This is to certify that the

dissertation entitled

CORRELATIONS OF STRESS AND STRAIN WITH ALERATIONS IN CARTILAGE AND UNDERLYING SUBCHONDRAL BONE FOLLOWING AN IMPACT IN AN IN VIVO ANIMAL AND AN IN VITRO EXPLANT MODEL

presented by

Benjamin James Ewers III

has been accepted towards fulfillment
of the requirements for

Ph.D. degree in Engineering Mechanics

Roger C Haut
Major professor

Date 03/14/01

CORRELATIONS OF STRESS AND STRAIN WITH ALTERATIONS IN CARTILAGE AND UNDERLYING SUBCHONDRAL BONE FOLLOWING AN IMPACT IN AN IN VIVO ANIMAL AND AN IN VITRO EXPLANT MODEL

By

Benjamin James Ewers III

A DISSERTATION

Submitted to
Michigan State University
In partial fulfillment of the requirements
For the degree of

DOCTOR OF PHILOSOPHY

Department of Materials Science and Mechanics

2001

ABSTRACT

CORRELATIONS OF STRESS AND STRAIN WITH ALTERATIONS IN CARTILAGE AND UNDERLYING SUBCHONDRAL BONE FOLLOWING AN IMPACT IN AN IN VIVO ANIMAL AND AN IN VITRO EXPLANT MODEL

By

Benjamin James Ewers III

Osteoarthritis (OA) is a degradative disease affecting both the articular cartilage and the underlying bone, with the final stages being loss of cartilage leading to bone on bone contact and pain. OA may cost society $54 billion annually in treatment and lost workdays. Excessive or abnormal loading has been implicated in initiating this joint degradation. Early signs of OA include fissuring, softening and increased permeability of the articular cartilage, chondrocyte death, and increased thickening of the underlying subchondral bone.

To better understand the mechanisms of mechanically induced changes to joint tissues our laboratory has developed an *in vivo* animal model that involves impacting the patellofemoral joint of Giant Flemish rabbits. At 12 months post-impact the retropatellar cartilage is fissured and softened and the subchondral plate is thickened. A computational model of the rabbit patella suggests that impact-induced shear stresses were associated with acute fissuring and chronic softening of the cartilage and thickening of the underlying bone. To better control mechanical loading, studies on cultured explanted cartilage have shown that a single severe impact can result in acute matrix damage (fissures) and chondrocyte death. Impact interfaces, impact orientation, and impact duration are all important parameters that could influence the state of stress and strain in joint tissues and therefore have an effect on both acute and chronic damages to the

tissues. Impact modeling of articular cartilage needs to take into account the well documented non-linear stiffening and time-dependent effect of cartilage.

The overall aims of this dissertation were threefold. First, to use the established animal model to examine the influence of impact interface, impact direction, and impact duration on chronic alterations in joint tissues. Second, use a cartilage explant system to examine the influence of impact duration on matrix damage and cell death, and attempt to correlate the state of stress and strain in the tissue and cells with these damages. Third, determine a method to estimate the non-linear viscoelastic material properties of cartilage from in situ indentation testing for the modeling of impact experiments.

This study found that distributing the impact load resulted in shear stresses being decreased in the bone, but not the cartilage. As predicted there were chronic alterations in the cartilage, but no thickening of the bone. Impacting the joint centrally compared to slightly medial resulted in shear stresses being increased in the bone and decreased in the cartilage. As expected there were no chronic changes in the cartilage, however, there was also no thickening of the bone. An increase in normal bone stresses in the central impacts could have helped protect the bone. Impacting at a higher rate of loading resulted in more damage compared to a lower rate of loading in both the animal and explant models. Modeling of the explant suggested that depth-dependent material properties are needed and matrix damage was associated with high shear stresses while cell death corresponded to high cell strains. Finally, in situ indentation testing was used to estimate the hyper-viscoelastic material properties of cartilage, which were able to predict experimental unconfined compression tests on cartilage. Future studies will be able to use these material properties of cartilage for more appropriate modeling of impact scenarios.

DEDICATION

I would like to thank my soul mate and wife who has supported me throughout our life together. I have endless love and respect for you, and all of my successes are because of you. I would also like to thank my parents and sister for all of their support throughout my entire life.

ACKNOWLEDGMENTS

I would like to acknowledge my major professor Dr. Roger Haut for giving me support, guidance and many opportunities throughout my time here at Michigan State University.

I am extremely grateful to Dr. Michael Orth, Dr. Thomas Pence, and Dr. John McGrath for serving on my committee and playing important roles in my education.

I would also like to thank Dr. Loic Dejardin, Dr. Steven Arnoczky, and Rhonda Clark, for allowing me to play an important role in research outside my dissertation topics.

Finally, I would like to express my gratitude to the many fellow research assistants that I had the pleasure of working with: William Newberry, Dana Dvoracek-Driksna, Richard Banglmaier, Brian Weaver, Vijay Jayaraman, Jill Krueger, Dr Patrick Atkinson, and Dr. Theresa Atkinson.

TABLE OF CONTENTS

LIST OF TABLES ix

LIST OF FIGURES x

CITATIONS OF PUBLISHED WORK CONDUCTED DURING GRADUATE SCHOOL: DISSERTATION RESEARCH xii

CITATIONS OF PUBLISHED WORK CONDUCTED DURING GRADUATE SCHOLL: ADDITIONAL PUBLISHED RESEARCH xiii

INTRODUCTION 1

CHAPTER 1
LONG TERM CHANGES IN RABBIT RETROPATELLAR CARTILAGE AND SUBCHONDRAL BONE AFTER BLUNT IMPACT LOADING OF THE PATELLOFEMORAL JOINT 9
- Abstract 9
- Introduction 10
- Methods and Materials 13
- Results 16
- Discussion 19
- References 25
- Tables 29
- Figures 32

CHAPTER 2
ALTERATIONS IN THE MECHANICAL PROPERTIES OF BONE UNDERLYING ARTICULAR CARTILAGE IN A TRAUMATIZED JOINT 34
- Introduction 34
- Methods and Materials 34
- Results 35
- Discussion 36
- References 37
- Figures 48

CHAPTER 3
CHRONIC SOFTENING OF CARTILAGE WITHOUT THICKENING OF UNDERLYING BONE IN A JOINT TRAUMA MODEL 39
- Abstract 39
- Introduction 40
- Methods and Materials 42
- Results 44

Discussion 45
References 49
Tables 51
Figures 52

CHAPTER 4
IMPACT SHEAR STRESSES IN AN ANIMAL JOINT PREDICTS CHRONIC SOFTENING OF CARTILAGE BUT NOT THICKENING OF UNDERLYING BONE 54
Abstract 54
Introduction 55
Methods and Materials 56
Results 61
Discussion 63
References 67
Tables 70
Figures 72

CHAPTER 5
THE EFFECT OF LOADING RATE ON THE DEGREE OF ACUTE INJURY AND CHRONIC CONDITIONS IN THE KNEE AFTER BLUNT IMPACT 76
Abstract 76
Introduction 77
Methods and Materials 81
Results 87
Discussion 92
References 97
Tables 101
Figures 107

CHAPTER 6
POLYSULPHATED GLYCOSAMINOGLYCAN TREATMENTS CAN MITIGATE DECREASES IN STIFFNESS OF ARTICULAR CARTILAGE IN A TRAUMATIZED ANIMAL JOINT 113
Abstract 113
Introduction 114
Methods and Materials 116
Results 118
Discussion 120
References 123
Tables 126
Figures 127

CHAPTER 7
THE EXTENT OF MATRIX DAMAGE AND CHONDROCYTE DEATH IN MECHANICALLY TRAUMATIZED ARTICULAR CARTILAGE EXPLANTS DEPENDS ON RATE OF LOADING 130
Abstract 130
Introduction 131
Methods and Materials 133
Results 135
Discussion 138
References 142
Tables 145
Figures 146

CHAPTER 8
THEORETICAL MODELS OF CARTILAGE EXPLANTS AND CORRELATIONS WITH EXPERIMENTAL MATRIX DAMAGE AND CELL DEATH AFTER IMPACTING LOADS 151
Abstract 151
Introduction 152
Methods and Materials 154
Results 158
Discussion 161
References 166
Tables 168
Figures 170

CHAPTER 9
DETERMINATION OF IN SITU MATERIAL PROPERTIES OF CARTILAGE BASED ON A NON-LINEAR VISCOELASTIC MODEL FOR IMPACT LOADING 176
Abstract 176
Introduction 177
Methods and Materials 179
Results 185
Discussion 187
References 190
Figures 193

APPENDIX A
A.1 Variables to define for user-defined isotropic hyperelastic subroutine 197
A.2 UHYPER for a "generalized" Fung exponential energy function 198
A.3 UHYPER for the expanded expanded exponential energy function 199

APPENDIX B - Infinitesimal elastic constants related to the strain-energy coefficients
B.1 Pure Shear 200
B.2 Uniform triaxial loading 200

LIST OF TABLES

CHAPTER 1
Table 1 29
Table 2 30
Table 3 31

CHAPTER 3
Table 1 51
Table 2 51

CHAPTER 4
Table 1 70
Table 2 70
Table 3 71
Table 4 71

CHAPTER 5
Table 1 101
Table 2 102
Table 3 103
Table 4 104
Table 5 105
Table 6 106

CHAPTER 6
Table 1 126
Table 2 126

CHAPTER 7
Table 1 145

CHAPTER 8
Table 1 168
Table 2 169
Table 3 169

LIST OF FIGURES

CHAPTER 1
Figure 1 32
Figure 2 32
Figure 3 33

CHAPTER 2
Figure 1 38

CHAPTER 3
Figure 1 52
Figure 2 52
Figure 3 53

CHAPTER 4
Figure 1 72
Figure 2 73
Figure 3 74
Figure 4 75

CHAPTER 5
Figure 1 107
Figure 2 107
Figure 3 108
Figure 4 108
Figure 5 109
Figure 6 109
Figure 7 110
Figure 8 110
Figure 9 111
Figure 10 112

CHAPTER 6
Figure 1 127
Figure 2 128
Figure 3 129

CHAPTER 7
Figure 1 146
Figure 2 147
Figure 3 148
Figure 4 149
Figure 5 150

CHAPTER 8

Figure 1 170
Figure 2 171
Figure 3 172
Figure 4 173
Figure 5 174
Figure 6 175

CHAPTER 9

Figure 1 193
Figure 2 193
Figure 3 194
Figure 4 194
Figure 5 195
Figure 6 195
Figure 7 196
Figure 8 196

CITATIONS OF PUBLISHED WORK CONDUCTED DURING GRADUATE SCHOOL: DISSERTATION RESEARCH

CHAPTER 1
Ewers BJ, Weaver BT, Sevensma ET, Haut RC: Long term changes in rabbit retropatellar cartilage and subchondral bone after blunt impact loading of the patellofemoral joint. *In Preparation*

CHAPTER 2
Ewers BJ, Newberry WN, Garcia JJ, Haut RC: Alterations in the mechanical properties of bone underlying articular cartilage in a traumatized joint. *Proceedings 44th Meeting of the Orthopaedic Research Society*, 1998.

CHAPTER 3
Ewers BJ, Newberry WN, Haut RC: Chronic softening of cartilage without thickening of underlying bone in a joint trauma model. *Journal of Biomechanics*, 33:1689-1694, 2000.

CHAPTER 4
Ewers BJ, Weaver BT, Newberry WN, Haut RC: Impact shear stresses in an animal joint predicts chronic softening of cartilage but not thickening of underlying bone. *Journal of Biomechanical Engineering*, In Review.

CHAPTER 5
Ewers BJ, Jayaraman VM, Banglmaier RF, Haut RC: The effect of loading rate on the degree of acute damage and chronic conditions in the knee after blunt impact. *Stapp Car Crash Journal*, 44:299-313, 2000.

CHAPTER 6
Ewers BJ, Haut RC: Polysulphated glycosaminoglycan treatments can mitigate decreases in stiffness of articular cartilage in a traumatized animal joint. *Journal of Orthopaedic Research*, 18:756-761, 2000.

CHAPTER 7
Ewers BJ, Dvoracek-Driksna D, Orth MW, Haut RC: The extent of matrix damage and chondrocyte death in mechanically traumatized articular cartilage explants depends on rate of loading. *Journal of Orthopaedic Research*, In Print.

CHAPTER 8
Ewers BJ, Krueger JA, Dvoracek-Driksna D, +Orth MW, Haut RC: Theoretical models of cartilage explants and correlations with experimental matrix damage and cell death after impacting loads. *Annals of Biomedical Engineering*, In Review.

CITATIONS OF PUBLISHED WORK CONDUCTED DURING GRADUATE SCHOLL: ADDITIONAL PUBLISHED RESEARCH

Atkinson TS, Ewers BJ, Haut RC: The tensile and stress relaxation responses of human patellar tendon varies with specimen cross-sectional area. *Journal of Biomechanics*, 32: 907-914, 1999.

Pruyn ML, Ewers BJ, Telewski FW: Thigmomorphogenesis: Changes in the morphology and mechanical properties of two Populus hybrids. *Tree Physiology*, 20:535-540, 2000.

Dejardin LM, Arnoczky SP, Ewers BJ, Haut RC, Clarke RB: Tissue engineered rotator cuff tendon using swine small intestinal submucosa: Histological and mechanical evaluation in dogs. *Journal of Sports Medicine*, In Print.

Atkinson PJ, Ewers BJ, Haut RC: Injuries to the patellofemoral joint resulting from transarticular loading are influenced by impactor mass and velocity. *Journal of Biomechaincal Engineering*, In Print.

Fiechtner J, Ewers BJ, Mackenzie CD, Haut RC: Prevention of lapine post-traumatic osteoarthritis with polysulphated glycosaminoglycans (PSGAG). *Proceedings 62nd Meeting of the American Collage of Rheumatology*, 1998.

Ewers BJ, Orth MW, Haut RC: Urinary markers of post-traumatic OA and effects of PSGAG treatment after insult. *Proceedings 45th Meeting of the Orthopaedic Research Society*, 1999.

Ewers BJ, Garcia JJ, Altiero NJ, Haut RC: Modeling of the rabbit's patello-femoral joint for studies of acute blunt injury to the knee. *Advances in Bioengineering ASME*, 1999.

Atkinson PJ, Ewers BJ, Haut RC: Is impact energy the most important parameter affecting transarticular loading of the patellofemoral joint? *Proceedings 46th Meeting of the Orthopaedic Research Society*, 2000.

Dejardin LM, Arnoczky SP, Ewers BJ, Haut RC: Tissue engineered rotator cuff tendon using swine small intestinal submucosa histological and mechanical evaluation in dogs. *Proceedings 46th Meeting of the Orthopaedic Research Society*, 2000.

Ewers BJ, Dvoracek-Driksna D, Orth MW, Altiero NJ, Haut RC: Matrix damage and chondrocyte death in articular cartilage depends upon loading rate. *Proceedings 46th Meeting of the Orthopaedic Research Society*, 2000.

Krueger J, Dvoracek-Driksna D, Ewers BJ, Haut RC, Orth MW: Effects of pretreatment with glucosamine on mechanically traumatized cartilage explants, *Proceedings 47th Meeting of the Orthopaedic Research Society*, 2001.

Ewers BJ, Krueger J, Dvoracek-Driksna D, Orth MW, Haut RC: Chondrocyte viability decreases over 24 hours post-impact in a mechanically traumatized cartilage explant. *Proceedings 47th Meeting of the Orthopaedic Research Society*, 2001.

Ewers BJ, Newberry WN, Garcia JJ, Orth MW, Haut RC: Early diagnosis, possible treatment, and etiology of osteoarthritis due to blunt impact of the rabbit patellofemoral joint. *8th Injury Prevention Through Biomechanics Symposium*, 1998.

Ewers BJ, Dvoracek-Driksna D, Orth MW, Haut RC: Urinary collagen crosslinks and lasting effects of polysulphated glycosaminoglycans in a traumatized animal joint. *9th Injury Prevention Through Biomechanics Symposium*, 1999.

INTRODUCTION

An articular joint, such as the knee, is a union of bones which are covered by a thin layer of articular cartilage. Articular cartilage consists of a fluid phase composed of water and a solid phase composed of chondrocytes and a dense network of collagen fibers interspersed with proteoglycans. It is this ultrastructure that gives cartilage its unique material properties. Cartilage is responsible for providing a near frictionless interface between the bones and the transmission and distribution of large loads. Osteoarthritis (OA) is a disease affecting both the articular cartilage and the underlying bone. Clinically, OA is diagnosed radiograpically by joint space narrowing which is indicative of the joint developing full thickness loss of cartilage. At this later stage of the disease, there is bone on bone contact that leads to severe pain and little intervention is possible apart from joint replacement. OA may cost society $54 billion annually in treatment and lost workdays (Hamerman, 1989).

Excessive or abnormal loading has been known to cause chronic alterations in cartilage and the underlying bone indicative of early stages of this disease. Early signs of OA include fissuring, softening and increased permeability of the articular cartilage, chondrocyte death, and increased thickening of the underlying subchondral bone plate (Brandt et al., 1986; Kim et al., 2000). Chondrocyte death might play a significant role in the development of OA (Blanco et al., 1998). In support of this Simon et al. (1976) using an animal model documented that chondrocyte death leads to chronic degradation of cartilage. Another proposed mechanism is that the thickening of the underlying bone causes abnormally high stresses to develop in the overlying cartilage which leads to its further softening and eventual loss (Radin et al., 1990). While the etiology is not well

understood, mechanical trauma has clinically been implicated in initiating this joint degradation (Chapchal, 1978; Felson, 1990).

Joint trauma routinely occurs during automobile crashes, sporting activities, and domestic and occupational accidents. To better understand the mechanisms of mechanically induced changes to joint tissues our laboratory has developed an *in vivo* animal model (Newberry et al., 1998a). Briefly, this involves impacting the right patellofemoral joint of Giant Flemish rabbits using a rigid impact interface directed slightly medial with a subfracture blunt impact. At 12 months post-impact the retropatellar cartilage is fissured and softened compared to an unimpacted control population (Newberry et al., 1998a). The impacted limb also has a thickened subchondral plate compared to the unimpacted controls (Newberry et al., 1998a). Using a computational model of the rabbit patella with boundary conditions obtained from pressure sensitive film, high impact-induced shear stresses were associated with acute fissuring and chronic softening of the retropatellar cartilage (Newberry et al., 1998b). This is in support of a previous study that found high shear stress was the best predictor of acute cartilage fissuring (Atkinson et al., 1998). Likewise, high shear and tensile stresses in the underlying subchondral bone corresponded with the chronic thickening of this tissue (Newberry et al., 1998b).

To better control loading and to examine possible mechanisms of cartilage damage, studies have been performed on cultured explanted cartilage tissue. These studies mechanically load the explanted tissue in simple loading configurations, such as unconfined compression. Previous studies have shown that a single severe impact to the

cartilage can result in acute matrix damage (fissures and increased water content) and chondrocyte death (Jeffrey et al., 1995; Repo and Finlay, 1977; Torzilli et al., 1999).

Impact interfaces, impact orientation, and impact duration are all important parameters that could influence the state of stress and strain in joint tissues and therefore have an effect on both acute and chronic damages to the tissues. Impact modeling of articular cartilage needs to take into account the non-linear stiffening effect of cartilage (Oloyede et al., 1992; Atkinson et al., 1998). We currently use an elastic modulus of 20 MPa for cartilage under impact loading (Newberry et al., 1998b). This elevated elastic modulus was based on matching experimental displacements of cartilage under impact loading (Atkinson et al., 1998). While there is no fluid flow in cartilage under one second of loading (Donzelli et al., 1999), Ewers et al., (2000) has shown that rates of loading under one second can affect the amount of deformation of cartilage. To fully model the apparent fast relaxation characteristics of cartilage under an impact, a model that incorporates viscoelasticity is needed (Suh and Bai, 1998).

The overall aims of the current study were threefold. First, to use the established animal model to examine the influence of impact interface, impact direction, and impact duration on chronic alterations in joint tissues, and to correlate impact-induced stresses with these changes. Second, to use a cartilage explant system to examine the influence of impact duration on matrix damage and cell death, and attempt to correlate the state of stress and strain in the tissue and cells with these damages. Third, determine a method to estimate the non-linear viscoelastic material properties of cartilage from in situ indentation testing for the modeling of impact experiments. Future studies will be able to

use these material properties of cartilage for more appropriate modeling of impact scenarios.

Below is an overview of the chapters contained in this dissertation:

Chapter 1 documents changes in retropatellar cartilage and subchondral bone in our established animal model out to 36 months post-impact. This study shows that this animal model does not develop an end-stage disease by 36 months, but that there are still progressive alterations going on in the joint tissues, such as increased thickening of subchondral bone, and a thinning of the articular cartilage.

Chapter 2 uses computational models to examine the influence of softened articular cartilage on the state of stress in the underlying bone. This study also examines the influence of the material properties of the subchondral bone on the state of stress in the overlying cartilage. This study shows that in our animal model there does not seem to be any mechanical interaction between retropatellar cartilage and underlying subchondral bone.

Chapter 3 examines the effects of using a deformable impact interface to change the load distribution on chronic alterations in joint tissues in our animal model. This study finds that a deformable interface reduced the impact-induced stresses in the underlying bone, mitigating any chronic thickening out to 12 months post-impact. However, the impact-induced stresses in the cartilage are still elevated leading to a chronic softening and fissuring of retropatellar cartilage.

Chapter 4 examines the effects of impacting the patellofemoral joint with a central oriented impact load. This study documents that there were no chronic alterations in the joint tissues out to 12 months post-impact. The impact-induced shear stresses are reduced

in the articular cartilage, but increased in the subchondral bone. However, there is also an increase in the compressive mean stress, which likely protected the underlying subchondral bone.

Chapter 5 examines the effect of impact duration on the acute injuries in cadaver knee impacts and chronic alterations in our animal model. This study indicates that a higher rate of loading results in more fracture and nonfracture injuries in the human cadaver impacts than low rates of loading. In support of this, there is more chronic damage to both the cartilage and underlying bone in our animal model with the high versus low rate of loading.

Chapter 6 examines the influence of a possible chondroprotective drug (polysulphated glycosaminoglycans) on joint tissues using our animal model. This study suggests that the drug did not have any effect on thickening of the underlying subchondral bone. However, the drug mitigated the usual decrease in cartilage moduli post-impact, suggesting a possible chondroprotective effect.

Chapter 7 examines the influence of loading rate on matrix damage and chondrocyte death using explanted cartilage plugs that were loaded in unconfined compression. This study indicates that a high versus low rate of loading results in significantly more matrix damage. In contrast, the low versus high rate of loading results in significantly more chondrocyte death.

Chapter 8 examines different computational models of cartilage and attempted to correlate high shear stresses with matrix damage and high cell strains with cell death. This study suggests that the isotropic model with depth-dependent material properties best associated areas of high stress with matrix damage and predicted the experimental

lateral expansion profiles documented in the recent literature. The study also suggestes that the extent of cell strain, and thus cell death in each layer, was most influenced by the shape of the cell, not the depth-dependent material properties of the matrix.

Chapter 9 describes a method to estimate the non-linear viscoelastic material properties of cartilage using in situ indentation testing. This study indicates that the short-time relaxation (less than 1 second) can be modeled by a linear viscoelastic response. This study also shows that the four material constants of the strain energy function can be approximated from the infinitesimal elastic constants, and the unrelaxed response of a spherical indentor indenting down to 50 % of the cartilage thickness. The method was validated using bovine cartilage in unconfined compression. The study suggests that the material properties determined from the above procedure can predict the experimental load within 17 %.

REFERENCES

1. Atkinson, TS, RC Haut, and NJ Altiero. (1998) Impact-induced fissuring of articular cartilage: an investigation of failure criteria. *J Biomech Eng.* 120:181-187.

2. Blanco FJ, Guitian R, Vazquez-Martul E, de Toro FJ, Galdo F (1998) Osteoarthritis chondrocytes die by apoptosis. A possible pathway for osteoarthritis pathology. *Arthritis Rhuem* 41:284-289.

3. Brandt KD, Mankin HJ, Shulman LE (1986) Workshop on etiopathogenesis of osteoarthrits. *J Rhuematol* 13:1126-1160.

4. Chapchal, G. (1978) Posttraumatic Osteoarthritis after Injury of the Knee and Hip Joint. *Reconstructive Surgery Traumatology* 16, pp. 87-94.

5. Donzelli, PS, RL Spilker, GA Ateshian, and VC Mow. (1999) Contact analysis of biphasic transversely isotropic cartilage layers and correlations with tissue failure. *J Biomech.* 32:1037-1047.

6. Ewers, BJ, D Dvoracek-Driskna, MW Orth, and RC Haut. (2000) The extent of matrix damage and chondrocyte death in mechanically traumatized articular cartilage explants depends on rate of loading. *J Orthop Res.* in press.

7. Felson DT. (1990) The epidemiology of knee osteoarthritis: results from the Framingham osteoarthristis study. *Sem Arth and Rheum*, 20:42-50.

8. Hamerman, D. (1989) The biology of osteoarthritis, *New Eng Journal of Med.* 320:1323-1330.

9. Jeffrey JE, Gregory DW, Aspden RM (1995) Matrix damage and chondrocyte viability following a single impact load on articular cartilage. *Arch Biochem Biophys* 322:87-96.

10. Kim, HA, YJ Lee, SC Seong, KW Choe, YW Song (2000) Apoptotic chondrocyte death in human osteoarthritis. *J Rheumatol.* 27(2):455-462.

11. Newberry WN, Mackenzie CD, Haut RC (1998a) Blunt impact causes changes in bone and cartilage in a regularly exercised animal model. *J Orthop Res* 16:348-354.

12. Newberry WN, Garcia JJ, Mackenzie CD, Decamp C, Haut RC (1998b) Analyses of acute mechanical insult in an animal model of post-traumatic osteoarthrosis. *J Biomech Eng*, 120:704-09.

13. Oloyede A, Flachsmann R, Broom N (1992) The dramatic influence of loading velocity on the compressive response of articular cartilage. *Conn Tiss Res*, 27:211-224.

14. Radin EL, Burr DB, Fyhrie D, Brown TD, Boyd RD (1990) Characteristics of joint loading as it applies to osteoarthrosis. In: Mow, VC, Ratcliffe, A., Woo, S.L-Y. (Eds.), Biomechanics of Diarthrodial Joints. Springer-Verlag, New York, pp. 437-451.

15. Repo RU, Finlay JB (1977) Survival of articular cartilage after controlled impact. *J Bone Joint Surg [Am]* 59: 1068-1076.

16. Simon WH, Richardson S, Herman W, Parsons JR, Lane J (1976) Long-term effects of chondrocyte death on rabbit articular cartilage in vivo. *J Bone Joint Surg [Am]* 58:517-526.

17. Suh, JK and S Bai (1998) Finite element formulation of biphasic poroviscoelastic model for articular cartilage. *J Biomech Eng* 120:195-201.

18. Torzilli PA, Grigiene R, Borrelli Jr. J, Helfet DL (1999) Effect of impact load on articular cartilage: Cell metabolism and viability, and matrix water content. *J Biomech Eng* 121:433-441.

CHAPTER 1

LONG TERM CHANGES IN RABBIT RETROPATELLAR CARTILAGE AND SUBCHONDRAL BONE AFTER BLUNT IMPACT LOADING OF THE PATELLOFEMORAL JOINT

Benjamin J Ewers, Brian T Weaver, Eric T Sevensma, and Roger C Haut

ABSTRACT

Animal models of OA are useful for the study of early changes in the joint tissues that may eventually lead to an end stage disease. Our laboratory has developed a joint trauma model using a single blunt impact to the patellofemoral joint of rabbits and has documented softening of retropatellar cartilage and thickening of underlying bone out to 12 months post-trauma. The objective of this study was to examine the changes in joint tissues with this animal model out to 36 months post-impact. Forty-nine Flemish Giant rabbits were impacted on the right patellofemoral joint and sacrificed at one of five times: 4.5, 7.5, 12, 24, and 36 months post-impact. The mechanical properties of cartilage and thickness of subchondral bone were documented. At 36 months the animals had not developed an end stage disease. A reduction in the compressive modulus of traumatized retropatellar cartilage, based on indentation testing, occurred at 4.5 months and remained constant to 36 months. The thickness of the cartilage, however, decreased from baseline over time resulting in overall structural mechanical stiffening of the retropatellar cartilage. Furthermore, the traumatized cartilage had a significant increase from baseline in its fluid permeability over time based on data from mechanical tests. In addition, the impacted patellae had progressive changes with a significant increase in thickness of the

subchondral bone over time from baseline. In conclusion, since there is a need to more fully understand the mechanisms of a post-traumatic OA, or a process of trauma with healing, this animal model may be of interest. While not developing into an end stage disease by 36 months, progressive changes were still occurring, so the model may be useful for the study of the mechanisms leading to a possible post-traumatic disease, early diagnostic protocols, and disease mitigating interventions. On the other hand, the model may also be one of trauma with a subsequent healing response over time.

INTRODUCTION

Osteoarthritis (OA) could cost society approximately 54 billion dollars a year (Yelin, 1998). Epidemiology studies of human OA have advanced our understanding of this disease; however, they do not provide much data on the mechanisms and temporal progression of joint degeneration. This is particularly true in the early stages of the disease. Experimentally, animal models provide a tool to study early changes in joint tissues that may eventually lead to an end stage disease. Many animal models of OA have been described using various species, various means of inducing joint degradation, and resulting in varying degrees of end stage disease. These models have included spontaneous disease (Okabe, 1989; Alexander, 1992), chemically induced disease models (Coulais et al., 1984; Van der Kraan et al., 1989), and mechanical or surgical models (Pond and Nuki, 1973; Ehrlich et al., 1975). Hallmark indicators of an end stage disease are the total loss of cartilage and exposure of bone, sclerosis of the underlying subchondral bone, and formation of osteophytes around the joint periphery (Brandt et al., 1986).

One surgical model, menisectomy in canines, has shown decreases in the tensile modulus of femoral surface-zone articular cartilage 12 weeks post-surgery (Elliot et al., 1999). This is significant because diseased human cartilage has decreased material stiffness (or modulus) in compression, tension, shear loading, and enhanced swelling (Akizuki et al., 1987; Armstrong et al., 1982; Maroudas and Venn, 1977; Setton et al., 1999). A more widely used surgical model is transection of the anterior cruciate ligament (ACL) in canines, which has been shown to result in a decreased compressive modulus, an increased fluid permeability, and a slight thickening of articular cartilage on the medial tibial plateau three months post-surgery compared to controls (Setton et al., 1994). Along with these mechanical alterations observed in cartilage, ACL transection has been shown to increase subchondral bone thickness on the medial tibial plateau over time (Dedrick et al., 1993). While this model appears to be self-limiting at two years, it develops an end-stage disease at 54 months (Brandt et al., 1991). A mechanical model using repetitive impulse loading of the rabbit tibiofemoral joint has shown an increase in tetracycline labeling and bone formation in the underlying subchondral plate before cartilage degradation (Radin et al., 1984). Nine weeks of repetitive loading, followed by 24 weeks of cage rest, leads to a complete loss of cartilage on the weightbearing surface of the tibia and the formation of osteophytes (Radin et al., 1990).

Previous knee injuries lead to an increased risk for the subsequent development of OA (Felson, 1990). A recent analysis of automobile accidents has shown that while safety features significantly reduce fatalities, lower extremity injuries are now more frequent (Otte, 1996; Pattimore et al., 1991). The current criterion for certifying new automobiles is based on a bone fracture in human cadavers. For the knee-femur-hip complex the

femoral loads cannot exceed 10 kN in a simulated crash. However, a majority of injuries to the knee are non-fracture, such as contusions and lacerations (Atkinson et al., 1997). Clinically, such non-fracture injuries can initiate diseases such as OA (Upadhyay et al. 1983; Chapchal, 1978). However, even major joint injuries with bone fracture take 2-5 years for development of disease symptoms. Less severe injuries may take 10 or more years for degenerative changes to be diagnosed (Wright, 1990).

A number of research animal models have been developed to study the pathogenesis of post-traumatic OA. An impact model using a single transarticular load to the canine patellofemoral joint has shown surface lesions on retropatellar cartilage and step-off fractures across underlying calcified cartilage (Thompson et al., 1991). One year after impact these fractures heal, and the density of cartilage proteoglycans appears normal (Thompson et al., 1993). The disease process looks to be self-limiting, but the model may need to be carried out over a longer time frame as in the ACL transection model. One difficulty, however, in such studies is the cost of maintaining these large animals over long periods of time (Brandt et al., 1991).

Our laboratory has been developing a small animal model, Giant Flemish rabbits, that involve less research costs than the canine model. A single blow to the patellofemoral joint leads to histological changes and decreased stiffness of retropatellar cartilage, along with thickening of the underlying subchondral bone (Newberry et al., 1998). To date post-traumatic changes in the joint have been documented for only 12 months. The current study was conducted to document the more long-term effects of a single blunt insult to the patellofemoral joint on retropatellar cartilage and its underlying subchondral bone using this animal model.

METHODS AND MATERIALS

Forty-nine mature Flemish Giant rabbits (4.8 ± 0.9 kg, 6-8 months) were used in the study. Random checks in prior pilot studies displayed closed epiphysis for animals weighing 5 kg at 6 – 8 months of age (Newberry et al., 1998). The blunt impact experiments have been described in previous studies (Newberry et al., 1998). Briefly, a 1.33 kg mass with a flat 1 in. diameter aluminum impact interface was dropped from 0.46 m onto the right hind limb and impacting the medial aspect of the joint, which was flexed approximately 120^0 (Figure 1). During the impact the animals were maintained at a surgical plane of anesthesia using Isoflurane and oxygen (2% Isoflurane). The mass was stopped electronically after the first impact, preventing multiple impacts. A load transducer (Sensotec, Columbus OH: model 31/1432, 500 lb capacity) recorded the impact load at a 10 kHz sampling rate.

After impact, all animals received one injection of Butorphenol for early post-surgical pain. After a five-day period of rest, a daily exercise program was initiated for all animals. This program consisted of ten minutes of exercise, five days a week, on a treadmill running at 0.3 mph (Oyen-Tiesma et al., 1998). The exercise schedule lasted the entire length of the study. A certified veterinary technician was devoted to this animal colony throughout the duration of the study (JA). The animals were housed in individual cages (48" x 24" x 19") when not being exercised. This study was approved by the MSU All-University Committee on Animal Use and Care.

Eight animals were sacrificed at each of the following timepoints: 0, 4.5, 7.5, 12, and 36 months post-impact. Nine animals were sacrificed twenty-four months after impact. Immediately after sacrifice the patellae were excised for mechanical indentation

tests on the retropatellar cartilage, as described previously (Ewers et al., 2000a). The patellae were immersed in a room-temperature phosphate buffered saline bath during the indentation tests. The tests were performed with a custom-built instrument that used a computer controlled stepper motor (Physik Instruments, Waldbronn, Germany : model M-168.30) to indent the cartilage. A fixture, which held the patella with its retropatellar surface facing the indenter, allowed X-Y-Z movement to position the site of indentation. A camera mount (Bogen, Ramsey, NJ) attached to the base of the fixture allowed rotation of the patella to insure that the indentation was performed normal to the cartilage surface. A 1 mm diameter flat, non-porous probe was pressed into the cartilage 0.1 mm in 30 ms and maintained for 150 seconds. The resistive loads were measured (Data Instruments, Acton MA : model JP - 25, 25 lb capacity), amplified, and collected at 1000 Hz for the first second and 20 Hz thereafter. After the tissue was allowed to recover for 5 minutes, the test was repeated with a 1.5 mm diameter, flat non-porous probe in the same location. The probe was then replaced with a needle that was slowly pressed into the cartilage to determine the thickness of cartilage at that location. The above procedure was performed at two sites adjacent to surface lesions that are typically produced on the lateral retropatellar facet during blunt impact to the patellofemoral joint at this severity of impact (Newberry et al., 1998).

Mechanical data was analyzed using a biphasic (poroelastic) model having a transversely isotropic (TI) solid structure (Garcia, 1998). Briefly, the model assumed isotropy in the plane of the cartilage and Poisson's ratio in the plane (ν_{12}) was set equal to zero. The remaining four elastic parameters and the two permeability measures, namely: a thickness direction modulus (E_{33}), an in-plane modulus (E_{11}), a shear modulus (G_{13}), a

Poisson's ratio (ν_{13}), a thickness direction permeability (k_3), and an in-plane permeability (k_1), were then computed using the Garcia curve fitting algorithm (Garcia, 1998).

After mechanical tests on each patella, they were stained with India ink to highlight surface lesions and photographed for permanent documentation. The patellae were then placed in 10% buffered formalin for a week, and decalcified in 20% formic acid for another week. Tissue blocks were cut medial to lateral across the patellae in the area known to produce high contact pressures during blunt impact to the patellofemoral joint at this flexion angle (Haut et al., 1995). Tissue blocks were processed in paraffin and six sequential sections, 8 μ thick, were prepared for analysis. The sections were stained with Safranin O-Fast Green and examined under light microscopy at 12-400 power. The thickness of the subchondral bone plate underlying retropatellar cartilage was measured at 25x for all six sections with a calibrated eye-piece at the center of each facet and the mid-line of the patella by three independent investigators, using established methods (Newberry et al., 1998). To quantify the degree of cartilage matrix damage, the gross photographic images were digitally scanned (ScanJet 6300C, Hewlett Packard, Singapore) and the total length of the surface lesions was measured using image software (Sigma Scan, SPSS Inc., Chicago, IL). The number and average depth of these surface fissures were also measured at 40x with the calibrated eye-piece for three sections for each patella by a single investigator (ES).

Signed Rank tests were used for comparisons between impacted and contralateral unimpacted limbs for the number of surface lesions and the average lesion depth. Paired t-tests were used to compare impacted to unimpacted contralateral limbs for all other parameters. ANOVAs with SNK post-hoc tests were used to determine statistical

differences in parameters between timepoints. ANOVAs with SNK post-hoc tests were also used to determine differences in subchondral bone thickness at each location between readers. A Spearman Rank Order correlation was performed to examine changes over time for the number of fissures and their average depth. A Pearson Product Moment correlation was used for the remaining parameters. Statistical significance was set at $p < 0.05$ for all tests.

RESULTS

Daily observations during treadmill exercise by the certified veterinary technician indicated that the rabbits did not favor the impacted limb. The 24 and 36 months post-impact groups had 4 and 5 animals, respectively, develop ulcerative pododermatitis (sore hocks). Sore hocks, which is treated with disinfecting ointments, is a common condition found in Giant Flemish rabbits associated with age, weight, and/or living quarter conditions. The 24 and 36 months post-impact groups had 6 and 4 animals, respectively, require antibiotics (Baytril, 5.0 mg/kg enrofloxacin) for an average of two weeks, for the treatment of various complications caused from chronic pasteurellosis. This is common for non-pathogen free animals.

Gross visual examination of the impacted joints revealed surface lesions on all impacted patellae typically occurring along the center ridge of the patella on the lateral facet (Figure 2A-B). Surface lesions on the contralateral unimpacted retropatellar cartilage were documented for three, two, and two patellae at 12, 24, and 36 months, respectively. At 36 months, three impacted patellae had osteophytes develop on the medial or lateral sides, while osteophytes were not documented on any unimpacted patellae (Figure 2C).

The results of mechanical indentation tests revealed that there were no significant differences between limbs in any mechanical parameter at time zero. Furthermore, there were no time-dependent changes from baseline in any mechanical parameter for the unimpacted sides. Significant reductions in the E_{11} and E_{33} moduli were, however, documented at all timepoints other than zero for the impacted retropatellar cartilage compared to the contralateral, unimpacted side (Table 1). Interestingly, these reductions occurred early (4.5 months) and remained constant at approximately 35 and 28% of contralateral values for E_{11} and E_{33}, respectively. There was a significant reduction in E_{11} compared to baseline values at all timepoints except 7.5 months. The reduction in cartilage moduli was accompanied by a significant increase in the k_1 and k_3 permeabilities for the traumatized cartilage versus the contralateral unimpacted side at all timepoints except zero. While the increase in the k_3 permeability remained constant over time, approximately 88% of the contralateral values, the k_1 permeability significantly increased with time at 0.18 $m^4/Ns \times 10^{-15}$ per month. The k_1 permeability was also significantly increased at 36 months compared to baseline values.

An analysis of the histological sections revealed an average variance of 1.0% for subchondral bone thickness between sections, so an average value was calculated at each location for each patella for each observer. There was no significant differences between the three independent observers in measured subchondral bone thickness at any location, with an average variance of 2.3% between observers. Therefore, an average value was calculated for each patellae at each location (medial, central, lateral) from the three independent readers and used in subsequent statistical analysis. At time zero and 4.5 months post-impact there were no significant differences in the thickness of the

subchondral plate for the impacted patellae compared to the unimpacted limb under any region (Table 2). At 7.5 months the thickness of the subchondral bone plate under the central region and the medial facet were significantly greater on the impacted patellae compared to those areas on the contralateral unimpacted limbs. At 12, 24, and 36 months the thickness of the subchondral bone under the central, the medial, and the lateral regions were significantly greater for the impacted patellae compared to those locations on the contralateral unimpacted limbs. There were also significant increases in subchondral plate thickness with time for the impacted patellae at all locations, and for the contralateral unimpacted patella in the medial and lateral facets. For the unimpacted patellae the thickness of the subchondral bone increased from 0.002 and 0.001 mm per month for the lateral and medial regions, respectively. For the impacted patellae, however, the thickness of the subchondral bone plate increased 0.013, 0.007, and 0.007 mm per month for the central, lateral, and medial regions, respectively. These differences in the rate of the subchondral bone thickening were statistically significant at each location. Finally, there was a significant increase in subchondral bone thickness at 36 months compared to baseline values at each location.

From the biomechanical testing protocol the thickness of retropatellar cartilage could be recorded over time. The traumatized retropatellar cartilage on the lateral facet was thicker than that of the contralateral unimpacted cartilage and baseline cartilage at 4.5 months post-trauma (Table 3). This thickening was followed by significant decreases in thickness for the traumatized cartilage compared to the contralateral unimpacted sides of 15 and 48% at 24 and 36 months, respectively. While there was no significant time-dependent change over baseline in articular cartilage thickness for the unimpacted limb,

the thickness of the traumatized retropatellar cartilage significantly decreased from the baseline level with time. Cartilage thickness decreased at 36 months compared to the baseline cartilage thickness.

Gross photographs of the retropatellar cartilage surface were studied and revealed significantly greater fissure lengths on impacted patellae versus contralateral unimpacted patellae at all timepoints post-trauma (Table 3). There was, however, no significant time-dependent change over baseline in the total length of surface fissures on retropatellar cartilage for impacted or unimpacted limbs.

Analysis of the histological sections revealed lesions in traumatized cartilage at all timepoints (Figure 3). There was a significant increase in average surface fissure depth and number of surface lesions for the impacted retropatellar cartilage compared to the contralateral unimpacted cartilage at 4.5, 7.5, 12, 24, and 36 months post-impact (Table 3). The average fissure depth and number of fissures for the unimpacted patellae were not significantly different than zero at any timepoint. There were no time-dependent changes over baseline in the average depth of the surface lesions or the number of surface fissures for either the impacted or unimpacted limb.

DISCUSSION

The current experimental study was undertaken to document the long-term effects of a single blunt insult to the rabbit patellofemoral joint on retropatellar cartilage and its underlying subchondral bone plate. While, the study showed no evidence of full thickness loss of cartilage, except in one animal at 24 months, there was a significant thinning. Furthermore, there was a progressive increase in the permeability of retropatellar cartilage and the thickness of underlying subchondral bone plate with time post-trauma

versus baseline. The elastic moduli of the cartilage, however, did not significantly decrease over time. Since the cartilage was shown to thin, these effects indicate that the cartilage became structurally stiffer with time post-trauma. This could have resulted in an altered stress state in the underlying subchondral bone, leading to its observed remodeling. This suggestion, however, would be in contrast to a recent mathematically simplified analysis of the rabbit patellofemoral joint which showed that a change in material properties of cartilage would not likely alter the state of stress in the underlying bone, and vise versa (Ewers et al., 1998). Furthermore, recent studies with this animal model suggest that damage to the retropatellar cartilage and the underlying subchondral plate may be initiated by acute overstressing, and that chronic softening of the retropatellar cartilage occurs independent of subchondral bone thickening (Ewers et al., 2000b). That study, however, was limited to 12 months post-impact. Thickening of subchondral bone underlying cartilage may be needed more for the progression to an end stage disease (Dedrick et al., 1993).

Our results compare well to earlier studies with this animal model in which the mechanical analysis of the cartilage was performed with an elastic versus a biphasic model. Newberry et al. (1998) showed a 42 and 25% reduction in the instantaneous modulus (G_U) and relaxed modulus (G_R), respectively, of traumatized cartilage compared to its contralateral unimpacted limb at 3, 6, and 12 months post-trauma. In the TI biphasic model analysis, changes in G_U and G_R are reflected largely by changes in E_{11} and E_{33}, respectively (Garcia, 1998). In the current study E_{11} of the impacted cartilage was reduced compared to the unimpacted side by approximately 35% at 4.5, 7.5, and 12 months, respectively. E_{33} was reduced by approximately 26% on the impacted versus

contralateral sides at these same timepoints. Newberry et al. (1998) also documented a 37, 29 and 72% increase in the thickness of underlying subchondral bone on the impacted patellae versus the contralateral unimpacted side at the center region for 3, 6, and 12 months post-trauma, respectively. This is similar to the current study which showed 15 and 46% increases in the thickness of subchondral bone underlying impacted cartilage versus the unimpacted side at 7.5 and 12 months, respectively, at the center region of the patella.

The mechanical results from the biphasic analysis of retropatellar cartilage in the current study also compare well to other animal models of OA. Setton et al. (1994) using a canine ACL-transection model, documented a 25% decrease in the aggregate and shear moduli of tibial cartilage and a 48% increase in its permeability and a thickening of cartilage at "covered" sites three months post-surgery. In the current study we documented 28% reductions in the elastic moduli of traumatized retropatellar cartilage, a 77% increase in its permeability, and a 15% increase in its thickness versus the contralateral unimpacted cartilage at 4.5 months post-trauma.

The reductions in the elastic moduli and increases in tissue permeability of retropatellar cartilage with trauma may reflect changes in its microstructure. The increased permeability of the tissue may reflect damage to the matrix that would likely increase tissue hydration. In fact, Setton et al. (1994) has documented a positive correlation between tissue permeability and its water content. This is significant since swelling or tissue edema has been documented in osteoarthritic human cartilage (Maroudas et al., 1977). In the current study, the E_{33} modulus is largely determined by the equilibrium response of the tissue (Garcia, 1998). Studies have shown that the

equilibrium response of cartilage is largely controlled by the content and integrity of tissue proteoglycans (Jurvelin et al., 1988). The in-plane modulus (E_{11}) has been shown to largely depend on the "instantaneous" response of cartilage. A study indicated that this characterization of cartilage may be reflective of the integrity of collagen network in the tissue (Mizrahi et al., 1986).

As previously stated above, the current impact model indicate early mechanical changes in the retropatellar cartilage similar to those that have been documented in the canine ACL-transection model (Setton et al., 1994). The increase in subchondral bone thickness is also similar. Dedrick et al. (1993) documented a trend for an increased tibial subchondral bone thickening on the ACL-transected side compared to the contralateral side at 18 and 54 months post-surgery, along with a statistical increase in thickness from three to 54 months post-surgery. At 24 to 36 months, the current study showed that in this impact model the joints did not develop an end stage disease. This is similar, however, to the ACL-transection model that showed only minimal degenerative changes in articular cartilage at 23 months post-surgery (Marshall and Olsson, 1971). It took 54 months post-surgery for this animal model to lead to a full loss of cartilage thickness (Brandt et al., 1991). This may suggest that we have to take the animals out further post-impact to develop an end stage disease. On the other hand, this model may be one of impact trauma and a subsequent healing response without development of an end stage disease.

Mazieres et al. (1987) using a similar impact model with New Zealand rabbits, have documented full thickness loss of cartilage at six months post-impact. A possible explanation for a difference in that study versus the current study is the use of a different breed of rabbit, and a higher impact energy (10 J versus 6 J in our model). Previous

studies with our animal model have shown that a high severity energy impact leads to a softening of the retropatellar cartilage and thickening of the underlying subchondral bone, while lower energies (and loads) do not result in any changes in joint tissues (Newberry et al., 1998b). Therefore, while causing some changes to the patellofemoral joint tissues, our impact energy (load) may not be as severe as the impacts in the Mazieres study so as to cause rapid joint degradation. Future studies with our model would be needed to see if an even more severe cases of blunt trauma, short of a gross fracture, would result in an accelerated disease process. In an impact model using canines, Thompson et al. (1991) documented multiple extensive fractures though the zone of calcified cartilage and the subchondral bone. These fractures heal one year post-impact and the density of cartilage proteoglycans appears normal. While the endpoint of the Thompson et al. (1991) level of joint trauma is yet unknown, these data may suggest that rapid progression to an end stage disease may only occur for a select range of joint impact intensities. If confirmed in future studies, this might suggest that the time frame for progressive disease may significantly depend on the intensity of acute trauma.

A limitation of the current study was the lack of a control population. Since for the contralateral unimpacted limb no parameter except subchondral bone thickness changed with time versus baseline, the chosen protocol may be justified given the expense of maintaining these animals over such a long time frame. Furthermore, the unimpacted side at time zero was not statistically different than the unimpacted limb at any timepoint for any parameter, except subchondral bone thickness. At the current severity of impact, primarily because of the life expectancy of the rabbits using the current experimental protocol, this model may not be appropriate to study end OA. More

severe insults to the patellofemoral joint need to be examined to determine if this would lead to a more progressive disease model.

In conclusion, since there is the need to more fully study joint injury after a blunt trauma, the current small animal model may be of interest. While the current model did not develop an end stage disease at 36 months post-impact, progressive changes are still occurring in the retropatellar cartilage and the underlying subchondral bone. This model may then be quite useful for the study of some early diagnostic protocols and/or the development of drugs to mitigate or limit early stages of disease post-trauma (Ewers and Haut, 2000). On the other hand, these data may also be indicative of a trauma model with subsequent healing over time. The study of the mechanisms of acute damage to tissues causing progressive degenerative changes, even with or without healing may also have utility in the design of "safer" impact interfaces in automobiles.

ACKNOWLEDGEMENTS

This study was supported by a grant for the Centers for Disease Control and Prevention (R49/CCR503607). Its contents are solely the responsibility of the authors and do not necessarily represent the official views of the Centers for Disease Control and Prevention. The authors wish to gratefully acknowledge William Newberry for assistance in the experimental impact protocol, Jane Walsh for her preparation of the histological sections, Jean Atkinson for her care of the animals and Cliff Beckett for technical assistance in the experimental phase of these studies.

REFERENCES

1. Akizuki S, Mow VC, Muler F, Pita JC, Howell DS. (1987) Tensile properties of human knee joint cartilage. II. Correlations between weight bearing and tissue pathology and the kinetics of swelling. *J Orthop Res*, 5:173-186.

2. Alexander JW. (1992) The pathogenesis of canine hip dysplasia. *Vet Clin North America: Small Animal Practice,* 22:503-11.

3. Armstrong CG, Mow VC. (1982) Variations in the intrinsic mechanical properties of human articular cartilage with age, degeneration, and water content. *J Bone Joint Surg [Am]*, 64:88-94.

4. Atkinson PJ, Garcia JJ, Altiero NJ, Haut RC. (1997) The influence of impact interface on human knee injury: implications for instrument panel design and the lower extremity injury criterion. *41st Stapp Car Crash Conference*, 167-180.

5. Brandt Kd, Mankin HJ, Shulman LE. (1986) Woprkshop on etiopathogenesis of osteoarthritis. *J Rheum*, 13:1126-60.

6. Brandt KD, Myers SL, Burr D, Albrecht M. (1991) Osteoarthritic changes in canine articular cartilage, subchondral bone, and synovium fifty-four months after transection of the anterior cruciate ligament. *Arth and Rheum*, 34:1560-70.

7. Chapchal G. (1978) Posttraumatic osteoarthritis after injury of the knee and hip joint. *Reconstr Surg*, 16:87-94.

8. Coulais Y, Marcelon G, Cros J, Guiraud R. (1984) An experimental model of osteoarthritis. II: biochemical study of collagen and proteoglycans. *Pathol Biol,* 32:23-8.

9. Dedrick DK, Goldstein SA, Brandt KD, O'Connor BL, Goulet RW, Albrecht M. (1993) A longitudinal study of subchondral plate and trabecular bone in cruciate-deficient dogs with osteoarthritis followed up for 54 months. *Arth and Rheum*, 36:1460-67.

10. Ehrlich MG, Mankin JH, Hones H, Grossman A, Crispen C, Ancona D. (1975) Biochemical confirmation of an experimental osteoarthritis model. *J Bone Joint Surg*, 57:392-6.

11. Elliot DM, Guilak F, Vail TP, Wang JY, Setton LA. (1999) Tensile properties of articular cartilage are altered by meniscectomy in a canine model of osteoarthritis. *J Orthop Res*,17(4):503-8.

12. Ewers BJ, Newberry WN, Garcia JJ, Haut RC. (1998) Alterations in the mechanical properties of bone underlying articular cartilage in a traumatized joint. *Proc 44th Annual Meeting Orthopaedic Research Society*, 459.

13. Ewers BJ, Jayaraman VM, Banglmaier RF, Haut RC. (2000a) The effect of loading rate on the degree of acute injury and chronic conditions in the knee after blunt impact. *STAPP Car Crash Conference*, 44:299-314.

14. Ewers BJ, Newberry WN, Haut RC. (2000b) Chronic softening of cartilage without thickening of underlying bone in a joint trauma model. *J Biomech*, 33:1689-1694.

15. Ewers BJ, Haut RC. (2000) Polysulphated glycosaminoglycan treatments can mitigate decreases in stiffness of articular cartilage without thickening of underlying bone in a joint trauma model. J Orth Res, 18:756-761.

16. Felson DT. (1990) The epidemiology of knee osteoarthritis: results from the Framingham osteoarthristis study. *Sem Arth and Rheum*, 20:42-50.

17. Garcia JJ. (1998) A transversely isotropic hypo-elastic biphasic model of articular cartilage under impact loading. Michigan State University, Ph.D. dissertation.

18. Haut RC, Ide TM, De Camp CE. (1995) Mechanical responses of the rabbit patello-femoral joint to blunt impact. *J Biomech Eng*, 117:402-08.

19. Jurvelin J, Saamanen A-M, Arokoski J, Helminen HJ, Kiviranta I, Tammi M. (1988) Biomechanical properties of the canine knee articular cartilage as related to matrix proteoglycans and collagen. *Eng Med*, 17:157-62.

20. Maroudas A, Venn M. (1977) Chemical composition and swelling of normal and osteoarthrotic femoral head cartilage. II. Swelling. *Ann Rheum Dis*, 36:399-406.

21. Marshall JL, Olsson S-E. (1971) Instability of the knee: a longterm experimental study in dogs. *J Bone Joint Surg [Am]*, 53:1561-70.

22. Mazieres B, Blanckaert A, Thiechart M. (1987) Experimental post-contusive osteoarthritis of the knee: quantitative microscopic study of the patella and the femoral condyles. *J Rheum*, 14:119-21.

23. Mizrahi J, Maroudas A, Lanir Y, Ziv I, Webber TJ. (1986) The "instantaneous" deformation of cartilage: effects of collagen fiber orientation and osmotic stress. *Biorheology*, 23:311-30.

24. Newberry WN, Mackenzie CD, Haut RC. (1998) Blunt impact causes changes in bone and cartilage in a regularly exercised animal model. *J Orth Res*, 16:348-54.

25. Newberry WN, Garcia JJ, Mackenzie CD, Decamp C, Haut RC. (1998) Analyses of acute mechanical insult in an animal model of post-traumatic osteoarthrosis. *J Biomech Eng*, 120:704-09.

26. Okabe T. (1989) Experimental studies on the spontaneous osteoarthritis in C57 black mice. *J Tokyo Med*, 47:546-57.

27. Otte D. (1996) Biomechanics of lower limb injuries of belted car drivers and the influence of intrusion and accident severity. *40th Stapp Car Crash Conference*, 193-206.

28. Oyen-Tiesma M, Atkinson J, Haut RC. (1998) A method for promoting regular rabbit exercise in orthopaedics research. *Contemp Topics in Lab Animal Sci*, 37:77-80.

29. Pattimore D, Ward E, Thomas P, Bradford M. (1991) The nature and cause of lower limb injuries in car crashes. *35th Stapp Car Crash Conference*, 177-188.

30. Pond MH, Nuki G. (1973) Experimentally induced osteoarthritis in the dog. Ann *Rheum Dis*, 32:387-8.

31. Radin EL, Martin RB, Burr DB, Caterson B, Boyd RD, Goodwin C. (1984) Effects of mechanical loading on the tissues of the rabbit knee. *J Orth Res*, 2:221-34.

32. Radin EL, Burr DB, Fyhrie D, Brown TD, Boyd RD. (1990) Characteristics of joint loading as it applies to osteoarthrosis. In: Mow VC, Ratcliffe A, Woo S L-Y, eds. Biomechanics of diarthrodial joints. Vol 1. New York: Springer-Verlag, pp. 437-51.

33. Setton LA, Mow VC, Muller FJ, Pita JC, Howell DS. (1994) Mechanical properties of canine articular cartilage are significantly altered following transection of the anterior cruciate ligament. *J Orth Res*, 12:451-63.

34. Setton LA, Elliott DM, Mow VC. (1999) Altered mechanics of cartilage with osteoarthritis: human osteoarthritis and an experimental model of joint degeneration. *Osteoarthritis Cart*, 7(1):2-14.

35. Thompson RC Jr., Oegema TR Jr., Lewis JL, Wallace L. (1991) Osteoarthritic changes after acute transarticular load. *J Bone Joint Surg*, 73-A(7):990-1001.

36. Thompson RC Jr., Vener MJ, Griffiths HJ, Lewis JL, Oegema TR Jr., Wallace L. (1993) Scanning electron-microscopic and magnetic resonance-imaging studies of injuries to the patellofemoral joint after acute transartricular loading. *J Bone Joint Surg*, 75-A(5):704-13.

37. Upadhyay S, Moulton A, Srikrishnamurthy K. (1983) An analysis of the late effects of traumatic posterior dislocation of the hip without fractures. *J Bone Joint Surg*, 65-B(2):150-52.

38. Van der Kraan PM, Vitters EL, van den Berg WB. (1989) Development of osteoarthritis models in mice by 'mechanical' and 'metobolical' alterations in the knee joints. *Arthritis Rheum*, 32:S107.

39. Wright V. (1990) Post-traumatic osteoarthritis – a medico-legal minefield. *J Rheum*, 29:474-78.

40. Yelin E. (1998) The economics of osteoarthritis. In: Brandt KD,Doherty M, Lohmander LS, eds. Osteoarthritis. New York: Oxford University Press Inc., pp. 23–30.

TABLES

Table 1: Mechanical data for the retropatellar articular cartilage were analyzed using a biphasic model having a transversely isotropic solid structure, with isotropy in the plane of cartilage (1) (Avg ± SD).

Time Point (months)	Limb	E_{11} (MPa)	E_{33} (MPa)	G_{13} (MPa)	υ_{13}	k_1 ($m^4/Ns10^{-15}$)	k_3 ($m^4/Ns10^{-15}$)
0 [a]	Imp	6.41 ± 1.52	1.21 ± 0.27	0.19 ± 0.03	0.09 ± 0.03	4.86 ± 2.60	1.87 ± 0.42
	Unimp	6.67 ± 2.62	1.16 ± 0.37	0.21 ± 0.08	0.10 ± 0.03	4.75 ± 1.72	2.09 ± 1.52
4.5 [a]	Imp	4.40 ± 2.32$^{+\#}$	0.85 ± 0.25^{+}	0.22 ± 0.05	0.10 ± 0.03	7.45 ± 3.43	5.92 ± 3.75^{+}
	Unimp	6.30 ± 1.83	1.15 ± 0.30	0.16 ± 0.08	0.10 ± 0.02	5.54 ± 4.79	2.70 ± 1.86
7.5 [a]	Imp	4.93 ± 1.76^{+}	0.95 ± 0.28^{+}	0.20 ± 0.06	0.10 ± 0.03	5.76 ± 3.88^{+}	3.43 ± 1.86^{+}
	Unimp	6.49 ± 1.61	1.34 ± 0.50	0.18 ± 0.05	0.11 ± 0.05	4.31 ± 2.86	1.77 ± 0.91
12 [a]	Imp	2.93 ± 0.94$^{+\#}$	0.78 ± 0.23^{+}	0.25 ± 0.14	0.10 ± 0.03	6.70 ± 2.62^{+}	4.20 ± 1.92^{+}
	Unimp	5.96 ± 2.42	1.14 ± 0.25	0.21 ± 0.14	0.11 ± 0.03	4.43 ± 2.49	2.55 ± 1.93
24 [b]	Imp	4.21 ± 1.23$^{+\#}$	1.00 ± 0.30^{+}	0.17 ± 0.03	0.13 ± 0.05	8.02 ± 4.35^{+}	3.19 ± 1.39^{+}
	Unimp	6.81 ± 1.59	1.41 ± 0.20	0.19 ± 0.03	0.13 ± 0.04	4.13 ± 2.15	1.77 ± 0.79
36 [a]	Imp	3.97 ± 1.62$^{+\#}$	0.96 ± 0.21^{+}	0.20 ± 0.07	0.10 ± 0.02	12.31 ± 5.11$^{+\#}$	2.57 ± 1.44^{+}
	Unimp	6.01 ± 1.83	1.23 ± 0.22	0.17 ± 0.05	0.11 ± 0.03	5.94 ± 2.67	1.42 ± 0.32

Imp – impacted limb
Unimp – unimpacted limb
a – n = 8
b – n = 9
Significant increase in k_1 over time for the impacted cartilage (Pearson Product Moment Correlation, $p < 0.05$).

+ – significantly different from contralateral unimpacted limb (paired t-test, $p < 0.05$)
# - significantly different from baseline (time 0) (ANOVA, SNK post-hoc, $p < 0.05$)

Table 2: Subchondral bone thickness (mm) was measured at 25x with a calibrated eye-piece at the central region of the patella and midline of the lateral and medial facets (Avg ± SD).

Time Point (months)	Limb	Lateral	Center	Medial
0[a]	Imp	0.54 ± 0.26	0.78 ± 0.44	0.54 ± 0.24
	Unimp	0.50 ± 0.16	0.74 ± 0.26	0.47 ± 0.08
4.5[a]	Imp	0.59 ± 0.08	0.77 ± 0.13	0.49 ± 0.10
	Unimp	0.54 ± 0.07	0.73 ± 0.11	0.51 ± 0.07
7.5[a]	Imp	0.59 ± 0.10	0.81 ± 0.18[+]	0.60 ± 0.09[+]
	Unimp	0.57 ± 0.07	0.69 ± 0.19	0.49 ± 0.06
12[a]	Imp	0.74 ± 0.15[+]	1.15 ± 0.34[+]	0.69 ± 0.18[+]
	Unimp	0.60 ± 0.12	0.79 ± 0.32	0.49 ± 0.11
24[b]	Imp	0.71 ± 0.12[+]	1.16 ± 0.23[+]	0.67 ± 0.13[+]
	Unimp	0.59 ± 0.09	0.68 ± 0.13	0.54 ± 0.07
36[a]	Imp	0.82 ± 0.17[+#]	1.23 ± 0.27[+#]	0.80 ± 0.09[+#]
	Unimp	0.59 ± 0.11	0.67 ± 0.21	0.58 ± 0.14

Imp – impacted limb
Unimp – unimpacted limb
a – n = 8
b – n = 9
Significant increase in thickness at all three locations over time for the impacted patellae (Pearson Product Moment Correlation, $p < 0.05$).
Significant increase in thickness at the medial and lateral locations over time for the unimpacted patellae (Pearson Product Moment Correlation, $p < 0.05$).

+ – significantly different from contralateral unimpacted limb (paired t-test, $p < 0.05$)
# - significantly different from baseline (time 0) (ANOVA, SNK post-hoc, $p < 0.05$)

Table 3: The cartilage thickness was measured at the sites of biomechanical testing on the lateral facet (Avg ± SD). Gross photographs of the patellae after staining with India ink were used to determine total fissure length (Avg ± SD). The histological sections were used to determine average fissure depth (Avg ± SD) and total number of fissures (median (range)).

Time Point	Limb	Cartilage Thickness (mm)	Total Fissure Length (mm)	Average Fissure Depth (%)	Number of Fissures (#)
0[a]	Imp	0.57 ± 0.07	7.5 ± 5.0 [+]	22 ± 18	1 (1-2)
	Unimp	0.57 ± 0.06	2.3 ± 3.5	10 ± 24	0 (0-1)
4.5[a]	Imp	0.70 ± 0.07 [+#]	11.2 ± 5.8 [+]	33 ± 15 [+]	4 (2-5) *
	Unimp	0.61 ± 0.06	3.1 ± 3.6	7 ± 18	0 (0-1)
7.5[a]	Imp	0.51 ± 0.07	13.1 ± 6.3 [+]	30 ± 12 [+]	4 (1-5) *
	Unimp	0.55 ± 0.07	4.0 ± 3.8	12 ± 15	0 (0-1)
12[a]	Imp	0.56 ± 0.09	25.7 ± 8.8 [+]	37 ± 14 [+]	7 (4-12) *
	Unimp	0.54 ± 0.07	4.4 ± 4.3	19 ± 22	2 (0-8)
24[b]	Imp	0.52 ± 0.10 [+]	14.8 ± 9.8 [+]	31 ± 10 [+]	4 (0-8) *
	Unimp	0.61 ± 0.06	3.2 ± 2.7	6 ± 17	0 (0-3)
36[a]	Imp	0.31 ± 0.13 [+#]	17.6 ± 9.6 [+]	41 ± 8 [+]	4 (0-8) *
	Unimp	0.60 ± 0.05	4.5 ± 3.7	13 ± 25	0 (0-5)

Imp – impacted limb
Unimp – unimpacted limb
a – n = 8
b – n = 9
Significant decrease in cartilage thickness over time for the impacted patellae (Pearson Product Moment Correlation, P <0.05).

+ – significantly different from contralateral unimpacted limb (paired t-test, $p < 0.05$)
* – significantly different from contralateral unimpacted limb (Signed Rank test, $p < 0.05$)
# - significantly different from baseline (time 0) (ANOVA, SNK post-hoc, $p < 0.05$)

FIGURES

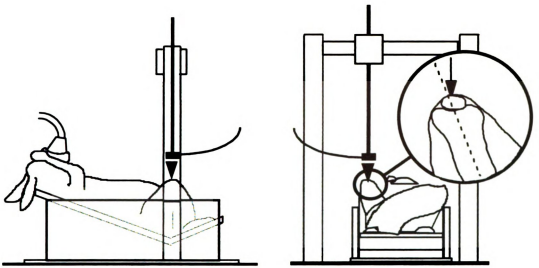

Figure 1: Impact experiments were performed by dropping a rigid mass onto the patellofemoral joint with 6.0 J of energy. The impacting mass was stopped electronically to prevent multiple impacts.

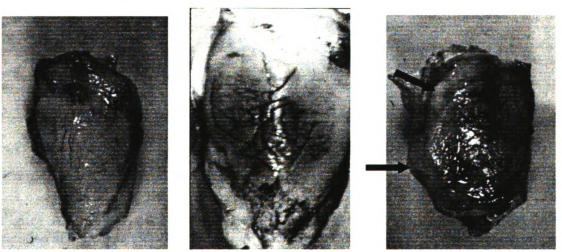

(A) (B) (C)

Figure 2: Gross visual examination of the impacted joints after application of India ink revealed small surface fissures on all impacted patellae at time zero typically along the center ridge of the patella on the lateral facet (A). By 12 months post-impact more lesions had developed (B).At 36 months post-impact osteophytes (➔) developed on the medial or lateral sides of three impacted patellae (C).

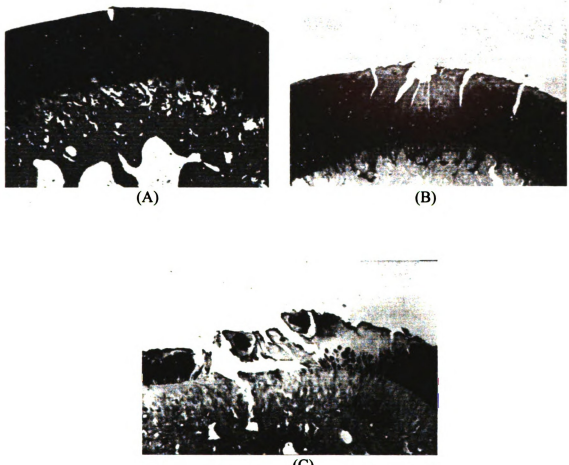

Figure 3: The histological sections revealed small acute surface fissures for the impacted patellae at time zero (A). At 12 months post-impact the lesions were more severe (B). At 36 months the lesions were similar in histological appearance compared to those at 12 months (C).

CHAPTER 2

ALTERATIONS IN THE MECHANICAL PROPERTIES OF BONE UNDERLYING ARTICULAR CARTILAGE IN A TRAUMATIZED JOINT

Benjamin J Ewers, William W Newberry, Jose J Garcia, and Roger C Haut

INTRODUCTION

Studies of the pathogenesis of osteoarthrosis (OA) have suggested that changes occur in both the underlying bone and articular cartilage. Changes in the mechanical properties of the subchondral bone have been thought to contribute to altered stresses in the overlying articular cartilage causing degradation of this soft material. Earlier studies have indicated both increases (Radin et al., 1973) and decreases (Serink et al., 1977) in subchondral bone stiffness. Our laboratory has been developing a small animal model of post-traumatic osteoarthrosis (Haut et al., 1995; Newberry and Haut, 1996). The studies indicate a decrease in the modulus of articular cartilage, and an increase in thickness of the underlying bone post-impact. The objectives of this current study were to determine the mechanical properties of the underlying bone as the disease progresses, and study the role of potential mechanical-based interactions between bone and overlying articular cartilage post-insult using mathematical analyses.

METHODS

The patello-femoral joints of 32 mature Flemish rabbits (4.7 ± 0.8 kg, 6-8 months of age) were impacted by a rigid, gravity-dropped impactor as described previously (Haut et al., 1995). The animals were sacrificed at 1, 3, 6, and 12 months, and the patellae were

excised. The integrity of the articular cartilage was examined along the lateral facet by indentation stress relaxation tests in a room temperature PBS bath (pH 7.2). The test consisted of indenting a 1 mm flat, non-porous probe 0.1 mm into the cartilage and holding it for 150 seconds while recording the resulting load. The shear modulus of the articular cartilage was determined based on load at 80 ms using an elastic analysis (Hayes et al., 1972). Sixteen pairs of patellae were histologically processed to determine the thickness of the underlying bone, using a calibrated eye-piece at 25x. The remaining patellae were stored at -20° C. Before mechanical testing of the underlying bone, the patellae were thawed and retro-patellar cartilage was removed under a dissecting microscope. Using the same probe as for cartilage tests, the subchondral plate was indented 0.04 mm and held for 150 seconds at six locations along the medial and lateral facets. An elastic modulus was computed using load at 50 ms based on the solution for an indentor on an elastic half-space (Timoshenko and Goodier, 1970). Paired t-tests were used to compare mechanical properties between impacted and non-impacted sides. The mathematical model of the rabbit patello-femoral joint was based on a 2-D plane strain contact analysis (ABAQUS). The geometry of the model was obtained by fixing *in situ* and sectioning a representative rabbit patello-femoral joint. Poisson's ratio for the cartilage and bone were assumed to be 0.49 and 0.3, respectively. The elastic modulus for the bone and articular cartilage was based upon the experimental data.

RESULTS

The elastic modulus for the unimpacted underlying bone was 230± 30 MPa. No change was recorded on the impacted side at 1 month. At 3 months the impacted side significantly decreased to 77% of the unimpacted value ($p<.05$). The properties of the

bone returned to contralateral levels at 6 and 12 months (Fig. 1). The elastic modulus of the unimpacted articular cartilage was 3.30 ±0.36 MPa. At 1 month post-insult no change from the unimpacted value was recorded. At 3 months the impacted side significantly decreased to 66% of the unimpacted level ($p<.05$). Unlike the bone, 42 and 33% reduction was observed at 6 and 12 months respectively (Fig. 1). The thickness of underlying bone on the impacted side was significantly greater, at all time points, compared to the contralateral unimpacted side. The mathematical model showed a 3% decrease in maximum shear stress at the cartilage surface when the elastic modulus of the bone was reduced by 23% at 3 months. The model also showed a 12% and 15% decrease in maximum shear stress and maximum tensile stress, respectively, in the underlying bone when the elastic modulus of the articular cartilage was reduced by 42%.

DISCUSSION

A current hypothesis for the progression of OA is that changes in the underlying bone cause increased stress in the articular cartilage which leads to degradation of this soft joint tissue (Radin et al., 1973). The degradation and subsequent softening of cartilage, in turn, leads to additional increased stress in underlying bone causing sclerosis and stiffening which further drives deterioration of the overlying cartilage. Our study showed only a subtle change in bone underlying traumatized and degrading articular cartilage 3 months after blunt impact, while the subchondral plate thickened significantly at all time points. Our mathematical analyses suggested only a minor decrease would occur in the stresses within articular cartilage with the documented decrease in modulus of underlying bone. Such a decrease in stress is not likely to cause softening of articular cartilage from disuse. Furthermore, the documented softening of overlying cartilage

would, as suggested by the model, result in lowered stresses in the underlying bone. This would not explain thickening of the subchondral plate. These data, and the corresponding model analyses, suggest that degradation of articular cartilage in this traumatized joint was independent of mechanical changes in the underlying bone. This implies that degradation of cartilage was not likely due to increased stress as a result of stiffening in the subchondral plate. The documented softening of cartilage was more likely due to wear and tear of the compromised tissue, and the subchondral bone thickening was a result of healing after microdamage produced by the initial insult. These conclusions are supported by other studies in which cartilage degrades without thickening of the subchondral plate (Dedrick et al., 1993). Our studies suggest that interventions in this disease process; surgical repair, pharmacological treatments, or specific physical therapies should focus on repair of the traumatized articular cartilage rather than thickening of underlying subchondral plate.

ACKNOWLEDGMENTS

This work was supported by the Centers for Disease Control and Prevention (R49/CCR503607).

REFREENCES

1. Radin EL, Parker HG, Pugh JW, Steinberg RS, Paul IL, Rose RM (1973) Response to impact loading – III: Relationship between trabecular microfractures and cartilage degeneration. *J Biomechanics* 6:51-57.

2. Serink MT, Nachemson A, Hansson G (1977) The effect of impact loading on rabbit knee joints. *Acta. Orthop. Scand.* 48:250-262.

3. Haut RC, Ide TM, De Camp CE (1995) Mechanical responses of the rabbit patello-femoral joint to blunt impact. *J Biomech Eng*, 117:402-08.

4. Newberry and Haut (1996) *Soc. Phys. Reg. Bio. Med.* 16th annual meeting 32-33.

5. Hayes WC, Keer LM, Herrmann G, Mockros LF (1972) A mathematical analysis for indentation tests of articular cartilage. *J Biomechanics* 5:541-551.

6. Timoshenko and Goodier (1970) *Theory of Elasticity* pp:380-409.

7. Dedrick DK, Goldstein SA, Brandt KD, O'Connor BL, Goulet RW, Albrecht M (1993) A longitudinal study of subchondral plate and trabecular bone in cruciate-deficient dogs with osteoarthritis followed up for 54 months. *Arth and Rheum*, 36:1460-67.

FIGURE

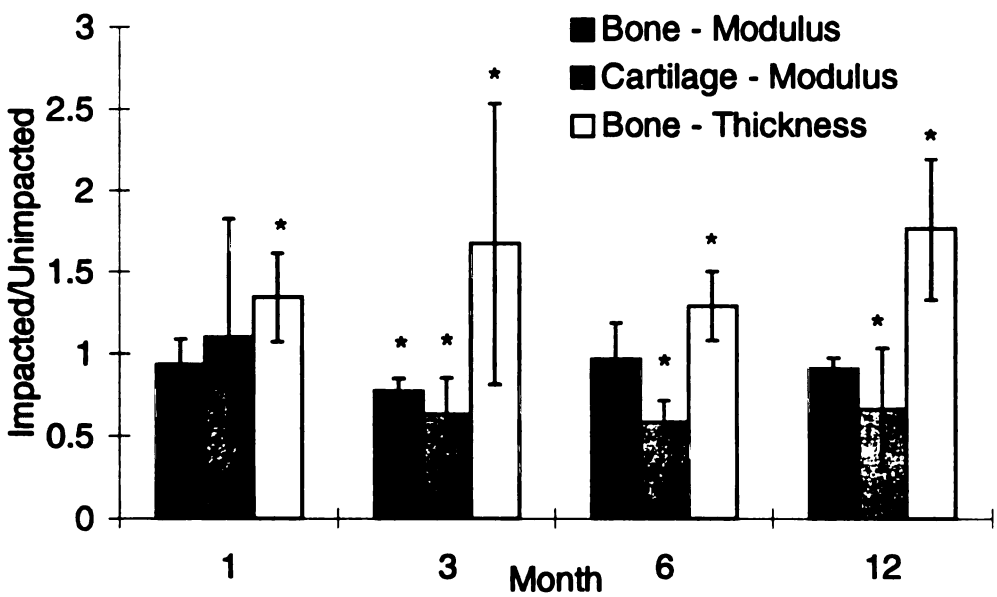

Figure 1: Ratios of mechanical data and subchondral bone thickness at each time point. n = 4 for bone modulus and thickness, n = 8 for cartilage modulus. * indicates significant difference between impacted and contralateral unimpacted sides using paired t-tests ($p<.05$).

CHAPTER 3

CHRONIC SOFTENING OF CARTILAGE WITHOUT THICKENING OF UNDERLYING BONE IN A JOINT TRAUMA MODEL

Ewers BJ, Newberry WN, and Haut RC

ABSTRACT

We have recently developed a trauma model to study degradation of the rabbit patello-femoral joint. Our current working hypothesis is that alterations in retropatellar cartilage and underlying bone in our model are initiated independently by acute overstresses developed in each tissue during blunt insult to the joint, and that the processes of chronic degradation in each tissue are not related in a mechanical sense. The current study was conducted in an attempt to help validate our hypothesis by impacting the patello-femoral joint with a padded interface. Based upon earlier human cadaver experiments, we believe this would reduce the acute overstresses in patellar bone while the stresses developed in the overlying retropatellar cartilage would be sufficient enough to initiate a chronic softening of the tissue. Twenty-four animals received an impact to the patello-femoral joint and were sacrificed at either 0, 4.5, or 12 months post-insult. Three acute animals were impacted to develop a simplified computational model to estimate the stresses in joint tissues. The study showed there was a significant softening of the retropatellar cartilage at 4.5 and 12 months post-trauma, compared to unimpacted controls. However, no thickening of the underlying subchondral bone was documented at

any timepoint. This was consistent with a reduction of stress in the bone compared to earlier studies, which document thickened subchondral bone post-insult at the same applied impact load. In conclusion, this study helped validate our hypothesis by documenting chronic softening of cartilage without remodeling of the underlying subchondral bone. Furthermore, this study, along with our earlier studies, suggest that impact load alone, which is currently used by the automobile industry to certify new automobiles, is not a good predictor of chronic injuries to a diarthrodial joint, and that simply the addition of padding to impact interfaces may not be adequate to protect occupants from chronic injuries.

INTRODUCTION

We have recently developed a trauma model to study degradation of the rabbit patello-femoral joint following a single, blunt impact. In various studies we have documented chronic alterations in retropatellar cartilage, as well as the underlying subchondral bone, out to one year post insult (Newberry et al., 1997; Newberry et al., 1998a). In one study with this joint trauma model we documented a significant decrease in the modulus of retropatellar cartilage three months post-insult with a significant increase in the thickness of underlying subchondral bone at 12 months (Newberry et al., 1998a). These data suggest that alterations in retropatellar cartilage may have occurred prior to alterations in the underlying bone. The results are in contrast to those suggested by Radin et al. (1978) where significant changes have been documented in underlying bone before histological alterations have been noted in the overlying cartilage using a repetitive trauma protocol on the rabbit tibial-femoral joint. These studies and others (Radin et al., 1990) have lead to the commonly accepted hypothesis that overloading a

diarthrodial joint may firstly result in damage to bone underlying cartilage, followed by a stiffening of the bone with a subsequent increase in the state of stress in the overlying cartilage resulting in its degradation over time. Studies with other models of joint injury, such as transection of the anterior cruciate ligament, have shown degradation of overlying cartilage before significant alterations are noted in the histology of underlying bone (Dedrick et al., 1993). Since bone changes are typically seen in the clinical setting, Burr (1998) suggested that alterations of bone underlying cartilage may occur late and be required to bring forth an end stage disease in the joint. Recently Ewers et al. (1998), using a simplified mathematical model of the rabbit patello-femoral joint, suggested that significant alterations in the mechanical properties of bone underlying cartilage in our joint trauma model would not influence the state of stress in the overlying cartilage. Nor will softening of the overlying cartilage, as a result of a severe blunt trauma, alter the state of stress in the underlying bone and initiate a remodeling process. That study has been used to establish the basis for our current working hypothesis that alterations in retropatellar cartilage and underlying bone in our joint trauma model are initiated independently by acute overstresses developed in each tissue during blunt insult to the joint, and that the processes of chronic degradation in each tissue are not related in a mechanical sense (Li et al., 1995; Newberry et al., 1998b).

The current study was conducted in an attempt to help partially validate the above hypothesis by impacting the rabbit's patello-femoral joint in such a way that acute overstresses in patellar bone would be minimized, while the stresses developed in the overlying retropatellar cartilage would be sufficient enough to initiate a chronic softening of the tissue. The idea was based on a study by Atkinson et al. (1997) using the isolated

human cadaver joint. That study suggests that by padding the impact interface loads can be distributed over a large area on the anterior surface of the patella to keep stresses in bone significantly low so as not to generate acute damage or initiate a chronic remodeling process of bone underlying retropatellar cartilage. On the other hand, by using an impact intensity sufficient enough to cause cartilage damage, the study further suggests that acute stresses in the overlying retropatellar cartilage could still be sufficient to induce injury and lead to a chronic degradation of this soft tissue.

METHODS AND MATERIALS

Thirty-five mature Flemish Giant rabbits (4.6 ± 0.8 kg, 6-8 months of age) were used in the study. The project was approved by the Michigan State University All-University Committee on Animal Use and Care. Twenty-four animals received a single impact to the right patello-femoral joint. Eight animals were sacrificed at each of three times post-insult: zero months, 4.5 months, and twelve months. Earlier studies with this animal model show no significant changes in the biomechanical properties of retropatellar cartilage or the thickness of underlying bone over time in control animals (Newberry et al. 1998a). Therefore a single, non-impacted control group of eight animals was used in the study. Three animals (acute animals) were sacrificed prior to impact for determination of the input boundary conditions for computational models.

These impact experiments have been described in an earlier study (Haut et al., 1995). In this study, however, a deformable impact interface (Hexcel, 3.76 MPa crush strength) was used to distribute the impacting load over the patella, versus a rigid interface used in earlier studies by our laboratory. Briefly, with the animal supine and maintained under anesthesia (2% isoflurane), the right hind limb was flexed 120° and a

1.33 kg mass was dropped onto the patello-femoral joint from 0.51 m, yielding 6.6 J of impact energy (Figure 1). The load-time history of the impact was recorded at 10 kHz. The peak contact load, time to peak, and total contact duration were documented in each experiment. Starting five days after impact the animals were regularly exercised, as previously described (Oyen-Tiesma et al., 1998).

Immediately after sacrifice, patellae were excised and the cartilage surface wiped with India ink to highlight defects on the retropatellar surface. Using previous documented biomechanical tests (Newberry et al., 1998a), the stiffness of the retropatellar cartilage was determined based on a shear modulus calculation at 50 ms (instantaneous shear modulus) and 150 s (relaxed shear modulus) using an elastic analysis (Hayes et al., 1972). Following mechanical testing the patellae were histologically processed and the thickness of the underlying subchondral plate was measured at 25x with a calibrated eye-piece at the center of each facet and at the mid-line of the patella (Newberry et al., 1998a).

To estimate the acute state of stress in the patella at impact, a two-dimensional, plane-strain, finite element model of the patella has been developed (Newberry et al., 1998b). Briefly, the geometry was taken from a slab cut of a representative patella, where the subchondral bone plate was distinguished from the cancellous bone. The retropatellar cartilage was treated as an incompressible elastic material with an elastic modulus and Poisson's ratio of 20 MPa and 0.49, respectively (Atkinson et al., 1998). Large deformations were allowed in the analysis. Due to the characteristics of the rabbit patella, with high-density cancellous bone, the patellar bone was assumed to have an equivalent elastic modulus of 350 MPa and a Poisson's ratio of 0.3, as previously computed for the

entire patella (Ewers et al., 1998). The boundary conditions on the patella were derived from pressure sensitive film (Prescale, single sheet, medium range, Fuji Film Ltd., Tokyo, Japan) inserted into the patello-femoral joint of the three acute animals, as previously described (Newberry et al., 1998b). The anterior surface of the patella was fixed in the area where the impact interface contacted the joint. The experimental retropatellar contact pressure distribution, medial to lateral across the region of highest contact pressure, was applied to the model of the patella (ANSYS 5.5). In the cartilage layer maximum shear stresses at the surface and at the interface with subchondral bone were reported. Maximum shear and peak principal stress distributions were also documented in the underlying subchondral plate.

An analysis of variance with S-N-K post-hoc tests was used to evaluate differences in moduli and subchondral bone thicknesses for unimpacted and impacted limbs between groups (Glantz, 1996). Paired t-tests were used for comparisons between the impacted and the contralateral, unimpacted limbs. Errors in the mean of data were reported as one standard deviation. Statistical differences were indicated for $p < 0.05$.

RESULTS

Qualitative examination after impact loading and daily observations during treadmill exercise by a veterinary technician (J.A.) indicated that the rabbits did not favor the impacted limb. Gross visual examination of the impacted joints revealed surface fissures typically along the center ridge of the patella on the lateral facet in 22 of 24 cases. No surface lesions were documented on the retropatellar cartilage of the unimpacted joints or that of controls. Contact loads on the patella for the three acute animals increased to a maximum of 636 ± 80 N in 5.4 ± 0.8 ms with a total contact

duration of 13.4 ± 1.0 ms. This was not significantly different from the chronic animals which increased to a maximum of 620 ± 50 N in 5.5 ± 1.0 ms with a total contact duration of 13.6 ± 0.9 ms (Figure 2).

The instantaneous and relaxed moduli of the retropatellar cartilage were significantly less on the impacted side compared to the unimpacted limb and those of control animals at 4.5 and 12 months post-impact (Table 1). The subchondral bone underlying the retropatellar cartilage was thicker at the central site than at the medial and lateral sites for each group. There was no statistical thickening of the subchondral bone for the impacted limb compared to either the unimpacted, contralateral limb or control animals at any time post-impact (Table 2).

The computational model showed a maximum shear stress in the retropatellar cartilage of 6.1 ± 0.9 MPa and 8.6 ± 2.0 MPa at the surface and interface, respectively (Figure 3). These maximum shear stresses were located at the center of the lateral facet near the impact-induced lesions. The maximum shear and tensile stress in the underlying bone were 15.6 ± 2.9 MPa and 7.7 ± 1.9 MPa, respectively, and also located under the lateral facet of the patella near the area of surface lesions.

DISCUSSION

The objective of the current study was to partially validate our working hypothesis that alterations in retropatellar cartilage and underlying bone are initiated independently by acute overstresses developed during blunt impact to the patello-femoral joint in this animal model. Furthermore, that the documented softening of retropatellar cartilage and thickening of the underlying subchondral bone occur independently post-trauma. In support of our hypothesis, there was a significant softening of traumatized

cartilage compared to controls at 4.5 and 12 months post-trauma, and with no thickening of subchondral bone at any timepoint in this study.

The shear moduli and subchondral bone thicknesses of the control population used in this study were statistically similar to previous control animals using this model (Newberry et al., 1998a). The degree of chronic softening in the retropatellar cartilage post-trauma was similar to other studies using this animal model. Newberry et al. (1998a) document 40 % and 30 % decreases in G_U for traumatized cartilage compared to controls at 6 and 12 months post-trauma, respectively. This was consistent with 41 % and 26 % decreases observed at 4.5 and 12 months post-trauma in the current study. Furthermore, Newberry et al. (1998a) document 19 % and 28 % decreases in G_R for impacted cartilage compared to unimpacted contralateral patellae at 6 and 12 months post-trauma. The current study documented 20 % and 32 % decreases in G_R at 4.5 and 12 months, respectively. In contrast to the current study, Newberry et al. (1998a) document a thickening of the subchondral bone at one month post-trauma compared to the unimpacted contralateral patella, and a significant thickening at 12 months compared to unimpacted controls. No such thickening was observed with padded impact interfaces in the current study.

The chronic observations of the current study could be explained by the acute stresses generated in these joint tissues during blunt impact. The acute stresses generated in the retropatellar cartilage of the current study were consistent with high severity impacts which have previously resulted in chronic softening of traumatized cartilage (Figure 2) (Newberry et al., 1998b). On the other hand, there was a 35 % and 52 % decrease, respectively in maximum shear and tensile stress in the subchondral bone

compared to the previous high severity impacts using a rigid impact interface, which produced chronic subchondral bone thickening (Newberry et al., 1998b). Previous studies have suggested that surface lesions on the retropatellar cartilage occur for impacts that generate a shear stress of 5.5 MPa (Atkinson et al., 1998). This compared well with the current study that documented surface lesions for an average maximum surface shear stress of 6.1 MPa in computational models using padded impact interfaces.

Our trauma model suggests that damage and subsequent alteration of joint tissues may be due to acute impact induced stresses that are generated during a single overloading of the joint. Therefore, cartilage softening and underlying bone thickening may occur independently, which would be in contrast to the currently accepted hypothesis due to Radin et al. (1990). In contrary to the current study, Radin et al. (1978) used low level repetitive overloadings that may have resulted in fatigue damage to the bone with a secondary effect of cartilage degeneration. The differences between a single overloading and repetitive overloadings may result in different pathways of joint degeneration. Additional studies will be needed to support this suggestion.

There were some limitations in the computational model used for the current study. It was assumed that the patella was a 2-D object, and that the retropatellar cartilage was isotropic, homogeneous and linearly elastic. This allowed direct comparisons to be made to previous published studies. In addition because of the large medial to lateral variation of contact pressure versus the proximal to distal variation, a plane strain analysis would likely be appropriate. It has also been suggested that the instantaneous response of biphasic cartilage is equivalent to that of an incompressible elastic material (Armstrong et al., 1984; Ateshian et al., 1994). It has been shown that the shear stress in a

cartilage layer under impact loading are the same for an incompressible elastic and biphasic material at time zero (Garcia et al., 1998). However since tensile stresses in the solid phase of articular cartilage might be responsible for acute damage to the matrix, there is the need for future biphasic analyses in order to decompose the stresses in the impacted tissue.

In conclusion, the current study helped to validate our current working hypothesis on the chronic alterations which have been documented in the patello-femoral joint of our model following blunt trauma. In addition this study, along with a previous study (Newberry et al., 1998b), suggests that load alone is not a good predictor of chronic injury to a diarthrodial joint. This is in contrast to a federally regulated lower extremity injury criterion that states that axial loads in the patella-femur complex can not exceed 10 kN for certification of new automobiles using anthropomorphic dummies. Atkinson et al. (1997), using isolated human cadavers, prevented microcracks in bone underlying retropatellar cartilage when using a particular padded impact interface. That study, however, did not address damage to articular cartilage. Assuming damage to articular cartilage can be correlated with diseases such as post-traumatic osteoarthritis, there may be a need to incorporate a method to better predict damage to joint cartilage in the certification of new automobiles. The current investigation suggests that simply the addition of padding to impact interfaces may not be adequate, and that optimized interfaces may be required.

ACKNOWLEDGEMENTS

This study was supported by a grant for the Centers for Disease Control and Prevention (R49/CCR503607). Its contents are solely the responsibility of the authors and

do not necessarily represent the official views of the Centers for Disease Control and Prevention. The authors wish to gratefully acknowledge Jane Walsh for her preparation of the histological sections, Jean Atkinson for her care of the animals and Cliff Beckett for technical assistance in the experimental phase of these studies.

REFERENCES

1. Armstrong, C.G., Lai, W.M., Mow, V.C., (1984) An analysis of the unconfined compression of articular cartilage. *Journal of Biomechanical Engineering* 106, 165-173.

2. Ateshian, G.A., Lai, W.M., Zhu, W.B., Mow, V.C., (1994) An asymptotic solution for the contact of two biphasic carilage layers. *Journal of Biomechanics* 27, 1347-1360.

3. Atkinson, P.J., Garcia, J.J., Altiero, N.J., Haut, R.C., (1997) The influence of impact interface on human knee injury: Implications for instrument panel design and the lower extremity injury criterion. *Society of Automobile Engineers*, Paper No. 973327.

4. Atkinson, T.S., Haut, R.C., Altiero, N.J., (1998) Impact induced fissuring of articular cartilage: An investigation of failure criteria. *Journal of Biomechanical Engineering* 120, 181-187.

5. Burr, D.B., (1998) Subchondral bone. In: Brandt, K.D., Doherty, M., Lohmander, L.S. (Eds.), Osteoarthritis. Oxford University Press Inc., New York, pp. 144-156.

6. Dedrick, D.K., Goldstein, S.A., Brandt, K.D., O'Conner, B.L., Goulet, R.W., Albrecht, M., (1993) A longitudinal study of subchondral plate and trabecular bone in cruciate-deficient dogs with osteoarthritis followed up for 54 months. *Arthritis and Rheumatism* 36, 1460-1467.

7. Ewers, B.J., Newberry, W.N., Garcia, J.J., Haut, R.C., (1998) Alterations in the mechanical properties of bone underlying articular cartilage in a traumatized joint. *Transactions of the 44th Annual Meeting of Orthopaedic Research Society*, New Orleans, LA.

8. Garcia, J.J., Altiero, N.J., Haut, R.C., (1998) An approach for the stress analysis of transversely isotropic biphasic cartilage under impact load. *Journal of Biomechanical Engineering* 120, 608-613.

9. Glantz, S.A., (1996) A better approach to multiple comparison testing. In: Wonsiewicz, M., McCurdy, P. (Eds.), Primer of Biostatistics. McGraw-Hill, New York, pp. 92-97.

10. Haut, R.C., Ide, T.M., Decamp, C.E., (1995) Mechanical responses of the rabbit patello-femoral joint to blunt impact. *Journal of Biomechanical Engineering* 117, 402-408.

11. Hayes, W.C., Keer, L.M., Herrmann, G., Mockros, L.F., (1972) A mathematical analysis for indentation tests of articular cartilage. *Journal of Biomechanics* 5, 541-551.

12. Li, X., Haut, R.C., Altiero, N.J., (1995) An analytical model to study blunt impact response of the rabbit P-F joint. *Journal of Biomechanical Engineering* 117, 485-491.

13. Newberry, W.N., Zukosky, D.K., Haut, R.C., (1997) Subfracture insult to a knee joint causes alterations in the bone and in the functional stiffness of overlying cartilage. *Journal of Orthopaedic Research* 15, 450-455.

14. Newberry, W.N., MacKenzie, C.D., Haut, R.C., (1998a) Blunt impact causes changes in bone and in cartilage in a regularly exercised animal model. *Journal of Orthopaedic Research* 16, 348-354.

15. Newberry, W.N., Garcia, J.J., Mackenzie, C.D., Decamp, C.E., Haut, R.C., (1998b) Analysis of acute mechanical insult in an animal model of post-traumatic osteoarthritis. *Journal of Biomechanical Engineering* 120, 704-709.

16. Oyen-Tiesma, M., Atkinson, J., Haut, R.C., (1998) A method for promoting regular rabbit exercise in orthopaedics research. *Contemporary Topics in Laboratory Animal Science* 37, 77- 80.

17. Radin, E.L., Ehrlich, M.G., Chernack, R., Abernethy, P., Paul, I.L., Rose, R.M., (1978) Effect of repetitive impulsive loading on the knee joints of rabbits. *Clinical Orthopaedics* 131, 288-293.

18. Radin, E.L., Burr, D.B., Fyhrie, D., Brown, T.D., Boyd, R.D., (1990) Characteristics of joint loading as it applies to osteoarthrosis. In: Mow, V.C., Ratcliffe, A., Woo, S.L-Y. (Eds.), Biomechanics of Diarthrodial Joints. Springer-Verlag, New York, pp. 437-451.

TABLES

Table 1: Measured instantaneous (G_U) and relaxed (G_R) moduli of retropatellar cartilage (MPa) from animals subjected to a single blunt impact with a padded interface and in the unimpacted, control animals (mean ± SD) (n = 8).

Time point	Side	G_U (MPa)	G_R (MPa)
	Control	1.00 ± 0.25	0.29 ± 0.06
Time-zero	Impacted	1.11 ± 0.46	0.29 ± 0.08
	Unimpacted	1.03 ± 0.48	0.27 ± 0.09
4.5 months	Impacted	0.59 ± 0.10 [a,b]	0.23 ± 0.03 [a,b]
	Unimpacted	0.88 ± 0.21	0.29 ± 0.09
12 months	Impacted	0.74 ± 0.24 [a,b]	0.23 ± 0.05 [a,b]
	Unimpacted	1.08 ± 0.29	0.34 ± 0.03

[a] Significantly different than unimpacted side by a paired students' t-test.
[b] Significantly different than controls by an analysis of variance.

Table 2: Measured subchondral bone thickness (mm) in animals subjected to a single impact with padded interface and in the unimpacted control animals (mean ± SD) (n=8). Subchondral bone thickness is greater in the center compared to the lateral or medial locations.

Time point	Side	Location		
		Medial	Central	Lateral
	Control	0.39 ± 0.04	0.59 ± 0.03	0.33 ± 0.05
Time-zero	Impacted	0.36 ± 0.09	0.55 ± 0.10	0.34 ± 0.07
	Unimpacted	0.39 ± 0.11	0.56 ± 0.22	0.35 ± 0.09
4.5 months	Impacted	0.33 ± 0.01	0.56 ± 0.07	0.39 ± 0.01
	Unimpacted	0.32 ± 0.03	0.55 ± 0.09	0.39 ± 0.01
12 months	Impacted	0.45 ± 0.09	0.67 ± 0.15	0.49 ± 0.10
	Unimpacted	0.45 ± 0.08	0.64 ± 0.16	0.52 ± 0.16

FIGURES

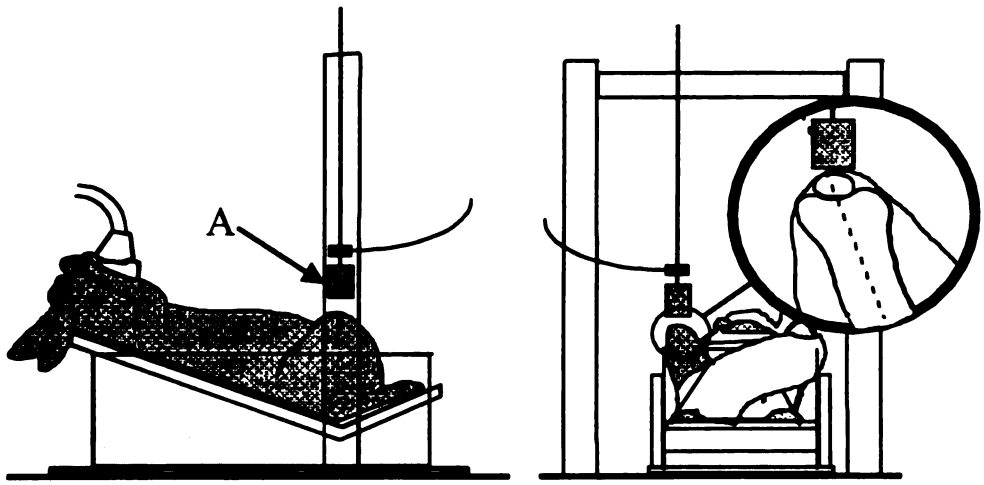

Figure 1: Impact experiments were performed by dropping a mass with a padded impact interface (A) (3.76 MPa crush strength – Hexcel) onto the patellofemoral joint with 6.6 J of energy.

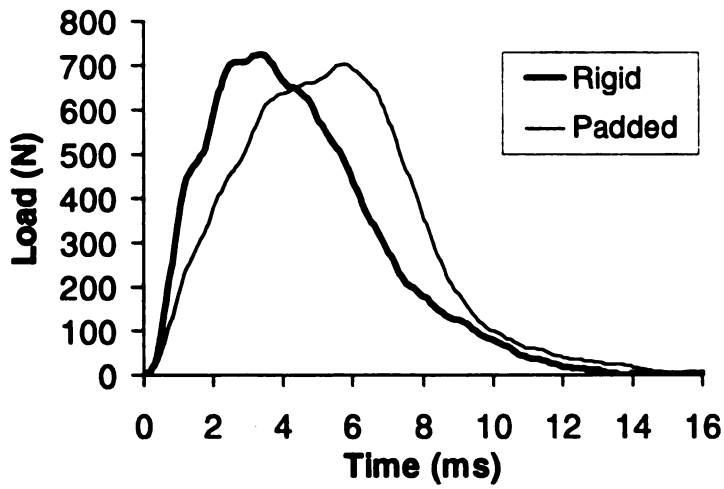

Figure 2: Representative force time plots for experiments with a rigid and padded impact interface. Notice the slightly longer time to peak with the padded interface but a similar contact duration. This representative rigid impact data is taken from a previous study (Newberry et al., 1998b).

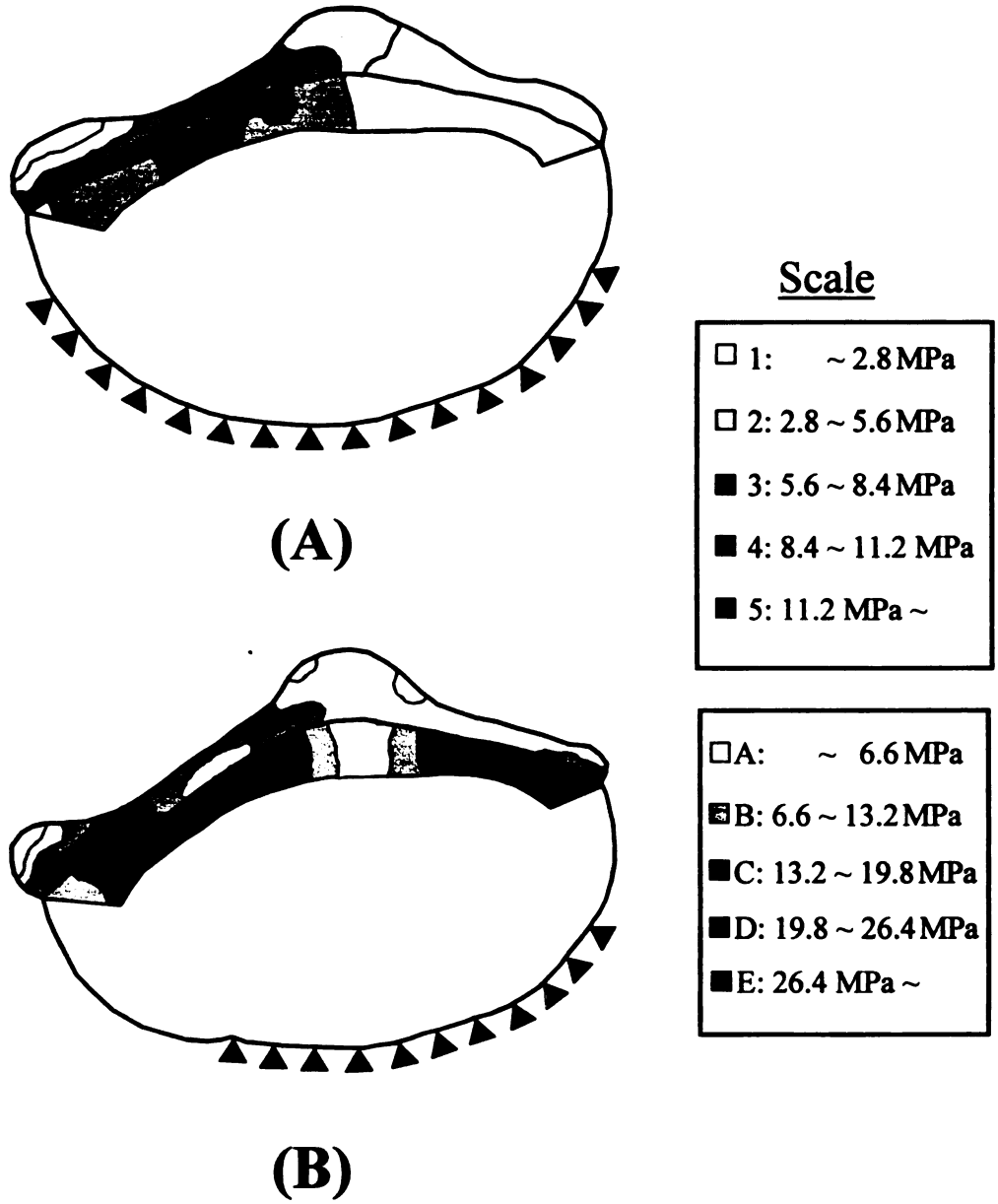

Figure 3: A representative shear stress distribution for padded (A) and rigid (B) impact interfaces. The cartilage is on the top with the subchondral plate underneath. Pressures were applied to the retropatellar surface and the anterior surface of the patella was fixed in the area of contact (▲). Notice that the shear stresses in the cartilage were similar for the two impact interfaces, but that there was a significant reduction in shear stresses in subchondral bone underlying the retropatellar cartilage for the padded interface experiment. The representative shear stress distribution for the rigid impact interface is based upon a previous study (Newberry et al., 1998b).

CHAPTER 4

IMPACT SHEAR STRESSES IN AN ANIMAL JOINT PREDICTS CHRONIC SOFTENING OF CARTILAGE BUT NOT THICKENING OF UNDERLYING BONE

Benjamin J. Ewers, Brian T. Weaver, William N. Newberry, and Roger C. Haut

ABSTRACT

Our laboratory has recently developed a joint trauma model, using rabbits, which exhibits chronic softening of retropatellar cartilage and thickening of underlying subchondral bone. We hypothesize that these alterations are initiated by acute shear stresses generated in each tissue during impact loading. With the use of a Finite Element Method (FEM), an earlier analytical study suggests shear stresses in the cartilage can be significantly reduced by reorientation of the impact load more centrally on the joint. The current study suggested that these types of impacts indicated reduced shear stresses and tensile strains in retropatellar cartilage with enhanced shear stresses in the underlying bone. In contrast to earlier studies we documented no degradation of retropatellar cartilage or remodeling of the underlying bone. The study supports our contention that degradation of cartilage may be related to the intensity of generated shear stress, but contradicts the role of shear stress alone in the remodeling of underlying bone.

INTRODUCTION

We have recently developed a trauma model to study degradation of the rabbit patellofemoral joint following a single, high severity blunt impact on the medial aspect of the anterior patella. In various studies we have documented acute superficial lesions on the retropatellar cartilage and chronic changes in cartilage, as well as the underlying subchondral bone, out to one year post-insult (Newberry et al., 1997; Newberry et al., 1998a). We document a significant decrease in stiffness of retropatellar cartilage beginning at three months post-insult with a significant increase in the thickness of underlying subchondral bone at 12 months (Newberry et al., 1998a). In a recent study with this joint trauma model we lowered the severity of the medial-oriented blunt impact and did not document any significant changes in these tissues post-insult (Newberry et al., 1998b). We hypothesize that changes in cartilage and underlying bone are correlated with the intensity of the blunt insult and the corresponding state of acute stress generated in these tissues.

In contrast to the above, Radin et al. (1990) have hypothesized that repetitive loading to a diarthrodial joint may first result in damage to bone underlying cartilage, followed by a stiffening of the bone with a subsequent increase in the state of stress in the overlying cartilage resulting in its degradation over time. Recently, however, Ewers et al. (1998) using a simplified mathematical model of the rabbit patellofemoral joint, suggest that significant alterations in the mechanical properties of bone underlying cartilage in our joint trauma model would probably not influence the state of stress in the overlying cartilage. Nor would a softening of the overlying cartilage, as a result of a severe blunt trauma, alter the state of stress in the underlying bone and initiate its remodeling. That

study has been used to establish the basis for our current working hypothesis that alterations in retropatellar cartilage and underlying bone in our joint trauma model are initiated independently by acute overstresses developed in each tissue during blunt insult to the joint, and that the processes of chronic degradation in each tissue are not related in a mechanical sense (Newberry et al., 1998b; Li et al., 1995). In a recent study supporting this hypothesis, we used a padded impact interface. This allowed us to lower the stresses in the subchondral bone, while keeping the same high level of stresses in the cartilage. Interestingly, at one-year post-insult we still documented a softening of retropatellar cartilage without a thickening of the underlying subchondral bone (Ewers et al., 2000).

The current study was conducted in an attempt to further validate our working hypothesis by impacting the rabbit's patellofemoral joint in such a way that acute overstresses in retropatellar cartilage would be minimized, while the stresses developed in the underlying subchondral bone would be sufficient enough to initiate its chronic thickening. The idea was based on an earlier study by Li et al. (1995), using a mathematical model of the rabbit patellofemoral joint. That study suggests that a single central-oriented impact would result in reduced tensile strains in the retropatellar cartilage, which might mitigate its acute damage. It also suggests that the shear stresses in the underlying subchondral bone would be greater than that for a single medial-oriented impact, so as to cause its chronic thickening. Our question was whether the overlying cartilage would degrade within one year post-impact.

METHODS

A total of twenty-nine mature Flemish Giant rabbits (4.8 ± 0.6 kg, 6-8 months of age) was used in this investigation. The study was approved by the Michigan State

University All-University Committee on Animal Use and Care. Twenty-four animals were randomly selected for the chronic aspect of the study (chronic animals). Eight animals received a single blunt impact to the right patellofemoral joint with a medial-oriented impact, while eight animals received a blunt impact to the patellofemoral joint that was central-oriented. An additional eight animals were not impacted, and served as controls. The chronic animals were all sacrificed at 12 months post-impact. Five additional animals (acute animals) were sacrificed prior to impact for the determination of boundary conditions in computational models.

The medial-oriented blunt impact protocol has been described in earlier studies (Newberry et al., 1998a; Haut et al., 1995). Briefly, the animals to be subjected to a blunt trauma were maintained under anesthesia (2% Isoflurane) with the right hind limb flexed approximately 120° (Figure 1A) with the animal supine. The medial-oriented impact required the femur to be positioned so that the impact load was aligned along the medial side of the anterior patella and directed towards the lateral patellar facet (Figure 1B), whereas the central-oriented impact was aligned along the medial-lateral center of the patellofemoral joint (Figure 1C). These orientations were verified in pilot studies using radiographic analyses. Impact was administered by dropping a rigid 1.33 kg mass onto the patellofemoral joint from a height of 0.46 m (6.0 J) [2]. The impact mass was arrested electronically to prevent multiple blows to the flexed limb. A load transducer (model 31/1432, 500 lb. capacity, Sensotec, Columbus, OH) was attached behind a one-inch diameter, flat aluminum interface to measure impact loads. The load-time history of the impact was recorded at 10 kHz. The peak contact load, time to peak, and total contact duration were documented for each experiment. The animals were given two weeks of

pre-impact exercise consisting of ten minutes of daily exercise on a treadmill running at 0.3 mph (Oyen-Tiesma et al., 1998). Blunt impact loading was followed by a five-day period of rest, and then the daily exercise program was resumed for the duration of the study. When not exercising, the animals were housed individually in cages (48"x24"x19").

Immediately after sacrifice, patellae from impacted and unimpacted limbs were excised. The patellae were then placed in a bath of room temperature phosphate buffered saline (pH 7.2) for mechanical tests in a servo-controlled hydraulic material testing machine (model 1331, retrofitted 8500+ electronics, Instron, Canton, MA). Structural integrity of the retropatellar cartilage was determined using indentation stress relaxation tests at two sites on the lateral facet near the central ridge (Newberry et al., 1998a). The stiffnesses of retropatellar cartilage from impacted, non-impacted, and control joints were compared by a calculation of the shear modulus from an elastic layer (Hayes et al., 1972), based on the load at 80 ms (instantaneous shear modulus - G_U) and at 150 s (relaxed shear modulus - G_R). The retropatellar cartilage was wiped with India ink to highlight surface lesions and then photographed.

Patellae were placed in 10% buffered formalin for seven days, and decalcified in 20% formic acid for another seven days. Only four of the central-oriented impacted patellae were randomly selected and histologically processed. Tissue blocks were cut transversely across the patella in the area of highest patellofemoral contact pressure, based on the acute experiments described below. The blocks were then embedded with paraffin according to an established protocol (Newberry et al., 1998a). Six sections, eight microns thick, were stained with Safranin O-Fast Green and examined in light

microscopy at 12-400 power. The thickness of the subchondral bone plate was measured at 25x with a calibrated eye-piece at the center of each facet and near the mid-line of the patella by a single investigator (BE), using an established protocol (Newberry et al., 1998a).

To estimate the impact-induced state of stress in the patella, a two-dimensional non-contact finite element model of the patella was developed consisting of 1537 3-noded plane strain elements (Figure 2A) (Ansys 5.5, SAS IP Inc., PA, USA). A representative model of the patellae was taken from a 0.5 mm transverse slab cut of a patellae. Briefly, the cross section of the patella was photographed and then used to form a digital image of the geometry by tracing the boundary of the cartilage and subchondral and trabecular bone. The layer of cartilage was assumed isotropic with an elastic modulus and Poisson's ratio of 20 MPa and 0.49, respectively (Newberry et al., 1998b; Atkinson et al., 1998). The instantaneous (impact) response of biphasic cartilage is equivalent to that of an incompressible elastic material (Armstron et al., 1984; Ateshian et al., 1994). Large deformations were allowed in the analysis. The bone had a Poisson's ratio of 0.3 and an elastic modulus of 3750 MPa and 300 MPa for the subchondral (Mente and Lewis, 1994) and trabecular bone (Townsend et al., 1975), respectively.

The determination of boundary conditions on the patella for the computational model has previously been described (Newberry et al., 1998b). Briefly, five acute animals were sacrificed in order to document the posterior and anterior pressure distributions on the patella during the impact experiments. Both a medial and central-oriented impact was conducted on each animal. Prior to impact, medial and lateral incisions were made in the joint capsule to insert pressure sensitive film (Prescale, single sheet, medium range, Fuji

Film, Ltd., Tokyo, Japan) into the patellofemoral joint. The film was encased in a packet of sterile polyethylene to protect it from joint fluids (Haut et al., 1995). In order to locate the pressure distribution on the patella, two holes were drilled through the center of the patella, anterior to posterior, at two locations away from the area of contact (one proximal, one distal) (Newberry et al., 1998b). Prior to impact, small needles were placed into these holes. The needles were cut so they extended approximately 1 mm beyond the anterior and posterior surfaces. The film was placed in the joint and wrapped around the anterior surface of the patella. The joint was impacted. The needles produced marks (holes) that were easily visible on the film. The pressure film was dynamically calibrated in a servohydraulic testing machine (Haut et al., 1995). The film was scanned at 150 dpi (~59 pixels per mm) using a video scanner (Microtek, model MRS-1200E6). The stained imprints were converted to pressure and post-processed with PC-based image analysis software (Image 1.6, NIH). The distributions of contact pressure and contact area were documented from the patellofemoral pressure imprints for each acute animal experiment. The anterior area of contact was located on the patella, and this area was fixed in space in the computational model to prevent rigid body motion. Patellofemoral pressure profiles were discretized in the area of the largest contact pressures, and located on a single representative patellar cross sectional geometry for each experiment (Figure 2A). A pilot study conducted with multiple impacts documented that there was less than an 8 % difference in contact area and average contact pressure, respectively.

The maximum shear stress and tensile strain were calculated along the retropatellar articular cartilage surface on the lateral facet where lesions are historically generated with this model (Figure 2B). Maximum shear stresses, principal stresses and

mean stresses were determined in the underlying subchondral bone in the center region of the patella where chronic thickening is typically observed (Figure 2C).

An analysis of variance with Bonferroni *post-hoc* tests were used to evaluate differences in the mechanical properties of retropatellar cartilage and the subchondral bone thickness differences between controls and unimpacted joints and between controls and impacted joints. Paired *t*-tests were used for comparisons of mechanical data from cartilage and subchondral thickness data between impacted and unimpacted sides of each animal. Experimental data in this manuscript has been reported as mean ± one standard deviation, and statistical significance was indicated for $p<0.05$.

RESULTS

Peak load, rise time, and duration of impact were similar for the acute and chronic medial-oriented impacts and for the acute and chronic central-oriented impacts (Table 1). The magnitude of the patellofemoral contact pressures varied across the area of contact, typically with the most intense pressure located in the middle of the lateral and medial facets (Figure 3A & 3B). Quantitative analysis of the pressure film from the acute impacts indicated that there was no significant difference in mean or peak pressures between the central-oriented and the medial-oriented impact groups (Table 1). The patellofemoral contact area slightly increased in the central-oriented versus medial-oriented acute groups, but again the result was not statistically different.

No surface lesions were documented on the retropatellar cartilage for the chronic central-oriented impacted animals. On the other hand, there were surface lesions on the retropatellar cartilage in all of the chronic medial-oriented impacted patellae. These lesions were typically on the lateral facet near the central ridge. Indentation tests on

retropatellar cartilage of the chronic animals showed no statistical differences in G_U or G_R between controls and the unimpacted limbs from the medial- or central-oriented groups (Table 2). There was a significant increase in G_R from the unimpacted limb in the central-oriented group compared to the unimpacted limb of the medial-oriented group. There was no significant difference in the central-oriented group in either G_U or G_R between the impacted and the contralateral unimpacted patellae. Conversely, there was a significant decrease in G_U and G_R on the impacted compared to the contralateral unimpacted patellae in the medial-oriented group. There was also a significant decrease in both G_U and G_R from the impacted limb of the medial-oriented group compared to the impacted limb of the central-oriented and the unimpacted control groups.

The computational models revealed that the maximum tensile strain on the surface retropatellar cartilage was significantly reduced from 0.44 ± 0.06 to 0.34 ± 0.01 in medial-oriented versus central-oriented acute impacts. The maximum shear stress on the surface of the retropatellar cartilage was also significantly decreased from 6.50 ± 0.94 MPa to 5.19 ± 0.20 MPa for the medial-oriented and central-oriented impacts, respectively. The contour plots of the maximum shear stress in the cartilage illustrate how these stresses increase along the lateral facet for the high severity medial-oriented impact group and are more constant and lower for the central-oriented impact group (Figure 4).

Quantitative analysis post-impact revealed that there was no statistical difference in the subchondral bone thickness between the unimpacted limbs in the medial- and central-oriented groups and controls at any location (Table 3). There was no significant difference in subchondral bone thickness at any location in the central-oriented group between the impacted and the contralateral unimpacted patellae. In contrast, at the medial

and central locations there was a significant increase in subchondral bone thickness in the impacted versus contralateral unimpacted limb in the medial-oriented group. There was also a significant increase in subchondral bone thickness at the central location for the impacted patellae in the medial-oriented group compared to controls.

As expected the computational models predicted a slight increase in average maximum shear stresses in the central region of the subchondral bone for the central-oriented versus medial-oriented impacts (Table 4). In the central region of the subchondral bone there was a significant increase in the average normal stresses for the central-oriented compared to the medial-oriented impacts (Figure 4).

DISCUSSION

The objective of this study was to validate our current working hypothesis that alterations in retropatellar cartilage and underlying bone are initiated independently by acute overstresses that are developed during a blunt impact to the patellofemoral joint in our animal model. Based on a previous study by Li et al. (1995), we hypothesized that a central-oriented patellar impact on our animal model would result in lower tensile strains and stresses in the retropatellar cartilage compared to a medial-oriented impact, thus mitigating the typically observed surface fissures and chronic softening of this tissue (Newberry et al., 1998a). On the other hand, the central-oriented impact would result in a higher state of shear stress in the underlying subchondral bone, compared to a medial-oriented impact, to cause a remodeling and subsequent thickening of this tissue post-trauma.

By impacting the joint centrally our computational model did indicate a reduction in tensile strains and maximum shear stresses in the retropatellar cartilage compared to a

medial-oriented impact. Subsequently, we did not observe any surface fissures or chronic softening of the cartilage in the chronic central-oriented impacted animals, whereas there was surface fissuring and chronic softening of retropatellar cartilage following a medial-oriented impact. The computational models indicated an increase in maximum shear stresses in the subchondral bone for the central-oriented versus medial-oriented impacts. However, while there was significant thickening of the subchondral bone in the chronic medial-oriented impacted animals, there was no thickening of the subchondral bone for the chronic central-oriented impacts.

One possible explanation for this result is that even though the shear stresses were similar for the medial and central-oriented impact configurations, the central-oriented impacts produced significantly greater mean compressive stresses compared to the medial-oriented impacts. Microdamage may form a basis for remodeling of bone (Burr et al., 1984; Mori and Burr, 1984). Impact induced microcracks may coalesce and be the precursors of gross fractures in bone (Atkinson et al., 1997; Vashishth et al., 1996). Therefore, since bone behaves similar to a brittle engineering material, a fracture criterion based on a Coulomb-Mohr model has been proposed by others (Keyak and Rossi, 2000; Plank et al., 1998; Shigley, 1977). In this model high mean stresses can effectively help protect brittle materials from shear induced damage. Interestingly, we documented a significant increase in the average mean stresses in the subchondral bone for the central-oriented impact group compared to the medial-oriented group (Table 4). Therefore, this might be indicative of a Coulomb-Mohr scenario. The combination of the shear and mean stresses in the medial-oriented impact group may have exceeded any threshold that

might exist for bone damage. This combination in the central-oriented group possibly lies below this threshold.

The current study suggested that since the chronic central-oriented experiments did not result in surface lesions or degradation of G_U and G_R post-impact, the impact-induced shear stresses were "safe". The computational model indicated an average maximum shear stress of 5.2 ± 0.2 MPa. This is in support of a previous study that proposed a shear stress of 5.45 MPa is required for impact induced fissuring of articular cartilage on the rabbit tibial plateau (Atkinson et al., 1998).

The chronic changes documented in the retropatellar cartilage and underlying subchondral bone in the medial-oriented impacts in the current study are similar to previous studies with this animal model. Newberry et al. (1998a) at 12 months post-impact documented a significant 43 and 28 % decrease in G_U and G_R, respectively, for the traumatized cartilage compared to the contralateral unimpacted limb. This is similar to the 38 and 27 % reduction in G_U and G_R, respectively, for the impacted versus the contralateral unimpacted cartilage in the current study. Newberry et al. (1998a) documented at 12 months post-impact a significant 72 % increase in subchondral bone thickness at the central location of the patellae for the traumatized limb compared to the contralateral unimpacted limb. This is also similar to the current study that documented a 74 % increase in subchondral bone thickness at the central location of the traumatized patellae compared to the contralateral unimpacted limb.

There were a number of limitations in our current computational model. We assumed the patella was a 2-D object, and that retropatellar cartilage was isotropic, homogeneous and linearly elastic. The model was selected so that the computational

aspects of the current study could be correlated with earlier studies by our laboratory (Newberry et al., 1998b; Li et al, 1995; Ewers et al., 2000). Because of large medial to lateral variation of contact pressure versus the proximal to distal variation, a plane strain analysis can be justified. Since the instantaneous response of biphasic cartilage has been shown equivalent to that of an incompressible elastic material, an elastic model was deemed appropriate for this study (Armstrong et al., 1984; Ateshian et al., 1994). On the other hand, earlier studies have suggested that articular cartilage in uniaxial compression under rapid loads responds linearly to only approximately 30% strain (Garcia et al., 2000). The effects of a nonlinear stress-strain response on the distribution of stress in our impact joint model are currently under investigation (Garcia et al., 2000). Another limitation is that an elastic model does not allow for the decomposition of stress into its fluid and solid phases. The analysis of solid stresses might provide vital information for fissuring and subsequent degradation of the cartilage.

In conclusion, this study suggested that shear stress alone might be a good predictor of cartilage damage; however, this is not the case for the subchondral bone. A slight relationship may exist between high shear stresses and mean stresses, which might be indicative of a Coulomb-Mohr scenario. If, as suggested by others, microdamage is the basis for such a response, then the proposed model may be useful as a conservative indicator of gross bone fracture. Gross fracture, based on total load applied to the joint, is currently used for the federally regulated lower extremity injury criterion in the automobile setting (Atkinson et al., 1997). The current study would suggest that the state of bone stress, and the probability for fracture, might also depend on the orientation of

the impacting load on the knee. This issue needs future study using a human knee joint model.

ACKNOWLEDGMENTS

This study was supported by a grant from the Centers for Disease Control and Prevention (R49/CCR503607). Its contents are solely the responsibility of the authors and do not necessarily represent the official views of the Centers for Disease Control and Prevention. The authors wish to gratefully acknowledge Jane Walsh for preparation of the histological slides, Jean Atkinson for care of the animals, and Charles DeCamp, D.V.M. for veterinary consultation.

REFERENCES

1. Armstrong, C. G., Lai, W. M. and Mow, V. C., (1984) An Analysis of the Unconfined Compression of Articular Cartilage. *Journal of Biomecanical Engineering* 106, pp. 165-173.

2. Ateshian, G. A., Lai, W. M., Zhu, W. B. and Mow, V. C., (1994) An Asymptotic Solution for the Contact of Two Biphasic Cartilage Layers. *Journal of Biomechanics* 27, pp. 1347-1360.

3. Atkinson, T. S., Haut, R. C., and Altiero, N. J., (1998) Impact Induced Fissuring of Articular Cartilage: An Investigation of Failure Criteria. *Journal of Biomechanical Engineering* 120, pp. 181-187.

4. Atkinson, P. J., Garcia, J. J., Altiero, N. J., and Haut, R. C., (1997) The Influence of Impact Interface on Human Knee Injury: Implications for Instrument Panel Design and the Lower Extremity Injury Criterion. *Proceedings, 41st Stapp Car Crash Conference* pp. 167-180.

5. Burr, D. B., Martin, B. R., Schaffler, M. B., and Radin, E. L., (1984) Bone Remodeling in Response to In Vivo Fatigue Microdamage. *Journal of Biomechanics* 18, pp. 189-200.

6. Ewers, B.J., Newberry, W.N., Garcia, J.J., and Haut, R.C., (1998) Alterations in the Mechanical Properties of Bone Underlying Articular Cartilage in a Traumatized Joint. *Proceedings, 44th Annual Meeting Orthopaedic Research Society* pp. 459.

7. Ewers, B. J., Newberry, W. N., and Haut, R. C., (2000) Chronic Softening of Cartilage Without Thickening of Underlying Bone in a Joint Trauma Model. *Journal of Biomechanics*, In Print.

8. Garcia, J. J., Altiero, N. J., and Haut, R. C., (2000) Estimation of in Situ Elastic Properties of Biphasic Cartilage Based on a Transversely Isotropic Hypo-Elastic Model. *Journal of Biomechanical Engineering* 122, pp. 1-8.

9. Haut R. C., Ide T. M., Decamp C. E., (1995) Mechanical Responses of the Rabbit Patello-Femoral Joint to Blunt Impact. *Journal of Biomechanical Engineering* 117, pp. 402-408.

10. Hayes, W. C., Keer, I. M., Herrmann, and Mockros, I. E., (1972) A Mathematical Analysis for Indentation Tests of Articular Cartilage. *Journal of Biomechanics* 5, pp. 541-551.

11. Keaveny, T. M., Wachtel, E. F., Ford, C. M., and Hayes, W. C., (1994) Differences Between the Tensile and Compressive Strengths of Bovine Tibial Trabecular Bone Depend on Modulus. *Journal of Biomechanics* 27, pp. 1137-1146.

12. Keyak, J. H., and Rossi, S. A., (2000) Prediction of Femoral Fracture Load Using Finite Element Models: An Examination of Stress- and Strain-Based Failure Theories. *Journal of Biomechanics* 33, pp. 209-214.

13. Li, X., Haut, R. C., and Altiero, N. J., (1995) An Analytical Model to Study Blunt Impact Response of the Rabbit P-F Joint. *Journal of Biomechanical Engineering* 117, pp. 485-491.

14. Mente, P. L., and Lewis, J. L., (1994) Elastic Modulus of Calcified Cartilage is an Order of Magnitude Less than that of Subchondral Bone. *Journal of Orthopaedic Research* 12, pp. 637-647.

15. Mori, S., and Burr, D. B., (1993) Increased Intracortical Remodeling Following Fatigue Damage. *Bone* 14, pp. 103-109.

16. Newberry, W. N., Zukosky, D. K., and Haut, R. C., (1997) Subfracture Insult to a Knee Joint Causes Alterations in the Bone and in the Functional Stiffness of Overlying Cartilage. *Journal of Orthopaedic Research* 15, pp. 450-455.

17. Newberry, W. N., Mackenzie, C. D., and Haut, R. C., (1998a) Blunt Impact Causes Changes in Bone and Cartilage in a Regularly Exercised Animal Model. *Journal of Orthopaedic Research* 16, pp. 348-354.

18. Newberry, W. N., Garcia J. J., Mackenzie, C. D., Decamp, C., and Haut, R. C., (1998b) Analyses of Acute Mechanical Insult in an Animal Model of Post-Traumatic Osteoarthrosis. *Journal of Biomechanical Engineering* 120, pp. 704-709.

19. Oyen-Tiesma, M., Atkinson, J., and Haut, R.C., (1998) A Method for Promoting Regular Rabbit Exercise in Orthopaedics Research. *Contemporary Topics in Laboratory Animal Science* 37, pp.77-80.

20. Plank, G. R., Kleinberger, M., and Eppinger, R. H., (1998) Analytical Investigation of Driver Thoracic Response to Out of Position Airbag Deployment. *Proceedings, 42nd Stapp Car Crash Conference* PA, pp. 317-329.

21. Radin, E. L., Burr, D. B., Fyhrie, D., Brown, T. D., and Boyd, R. D., (1990) "Characteristics of Joint Loading as it Applies to Osteoarthrosis. *Biomechanics of Diarthrodial Joints,* Springer-Verlag, New York, pp. 437-451.

22. Shigley, J. E., (1977) *Mechanical Engineering Design, 3rd Edition*, McGraw-Hill, New York, pp. 173-175.

23. Townsend, P. R., Raux, P., Rose, R. M., Miegel, R. E., and Radin, E. L., (1975) The Distribution and Anisotropy of the Stiffness of Cancellous Bone in the Human Patella. *Journal of Biomechanics* 8, pp. 363-367.

24. Vashishth, D., Behiri, J. C., and Bonfield, W., (1996) Crack Growth Resistance in Cortical Bone: Concept of Microcrack Toughening. *Journal of Biomechanics* 30, pp. 763-769.

TABLES

Table 1: Impact characteristics for chronic and acute central-, and acute medial-oriented impacts (mean ± SD). The peak pressure, mean pressure and contact area are from the patellofemoral contact pressure distributions.

	Group	Peak Load (N)	Rise Time (ms)	Duration (ms)	Peak Pressure (MPa)	Mean Pressure (MPa)	Area (mm^2)
Acute[a]							
	Medial	575 ± 32	4.3 ± 0.9	11.7 ± 1.0	42.4 ± 1.9	23.8 ± 2.5	22.2 ± 1.0
	Central	575 ± 70	4.0 ± 0.3	10.8 ± 0.6	40.2 ± 2.2	25.1 ± 2.9	24.3 ± 2.5
Chronic[b]							
	Medial	630 ± 94	4.2 ± 0.5	10.5 ± 1.8	-----	-----	-----
	Central	604 ± 38	4.5 ± 0.5	10.8 ± 3.0	-----	-----	-----

[a] N = 5
[b] N = 8

Table 2: Measured indentation response of cartilage in control and chronic animals at 12 months post impact (MPa, mean ± SD).

	Central[a]		Medial[b]		Control[a]
	Impacted	Unimpacted	Impacted	Unimpacted	
Gu	1.23 ± 0.29	1.28 ± 0.19	0.55 ± 0.14*+	0.88 ± 0.36	1.06 ± 0.35
Gr	0.43 ± 0.12	0.43 ± 0.08#	0.19 ± 0.07*+	0.26 ± 0.07	0.35 ± 0.11

[a] N = 8
[b] N = 7
* *Significantly less than Unimpacted group, by paired t-test ($p < 0.05$).*
\# *Significantly greater than Unimpacted Medial group, by ANOVA Bonferroni t-test ($p < 0.05$).*
\+ *Significantly less than Control and Impacted Central group, by ANOVA Bonferroni t-test ($p < 0.05$).*

Table 3: Thickness of the subchondral plate of the patella in chronic and control animals 12 months post impact (mm, mean ± SD).

Impact Group		Location		
		Medial	Central	Lateral
Medial[a]	Impacted	0.74 ± 0.23*	1.10 ± 0.38*#	0.60 ± 0.20
	Unimpacted	0.49 ± 0.13	0.63 ± 0.26	0.51 ± 0.21
Central[b]	Impacted	0.48 ± 0.06	0.69 ± 0.12	0.46 ± 0.08
	Unimpacted	0.40 ± 0.08	0.69 ± 0.08	0.42 ± 0.08
Control[a]		0.52 ± 0.14	0.72 ± 0.14	0.52 ± 0.12

[a] N = 8
[b] N = 4
* *Significantly thicker than Unimpacted group, by paired t-test ($p < 0.05$).*
# *Significantly thicker than Control group, by ANOVA Bonferroni t-test ($p < 0.05$).*

Table 4: Average maximum shear stresses and average mean stresses in the central region of the subchondral bone of the Finite Element Model for central- and medial-oriented impact groups (MPa, mean ± SD).

FEM model #	Central		Medial	
	τ_{max}	σ_{normal}	τ_{max}	σ_{normal}
1	10.51 ± 3.37	-30.82 ± 6.02	9.29 ± 3.32	-21.43 ± 8.71
2	9.58 ± 2.85	-26.37 ± 5.82	8.81 ± 2.33	-19.45 ± 4.32
3	8.95 ± 1.26	-26.16 ± 1.53	8.50 ± 1.58	-24.22 ± 1.63
4	14.24 ± 4.76	-29.01 ± 10.16	6.03 ± 1.91	-12.95 ± 1.45
5	8.95 ± 1.26	-26.17 ± 1.54	6.74 ± 2.07	-15.58 ± 1.59
MEAN	10.45	-27.71*	7.87	-18.73
SD	2.21	2.12	1.41	4.51

* *Significantly greater than Medial group, by Unpaired t-test ($p < 0.05$).*

FIGURES

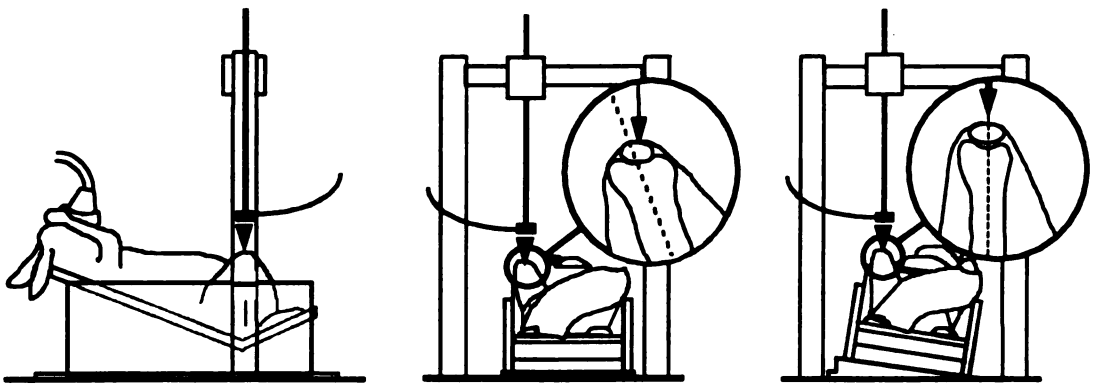

(A) (B) (C)

Figure 1. Impact experiments were performed by dropping a rigid mass onto the patellofemoral joint with 6.0 J of energy **(A)**. medial-oriented impacts required the femur to be positioned so that the impact load was aligned along the medial side of the anterior patella and directed towards the lateral patellar facet **(B)**, while the Central-oriented impacts were aligned along the medial-lateral center of the patellofemoral joint **(C)**.

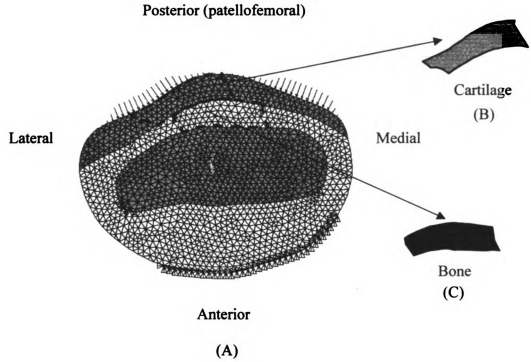

Figure 2. A two-dimensional non-contact finite element model **(A)** of the patella consisting of 1537 3-noded plane strain elements. The lateral facet on the retropatellar articular cartilage **(B)** surface where lesions were generated in acute experiments was used for documenting the impact induced stresses. The central one third of the subchondral bone **(C)** where chronic thickening is typically observed was used to document the impact induced stresses.

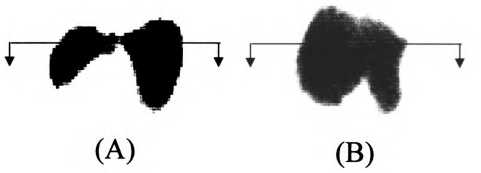

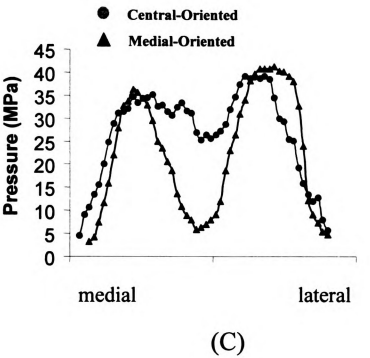

Figure 3. Contact pressure distributions for medial-oriented **(A)** and central-oriented **(B)** impacts, as measured by pressure sensitive film. The graph **(C)** represents the digital processed mean contact pressures of the medial-oriented (▲) and central-oriented (•) impacts.

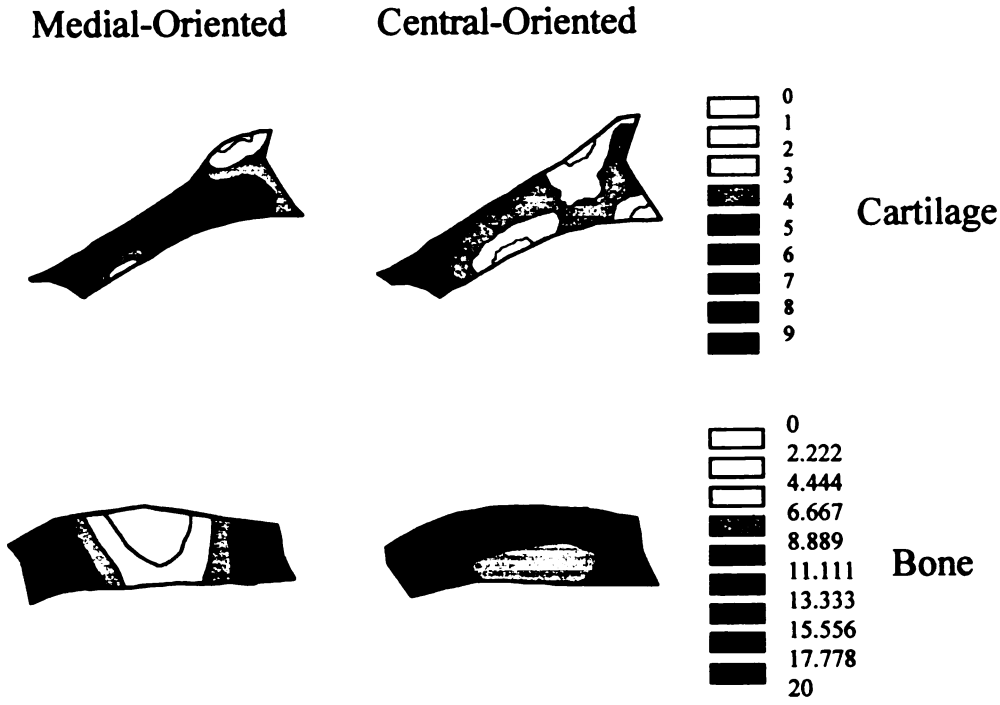

Figure 4. Acute impact-induced maximum shear stress (MPa) distributions in the lateral facet of retropatellar cartilage and central region of underlying subchondral bone medial-oriented and central-oriented impacts.

CHAPTER 5

THE EFFECT OF LOADING RATE ON THE DEGREE OF ACUTE INJURY AND CHRONIC CONDITIONS IN THE KNEE AFTER BLUNT IMPACT

Ewers BJ, Jayaraman VM, Banglmaier RF, Haut RC

ABSTRACT

Lower extremity injuries due to automobile accidents are often overlooked, but can have a profound societal cost. Knee injuries, for example, account for approximately 10% of the total injuries. Fracture of the knee is not only an acute issue but may also have chronic, or long term, consequences. The criterion currently used for evaluation of knee injuries in new automobiles, however, is based on experimental impact data from the 70's using seated human cadavers. These studies involved various padded and rigid impact interfaces that slightly alter the duration of contact. Based on these data and a simple mathematical model of the femur, it appears fracture tolerance increases as contact duration shortens. In contrast, more recent studies have shown mitigation of gross fractures of the knee itself using padded interfaces. The use of padded interfaces, however, result in coincidental changes in contact duration and knee contact area. Therefore, it is difficult to extract the direct effect of loading rate on fracture tolerance of the knee. The object of the current study was to isolate the effect of loading rate alone on fracture tolerance of the human knee joint. Paired experiments were conducted on eight pairs of isolated cadaver knees impacted with a rigid interface to approximately 5 kN at a

high (5 ms to peak) or low (50 ms to peak) rate of loading. Gross fracture and occult microfractures of the knee joint were documented. A second part of the study examined some chronic effects of loading rate on "subfracture" injuries in an animal. Thirty-four rabbits were subjected to a "subfracture" knee load at the same rates as used in the human studies. Alterations in the mechanical properties of retropatellar cartilage and thickening of subchondral bone were documented out to one year post "subfracture" trauma to the joint.

The current study documented an opposite effect than that expected based on 70's experiments with seated cadavers. There was an increase in the number of gross fractures and occult microfractures in high versus low rate of loading experiments. A similar effect was also seen in the "subfracture" chronic animal experiments, which showed relatively more degradative change in the mechanical properties of cartilage following high versus low rate of loading experiments. There was also a significant increase in subchondral bone thickening underlying cartilage and increased fissuring of cartilage in high versus low rate of loading experiments. The current study suggests a relative decrease in tolerance of the knee at high versus low rates of loading in acute experiments with human cadavers and in the chronic setting with animals. Therefore, it would appear that rate of knee loading may be an important issue in establishing a future injury criterion for the knee itself.

INTRODUCTION

Lower extremity injuries due to automobile accidents are often overlooked, but can have a profound societal cost. One study documented that 40 % of total annual trauma treatment charges from automobile collisions were for lower extremity injuries

(MacKenzie et al., 1988). Additionally, it has been estimated that approximately $21.5 billion is spent annually on treatment, rehabilitation, and lost workdays associated with lower extremity injuries (Miller et al., 1995). A previous study, analyzing a survey of accident statistics (The National Accident Sampling System), documents that injuries to the knee account for approximately 10 % of total annual injuries (Atkinson et al., 1998). Knee injuries in an automobile accident typically occur when the knee contacts the instrument panel, or a front knee bolster. Gross fracture of the femur or patella may occur in severe load cases, however, the majority of knee injuries are non-fracture, such as contusions, abrasions, and lacerations (Atkinson et al., 1998). Fracture of the knee is not only an acute issue but may initiate chronic problems, such as a secondary post-traumatic osteoarthritis (OA) (Chapchal, 1978; States, 1986; Wright, 1990). Less severe damage to joint tissues, such as fibrillation of articular cartilage or occult microcracks at the cartilage-bone interface can also occur without radiographic evidence of bone fracture (Pritsch et al., 1984). Subfracture injuries, such as occult microcracks (bone bruises), have been documented in recent years with improvements in magnetic resonance imaging. Often cartilage overlying certain types of bone bruises is fissured, softened, or indicates an occult fracture (Johnson et al., 1998). It has be suggested that these occult microcracks of bone are precursors to a gross fracture (Atkinson et al., 1997).

The current criterion used for evaluation of knee injuries in new automobiles is based on axial load in the femur. This criterion was largely established from experimental impact data on seated human cadavers that caused gross fracture of the patella, femur, or hip (Powell et al., 1975; Melvin et al., 1975; Patrick et al., 1965; Viano and Stalnaker, 1980). These hallmark studies from the 70's were performed with rigid, slightly padded

and heavily padded impact interfaces. The rigid interfaces were shown to generate more patellar fractures than did the padded interfaces. The padded interface experiments generally indicated a slightly increased contact duration of 19.9 ± 9.8 ms versus 3.9 ± 0.7 ms for the rigid interface experiments. Atkinson et al. (1997), using impacts to isolated cadaver knees, have also shown that using a padded interface causes increased contact area on the knee compared to the use of a rigid interface. These increased contact areas were shown to result in a reduction of the impact-induced stresses in joint tissues, resulting in relatively less joint damage than in comparative load experiments with a rigid interface. Hayashi et al. (1996) documented similar results. These data would suggest impacts with padded interfaces yield longer contact durations on the knee and increase its fracture tolerance. Using a finite element model of the human femur under impact loads Viano and Khalil (1976) suggest that fracture tolerance is constant for pulse durations longer than approximately 20 ms, whereas the fracture tolerance of the femur is increased as pulse duration is shortened. The model predicts a doubling of the fracture load as the pulse duration decreases from 20 ms to approximately 2 ms. The experimental data from the rigid and padded cadaver impacts from the 70's was also fit to the model of Viano and Khalil (1976). King et al. (1973) uses this result and states "In the case of short-duration impacts, this femur load criterion is much too conservative because the ultimate strength of the femur bone increases markedly due to the effect of strain rate sensitivity of bone on fracture tolerance". So, the accepted notion is that the fracture tolerance of the knee complex also increases for short versus long duration loads. This suggests that impacts on the knee with padded interfaces, which generally produce longer contact durations, would result in a decrease in the fracture tolerance of the knee rather than an

increase as suggested by Atkinson et al. (1997). This being true would indicate that the rate of loading effects on tissue strength in short duration pulses must have more of an effect on knee fracture tolerance than does the reduction of impact stress in joint tissues due to an increase in contact area. In fact, studies on isolated specimens of cortical bone have documented significant increases in the tensile and compressive strength of cortical bone with increasing strain rate (McElhaney, 1966; Wright and Hayes, 1976). However this dependency of strength on strain rate appears relatively weak, with only a 20 – 50 % increase of strength with an order of magnitude increase in strain rate. And therefore any difference in the strength of the knee for the contact duration of 2 to 20 ms would not explain the 70's data as presented by Viano (1977), unless the patella-femur-hip complex is more rate sensitive than that represented in experimental data from isolated bone coupons.

It is not currently possible, however, to extract the direct effect of loading rate on impact to the knee joint from the previous 70's studies, since padded interfaces result in coincidental changes in contact duration and contact area. The object of the current study was to isolate the effect of loading rate alone on tolerance of the intact human knee joint to blunt impact.

Paired experiments were conducted on eight pairs of isolated human cadaver knees, which were impacted with a rigid interface at a high rate of loading (5 ms to peak) or a lower rate of loading (50 ms to peak). Gross fractures and occult microfractures were documented after loads of approximately 5 kN were applied to the knee specimens. In a second part of the study some of the chronic effects of rate-of-loading on "subfracture" injury to the knee were investigated in an animal. Thirty-four rabbits were subjected to

loads on the knee with a rigid interface at the same high or low rate of loading used in the human studies. Alterations in the mechanical properties of retropatellar cartilage and thickness of underlying subchondral bone were documented out to one year post "subfracture" trauma.

METHODS

HUMAN IMPACTS - ACUTE STUDY

Paired impact experiments were conducted on eight pairs of isolated human knee joints (aged 74.8 ± 13.3 years). The limbs were obtained via a willed-bodied program (see Acknowledgment), and stored at -20°C until testing. The limbs were thawed at 27°C for 24 hours. The tibia and femur were sectioned 15 cm proximal and distal to the knee. Superficial tissues proximal to the femoral condyles were excised, the femoral shaft was cleansed with 70% alcohol, and potted in a cylindrical aluminum sleeve with room temperature curing epoxy using a previously documented protocol (Atkinson and Haut, 1995).

One knee from each subject pair was randomly selected for a single patellofemoral joint impact at a high rate of loading. This protocol followed previous studies by our laboratory, and results in peak loads being applied in approximately 5 ms (Atkinson et al., 1997). The potted femur and sleeve were mounted horizontally to a rigid test fixture with a flexion angle of 90° by a loosely tied tether to the quadriceps tendon and the test fixture (Figure 1). In order to measure patellofemoral joint and anterior patella contact pressures and areas, pressure sensitive film was used (Prescale, Fuji Film Ltd., Tokyo, Japan). On the anterior side of the patella, low range (0-10 MPa), medium range (10-50 MPa), and high range (50-126 MPa) pressure films were stacked together.

In the patellofemoral joint, high pressure film was not used, because previous studies have indicated that pressures within the joint do not exceed 50 MPa (Atkinson et al., 1997). The film was encased in a polyethylene packet to prevent exposure to body fluids and reduce shear loading artifacts. The packet was inserted into the joint prior to each impact through medial and lateral incisions, and wrapped around the anterior surface of the patella (Figure 1). The joint was impacted with a rigid interface at an energy of 27 J. This was based on a logistic regression analysis from a previous study that suggests 27 J would provide the greatest risk of producing an occult trauma, with a 50% chance of generating a gross fracture (Atkinson et al., 1997; Atkinson and Haut, 1995). Impact was delivered to the patellofemoral joint via a 4.5 kg horizontal impact sled accelerated along steel rails to the required pre-impact velocity by a pneumatic cannon. A 5.7 × 5.7 cm, 6061-T6 aluminum impact interface was mounted to the front of a load transducer (Model 3173-2k, Lebow Products, Troy, MI). Load data were collected at 20 kHz continuously via a 16 bit A/D board (Model DAS 1600, Computer Boards Inc., Mansfield, MA), and inertially compensated with an accelerometer (Model #72624a-2000, Endevco, San Juan Capistrano, CA). The velocity of the impact sled was measured prior to the impact event using two infrared optical sensors separated by 76.2 mm (Part No. OR518-ND, Digi-Key Corporation, Thief River Falls, MN). The energy input into the knee was further computed by integration of the force-deflection curve. The deflection data was determined by double integration of the deceleration curve from the impact mass.

Following the high rate of loading impact, the opposite limb underwent a single patellofemoral joint impact using a low rate of loading. The potted femur and sleeve were

vertically mounted to the base of a servo-hydraulic material test machine (Model 1331, Instron Corp., Canton, MA), with the joint flexion angle maintained at 90°. The same impact interface was mounted to the front of a load transducer (Model #10101a-2500, Instron Corp). Prior to application of load, pressure film was inserted into the patellofemoral joint, as described above. Impact was delivered to the patellofemoral joint via the actuator of the test machine under computer control (Flaps 5+, Instron Corp). The impact pulse was a haversine waveform designed to generate the required peak load within 50 ms. The desired peak load was based on the maximum load generated in the contralateral limb during the high rate of loading experiment. Load data were recorded continuously at 1000 Hz. Energy input into the knee was computed by integration of the load-displacement curve, based on hydraulic actuator motion.

The individual pressure films were scanned on a flatbed scanner (ScanJet 6300C, Hewlett Packard, Singapore) using commercial software (PhotoStyler, Aldus Corporation, Seattle, WA). The scanning resolution was 101 dpi, which is equivalent to 25 pixels per square millimeter. The images from the pressure sensitive film were represented digitally as gray scale values using public domain software (NIH, ver. 1.6). The gray scale values were then converted to pressure using a previously established methodology (Atkinson et al., 1998). Briefly, calibration tests on low and medium stacked film were performed using a haversine waveform to generate peak loads within 50 ms with the servohydraulic-testing machine. Past studies have shown that film calibrated at this rate can accurately represent loads with a time to peak of 5 ms (Haut et al., 1995). Peak loads ranged from 135 N to 6600 N, in increments of approximately 150 N. The calibration films were scanned, as stated above, and calibration curves were

created relating the grayscale values to pressure. The calibration curves also determined the range for which each film was usable under these relatively high rates of loading (Figure 2). The ranges were 3 - 10 MPa and 10 - 49 MPa for the low and medium films, respectively. The same calibration procedure was performed for the low, medium, and high pressure film stacks. A macro program (Microsoft Excel 97) was written to eliminate sections of the digitized pressure film images that were not in the useable range. The images from the pressure films were combined to obtain the average contact pressure and area on the anterior surface of the patella and within the patellofemoral joint (Figure 3).

The patellae were grossly examined for evidence of gross bone fracture, and then placed in 10 % buffered formalin for 10-14 days. The tissue was decalcified in 20 % formic acid. Each patella was cut into a 2-3 mm sample block on the center of the medial and lateral facets, processed for routine paraffin embedding, slab-cut and stained with Safranin O-Fast Green. All sections were examined in light microscopy at 12-400 power and photographed. Injuries were classified as to the number of gross fractures, histological fractures (slight fractures through the cartilage and into the underlying bone), and the number of occult microcracks or splits in the zone of calcified cartilage that do not propagate to the cartilage surface.

Paired t-tests were performed to evaluate the following differences in impact characteristics for high versus low rate experiments: peak load, time to peak load, contact duration, input energy, retropatellar contact area and pressure, and contact area on the anterior surface of the patella. McNemar's test was used to examine the difference in the number of gross fractures between high and low rate of loading experiments. Signed

Rank tests were used to examine the differences in the number of histological fractures and occult microfractures between the high and low rate of loading experiments. Significant statistical differences were reported for $p < 0.05$.

ANIMAL MODEL - CHRONIC STUDY

Thirty-four mature Flemish Giant rabbits (4.9 ± 1.2 kg; 6-8 months old) were used. Sixteen animals received a blunt insult to the right patellofemoral joint with a high rate of loading (~5 ms to peak). The impact protocol has been described in earlier studies (Newberry et al., 1998). Briefly, a 1.33 kg mass with a flat 1 in. diameter impact surface was dropped from 0.46 m onto the right flexed (120^0) hind limb. During the impact the animals were maintained at a surgical plane of anesthesia using Isoflurane and oxygen (2% Isoflurane). The impactor was stopped electronically to prevent multiple impacts. A load transducer (Sensotec, Columbus OH: model 31/1432, 500 lb capacity) recorded the impact load at 10 kHz. The remaining eighteen animals received a blunt insult to the right patellofemoral joint with a low rate of loading (~50 ms to peak). These impacts were performed as described above, but with a servo-hydraulic testing machine (Model 1331, Instron Corp) using a single haversine waveform to generate loads comparable to the average load generated in the high rate of loading experiments.

After trauma, all animals received one injection of Butorphenol for post-surgical pain, and were carefully monitored by the veterinary technician. After a five day period of rest following the impact, a daily exercise program was initiated for all animals. This program consisted of ten minutes of exercise, five days a week, on a treadmill running at 0.3 mph (Oyen-Tiesma et al., 1998). The exercise schedule lasted the entire length of the

study. This study was approved by the MSU All-University Committee on Animal Use and Care.

Eight animals from each of the high and low rate of loading groups were sacrificed at 4.5 months post-impact. The remaining animals were sacrificed at 12 months. Immediately after sacrifice, the patellae were excised for mechanical indentation tests on the retropatellar cartilage, as previously described (Ewers et al., 2000). Briefly, the patellae were immersed in a room-temperature phosphate buffered saline bath during the indentation tests. These tests were performed with a custom built instrument that used a computer operated stepper motor (Physik Instruments, Waldbronn, Germany: model M-168.30) to indent the cartilage. A 1 mm diameter flat, non-porous probe was pressed into the cartilage 0.1 mm in 30 ms and maintained for 150 seconds. The resistive loads were measured (Data Instruments, Acton MA: model JP - 25, 25 lb capacity), amplified, and collected at 1000 Hz for the first second, and 20 Hz thereafter. After the tissue was allowed to recover for 5 minutes, the test was repeated with a 1.5 mm diameter, flat non-porous probe at the same location. The probe was then replaced with a needle, which was slowly pressed into the cartilage to determine tissue thickness at that location. The above procedure was performed at two sites on the lateral retropatellar facet adjacent to impact-induced surface lesions, if present.

The analysis of the mechanical data from the retropatellar cartilage was performed using a biphasic model having a transversely isotropic (TI) solid structure. A technique has been developed to determine the mechanical constants using the indentation relaxation data (Garcia, 1998). Briefly, the model assumed isotropy in the plane of the cartilage and the Poisson's ratio in this plane (ν_{12}) was set equal to zero. The

remaining four independent mechanical properties and two permeabilities, namely: a thickness direction modulus (E_{33}), an in-plane modulus (E_{11}), a shear modulus (G_{13}), a Poisson's ratio (ν_{13}), a thickness direction permeability (k_3), and an in-plane permeability (k_1), were then computed using the Garcia algorithm.

After the mechanical tests, each patella was stained with India ink to highlight surface lesions and then photographed. The patellae were then placed in 10% buffered formalin for a week, and decalcified in 20% formic acid for another week. Tissue blocks were cut medial to lateral across the patellae in the area known to produce high contact pressure during impact to the joint (Haut et al., 1995). The tissue blocks were processed in paraffin, and six sections, 8 μ thick, were cut medial to lateral. The sections were stained with Safranin O-Fast Green and examined under light microscopy at 12-400 power. The thickness of the subchondral bone plate underlying retropatellar cartilage was measured at 25x with a calibrated eye-piece at the center of each facet and mid-line of the patella by a single investigator (BE), using existing methods (Newberry et al., 1998).

To help assess cartilage matrix damage, the gross photographic images were scanned and the total length of surface fissuring was measured for each patella using image software (Sigma Scan, SPSS Inc., Chicago, IL). Using the histological sections, the number and average depth of the surface fissures were also measured at 40x with a calibrated eye-piece by one investigator (ES) (Figure 4).

RESULTS

HUMAN IMPACTS - ACUTE STUDY

The typical load-time response for the high rate of loading experiments was a nearly symmetrical haversine, while the low rate of loading experiments resulted in a

skewed haversine (Figure 5). There was no significant difference in peak loads between the high rate of loading (4.6 ± 1.0 kN) and the low rate of loading (4.5 ± 1.2 kN) experiments (Table 1). The high rate of loading experiments produced an average time to peak of 4.9 ± 0.9 ms, while the low rate of loading experiments resulted in a time to peak of 54.2 ± 2.6 ms. The total contact duration for the high rate of loading experiments was 10.3 ± 2.6 ms, while the low rate of loading experiments produced a contact duration of 218.8 ± 23.4 ms. While not statistically significant, the input energy for the high rate of loading experiments (26.2 ± 9.6 Nm) had a tendency to be greater than the low rate of loading experiments (15.8 ± 8.6 Nm) (Figure 6).

The retropatellar pressure film indicated that the region of contact typically had a "kidney" shaped appearance for the high and low rate of loading experiments. There were no significant differences in the retropatellar contact area between the high at 749.6 ± 185.8 mm^2 and the low rate of loading experiment at 587.3 ± 224.1 mm^2 (Table 2). Retropatellar contact area from two high rate of loading experiments had to be removed from the study because of contamination from unknown sources. The retropatellar contact pressures were also similar for experiments at the high rate having a contact pressure of 13.7 ± 3.3 MPa, while the low rate pressure was 14.4 ± 2.7 MPa. The pressure distribution on the anterior surface of the patella for the high and low rate of loading experiments was typically circular. There was also no significant difference in the area of contact between the high (740.1 ± 176.5 mm^2) and the low (586.9 ±153.9 mm^2) rate of loading experiments.

Six pairs of specimens were histologically processed (Table 3). As predicted from earlier studies, the high rate of loading experiments produced transverse patellar fractures

in 50 % of the experiments (Figure 7). On the other hand, the low rate of loading experiments resulted in gross fracture of the patella in only 17 % of the cases. The character of the gross fractures for high and low rate loading was similar. The high rate of loading resulted in approximately twice the number of histological fractures than the low rate of loading experiments. The occult microcracks were typically horizontal (Figure 8). The high rate of loading impacts also produced approximately 50 % more microcracks than the low rate of loading experiments, for the same impact load intensity.

ANIMAL MODEL - CHRONIC STUDY

Examination after impact and daily observations by a certified veterinary technician (JA) assigned only to this project indicated no noticeable joint effusions, and the rabbits did not appear to favor their impacted limbs. A typical load-time response for the high rate of loading experiments was a nearly symmetrical haversine, while the low rate of loading experiments resulted in a skewed haversine. The average peak impact loads of 590 ± 45 N and 630 ± 94 N for the low and high rate of loading, respectively, were not statistically different. However, as expected, there were significant increases in time-to-peak and contact duration for the low rate of loading compared to the high rate of loading experiments. The low rate of loading experiments resulted in a time-to-peak of 60 ± 8 ms and a contact duration of 257 ± 26 ms. In contrast, the high rate of loading experiments produced a time-to-peak of 4.2 ± 0.5 ms and a contact duration of 10.5 ± 1.8 ms.

The data for one animal in the low rate of loading group at 12 months was removed from the study because of excessive pathology in both limbs. Gross visual examination of the remaining patellae in the study, after wiping with India ink, indicated

surface fissures on the retropatellar cartilage in 13 of 17 low rate of loading impacts and in all high rate of loading impacts. These lesions typically ran proximal to distal on the lateral facet near the central ridge of the patella.

The high rate of loading experiments resulted in greater changes in the mechanical properties of the traumatized retropatellar cartilage compared to the low rate of loading experiments at both timepoints. There was no significant difference in any mechanical parameters between unimpacted limbs of the high and low rate of loading experiments at both 4.5 and 12 months post-trauma. At 4.5 months after a high rate of loading on the patellofemoral joint, statistically significant reductions of 39% and 29% in E_{11} and E_{33}, respectively, were documented for the traumatized cartilage compared to the unimpacted limb. There was also significant increases of 57% and 119% in permeabilities k_1 and k_3, respectively, for the traumatized versus contralateral, unimpacted cartilage (Table 4). The low rate of loading experiments resulted in 32% and 21% reductions in E_{11} and E_{33}, respectively, for the traumatized cartilage compared to the contralateral unimpacted limb, and a 48% increase in permeability k_1. At 12 months post-trauma, the high rate of loading experiments resulted in 51% and 32 % reductions of E_{11} and E_{33}, respectively, for the traumatized cartilage compared to the unimpacted contralateral limb. A 51% and 65% increase in k_1 and k_3, respectively, was obtained in the traumatized versus the unimpacted cartilage at this timepoint. However, the low rate of loading resulted in only 25% and 22% decreases in E_{11} and E_{33}, respectively, for the impacted cartilage compared to the unimpacted limb, and no significant difference in permeability at 12 months past impact.

The high rate of loading experiments caused more thickening of the underlying subchondral bone compared to the low rate of loading experiments. At 4.5 months, the high rate impacts resulted in 27%, 28%, and 18% increases in subchondral bone thickness under the lateral, central, and medial sites on the patella, respectively, for the impacted patellae compared to the contralateral unimpacted limbs (Table 5). The low rate experiments resulted in only 10% and 20% increases in subchondral bone thickness at the lateral and central sites, respectively, for the impacted patellae compared to the unimpacted limbs, while there was no significant increase at the medial site. These types of results were also documented at 12 months post-trauma. The high rate of loading experiments again resulted in 29%, 60%, and 44% increases in subchondral bone thickness for the impacted patella compared to the unimpacted limb at the lateral, central, and medial sites, respectively. The low rate impacts resulted in only 9% and 24% increases in subchondral bone thickness at the lateral and central sites, respectively, with no significant increase at the medial site (Figure 9). Importantly, at the lateral and medial sites the subchondral bone of the impacted patellae from the high rate of loading experiments was significantly thicker than that of the impacted patellae from the low rate of loading experiments.

The histological sections showed that the typical depth of surface fissures on traumatized cartilage was approximately 30 - 40% of the cartilage thickness (Figure 10). The average fissure depth for the impacted cartilage was significantly greater than any fissures appearing on the unimpacted limbs (Table 6). There was a significant increase in the number of fissures for the traumatized cartilage compared to the contralateral unimpacted sides. At 12 months, the high rate of loading experiments produced

significantly more surface fissures on retropatellar cartilage than in the low rate of loading experiments. The high rate of loading also resulted in greater length of total surface fissuring on retropatellar cartilage than in the low rate of loading experiments at 12 months post-trauma. In effect, the high rate of loading experiments resulted in more surface fissuring of the retropatellar cartilage than produced in the low rate of loading experiments.

DISCUSSION AND CONCLUSIONS

The criterion for evaluation of knee injuries in new automobiles is based on experimental impact data from the 70's using seated human cadavers. These studies used various padded impact interfaces that only slightly altered contact durations. However, Viano and Khalil (1976) used a FEM model of the human femur to suggest that its fracture tolerance would increase for shortened contact durations. Viano (1977) has also shown that the experimental data from the 70's whole cadaver experiments fit this model. On the other hand, Atkinson et al. (1997), document that by using a padded interface the contact duration increases and gross fracture can be mitigated, suggesting that fracture tolerance of the knee increases with increasing contact durations. However, the use of padded interfaces results in coincidental changes in the contact duration and contact area. Therefore, it is not currently possible to extract the direct effect of loading rate on fracture tolerance of the knee. The object of the current study was to isolate the effect of loading rate alone on tolerance of the knee joint to blunt trauma.

The current study documented an opposite rate of loading effect than that expected based on a model of the femur alone (Viano and Khalil, 1976). As the experimental time to peak load was decreased from 50 ms to 5 ms, there was an increase

in the frequency of gross fractures, indicating a decrease in fracture tolerance of the knee as contact duration was shortened. This result likely suggests that the model analysis of the femur alone, presented by Viano and Khalil (1976), may not be suitable for studying fracture of the patella. The mechanism of injury is significantly different and because of the way soft tissue and the bones make up the knee, the rate sensitivity may be radically different from that of the femur. Therefore, a knee load tolerance criterion should probably not be based on the curve presented in Viano (1977). There was also a doubling of the number of histologically observed fractures, and a 50% increase in occult microcracks for the high versus low rate of loading experiments. Histological fractures and occult microcracks have been suggested to be precursors of gross fractures, and therefore these data support the documented increase in the number of gross fractures generated in the high rate of loading experiments (Atkinson et al., 1997). Occult microcracks of subchondral bone have also been implicated in so-called "subfracture" injuries to the knee (Johnson et al., 1998).

The animal was used in this study to examine some effects of the rate of loading in a chronic experiment. Groups of rabbits were exposed to loads with the same rate of loading used in the human cadaver impacts and examined 4.5 and 12 months post-trauma. There was a tendency for increased softening and increased permeability of the traumatized versus unimpacted retropatellar cartilage in the high rate of loading experiments compared to the low rate of loading experiments. There was also significantly more fissuring on the surface of this cartilage in the high versus low rate of loading experiments. Furthermore, there was significantly more subchondral bone thickening in traumatized patellae for the high versus low rate of loading experiments.

This thickening has been suggested due to a remodeling of the bone as a result of microfractures (Radin et al., 1990). These data could then be in agreement with the results from the human impacts that documented more occult microcracks in the high versus low rate of loading experiments, however microcracks per se were not seen in the animal patellae.

One possibility for the reduction in injuries at low versus high rates could be due to rigid body motion. The low rate of loading might have allowed sliding of the patella, which could result in larger contact areas. The pressure sensitive film, however, showed no increase in contact areas for the low versus high rate of loading experiments. This may be due, however, to the fact that the film was encased in a polyethylene packet, which was meant to mitigate or reduce shear loading artifacts on the film. Since the force-deflection curve was stiffer for the high versus the low speed experiments, there is still a strong possibility that more of the available impact energy on the knee went into patellar deformation in the high rate of loading experiments resulting in a high incidence of gross and microfractures of the patella. However, in order to confirm this conclusion, high speed films would be required. Atkinson et al. (1997) has suggested that acute impact-induced stresses are responsible for injury. Even if there was some rigid body movement of the patella, the retropatellar contact pressures and anterior contact areas were the same for the high and low rate of loading experiments. This would suggest that impact-induced stresses in the joint tissues were the same for both rates of loading, and therefore the two rates of loading should result in the same frequency of injury.

Another possibility may be the rate-sensitive or viscoelastic nature of bone. A load applied over a short time period would cause less tissue strain, and therefore would

be less damaging for a strain failure criterion than the same load applied over a longer time frame, assuming the strain at failure does not depend on time. Furthermore, previous studies have documented with isolated bone coupons that the ultimate strength of bone is increased with increasing strain rate (McElhaney, 1966; Wright and Hayes, 1976). This would not seem to explain our results, because impact loads were the same in our high and low speed tests and we documented more fractures in the high rate test. Therefore, our results do not seem to be explained based on the documented strain rate sensitivity of bone strength alone. On the other hand, the mechanical behavior of isolated bone specimens may be different than bones in a whole joint model.

A third possibility may be proposed assuming bone behaves similar to other engineering materials. An increase in strain rate typically tends to promote brittleness in engineering materials (Felbeck and Atkins, 1984). This would result in more energy going into crack propagation to develop a versus plastic zone at the crack tip for high compared to low rate of loading experiments. The increase in crack propagation could lead to more connected cracks resulting in a greater number of microcracks. This process would result in a greater frequency of gross fractures in the high compared to the low rate of loading experiments.

A forth possibility is based on the complex microstructure of bone. Since bone is composed of solid and fluid phases, it has been modeled as poroelastic (Cowin, 1999). Experimentally, whole bones have shown a degree of hydraulic stiffening (Ochoa et al., 1997). The same effect has been surmised in a fluid-saturated model of cortical bone (Zeng et al., 1994). Hydraulic stiffening of cortical bone is likely to occur under impact loading (Zhang et al., 1998). It has been documented that the pore fluid pressure

relaxation time is approximately 5 ms, and that for a uniaxial impact the fluid pressure differential in the bone can approach 13% of the applied boundary stress (Zhange et al., 1998). These internal compressive fluid pressures must be balanced by tensile stresses in the solid phase of the bone. We hypothesize that these increased tensile stresses in the solid phase could be responsible for the generation of occult microcracks, and eventual gross fracture of bone under an impact load. This notion would support our observation of a greater number of microscopic and gross fractures in high versus low rate of loading experiments.

A similar poroelastic hypothesis has been described for articular cartilage. Garcia et al. (1998) suggested that increases in tensile stress in the solid phase of cartilage may be responsible for impact-induced fissures. Indeed, with a simple geometry and a poroelastic analysis, Garcia et al. (1998) documented the largest tensile stresses in the solid phase of cartilage to be at the surface, where fissures have been documented following impact experiments (Newberry et al., 1998). The current study documented more fissures in the high versus low rate of loading experiments. This may be the result of the high rate of loading causing larger fluid pressures and correspondingly higher tensile stresses in the solid matrix of the retropatellar cartilage. A previous study that traumatized isolated cartilage explants supports this hypothesis by documenting more surface fissures with a high versus low rate of loading (Ewers et al., 2000).

One implication of these new data is that previous impact data from our laboratory with a high rate of loading maybe too conservative with respect to normal instrument panel loading scenarios (Atkinson et al., 1997). The current study would suggest a relative decrease in the tolerance of the knee for high versus low rates of

loading acutely using the cadaver and chronically in an animal. There is still, however, a need for a better understanding of the behavior of cartilage and bone as poroelastic materials at these relatively high rates of loading. While it has been suggested that the impact-induced stresses in joint tissues cause gross fractures, based on the current study it seems that the rate of loading may be another important issue in establishing an injury criterion for the knee joint.

ACKNOLWEDGMENTS

This study was supported by a grant for the Centers for Disease Control and Prevention (R49/CCR503607). Its contents are solely the responsibility of the authors and do not necessarily represent the official views of the Centers for Disease Control and Prevention. The authors wish to gratefully acknowledge Jane Walsh for preparation of the histological slides, Jean Atkinson for care of the animals, Eric Sevensma for help reading the slides, and Cliff Beckett for technical assistance in this study. We also thank Mr. R.S. Wade, Director of the Anatomical Services Division / State Anatomy Board, University of Maryland for help procuring human test specimens.

REFERENCES

1. Atkinson, P.J. and Haut, R.C. (1995) Subfracture Insult to the Human Cadaver Patellofemoral Joint Produces Occult Injury. *Journal of Orthopaedic Research* 13(6), pp. 936-944.

2. Atkinson, P.J., Garcia, J.J., Altiero, N.J., and Haut, R.C. (1997) The Influence of Impact Interface on Human Knee Injury: Implications for Instrument Panel Design and the Lower Extremity Injury Criterion. *Society of Automotive Engineers* 973327, pp. 167-180.

3. Atkinson, P.J., Newberry, W.N., Atkinson, T.S., and Haut, R.C. (1998a) A Method to Increase the Sensitve Range of Pressure Sensitive Film. *Journal of Biomechanics* 31(9), pp. 855-859.

4. Atkinson, P.J., Atkinson, T.S., Haut, R.C., Eusebi, C., Maripudi, V., Hill, T., and Sambatur, K. (1998b) Development of Injury Criteria for Human Surrogates to Address Current Trends in Knee-to Instrument Panel Injuries. *Society of Automotive Engineers* 983146, pp. 13-31.

5. Chapchal, G. (1978) Posttraumatic Osteoarthritis after Injury of the Knee and Hip Joint. *Reconstructive Surgery Traumatology* 16, pp. 87-94.

6. Cowin, S. (1999) Bone Poroelasticity. Journal of Biomechanics. 32(3), pp. 217-238.

7. Ewers, B.J. and Haut, R.C. (2000) Polysulphated Glycosaminoglycan Treatments Can Mitigate Decreases in Stiffness of Articular Cartilage in a Traumatized Animal Joint. *Journal of Orthopaedic Research*, 18:756-761.

8. Ewers, B., Dvoracek-Driksna, D., Orth, M., Altiero, N., and Haut, R. (2000) Matrix Damage and Chondrocyte Death in Articular Cartilage Depends Upon Loading Rate. *46th Annual Meeting of Orthopaedic Research Society.*

9. Felbeck, D.K., and Atkins, A.G. (1984) Strength and Fracture of Engineering Solids. Prentice-Hall, pp. 327-330.

10. Garcia, J.J. (1998) A Transversely Isotropic Hypo-Elastic Biphasic Model of Articular Cartilage Under Impact Loading. PhD Dissertation. Michigan State Univerisity.

11. Haut, R.C. and Atkinson, P.J. (1995) Insult to the Human Cadaver Patellofemoral Joint: Effects of Age on Fracture Tolerance and Occult Injury. *Society of Automotive Engineers*, 952729, pp. 281-294.

12. Haut, R.C., Ide, T.M., and DeCamp, C.E. (1995) Mechanical Responses of the Rabbit Patello-Femoral Joint to Blunt Impact. *Journal of Biomechanical Engineering* 117(4), pp. 402-408.

13. Hayashi, S., Choi, H., Levine, R., Yang, K., and King, A. (1996) Experimental and Analytical Study of Knee Fracture Mechanisms in a Frontal Knee Impact. *40th Stapp Car Crash Conference*, pp. 161-171.

14. Johnson, D.L., Urban, W.P., Caborn, D.N.M., Vanarthos, W.J., and Carlson, C.S. (1998) Articular Cartilage Changes Seen With Magnetic Resonance Imaging-Detected Bone Bruises Associated With Acute Anterior Cruciate Ligament Rupture. *American Journal of Sports Medicine* 26(3), pp. 409-414.

15. King, J.J., Fan, W.R.S., and Vargovick, R.J. (1973) Femur Load Injury Criteria--A Realistic Approach. *17th Stapp Car Crash Conference*, pp. 509-525.

16. MacKenzie, E.J., Siegel, J.H., Shapiro, S., et.al. (1988) Functional Recovery and Medical Costs of Trauma: An Analysis by Type and Severity of Injury. *Journal of Trauma* 28, pp. 281-298.

17. McElhaney, J. (1966) Dynamic Response of Bone and Muscle Tissue. *Journal of Applied Physiology* 21, pp. 1231-1236.

18. Melvin, J., Stalnaker, R., Alem, N., Benson, J., and Mohan, D. (1975) Impact Response and Tolerance of the Lower Extremities. *19th Stapp Car Crash Conference*, pp. 543-559.

19. Miller, T., Martin, P., and Crandell, J.R. (1995) Cost of Lower Limb Injuries in Highway Crashes. *Proceedings of the International Conference on Pelvic and Lower Extremity Injuries*, pp. 47-57.

20. Newberry, W.N., MacKenzie, C., and Haut, R.C. (1998) Blunt Impact Causes Changes in Bone and Cartilage in a Regularly Exercised Animal Model. *Journal of Orthopaedic Research*, 16(3), pp. 348-354.

21. Ochoa, J.A., Sanders, A.P., Kiesler, T.W., Heck, D.A., Toombs, J.P., Brandt, K.D., and Hillberry, B.M. (1997) In Vivo Observations of Hydraulic Stiffening in the Canine Femoral Head. J*ournal of Biomechanical Engineering*, 119(1), pp. 103-108.

22. Oyen-Tiesma, M., Atkinson, J., and Haut, R.C. (1998) A Method for Promoting Regular Rabbit Exercise in Orthopaedics Research. *Contemporary Topics in Laboratory Animal Science*, 37, pp. 77-80.

23. Patrick, L., Kroell, C., and Mertz, H. (1965) Forces on the Human Body in Simulated Crashes. *9th Stapp Car Crash Conference*, pp. 237-259.

24. Powell, W., Ojala, S., Advani, S., and Martin, R. (1975) Cadaver Femur Responses to Longitudinal Impacts. *19th Stapp Car Crash Conference*, pp. 561-579.

25. Pritsch, M., Comba, D., Frank, G., and Horoszowski, H. (1984) Articular Cartilage Fractures of the Knee. *Journal of Sports Medicine*, 24(4), pp. 299-302.

26. Radin, E. L., Burr, D. B., Fyhrie, D., Brown, T. D., and Boyd, R. D. (1990) Characteristics of Joint Loading as It Applies to Osteoarthrosis. In: Biomechanics of Diarthrodial Joints. Springer-Verlag, pp.437-451.

27. States, J. (1986) Adult Occupant Injuries of the Lower Limb. In: Biomechanics andMedical Aspects of Lower Limb Injuries. Warrendale, pp.97-107.

28. Viano, D.C. and Khalil, T.B. (1976) Investigation of Impact Response and Fracture of a Human Femur by Finite Element Modeling. *20th Stapp Car Crash Conference*, pp. 412.

29. Viano, D.C. (1977) Considerations for a Femur Injury Criterion. *21st Stapp Car Crash Conference*, pp. 445-473.

30. Viano, D.C. and Stalnaker, R.L. (1980) Mechanisms of Femoral Fracture. *Journal of Biomechanics*, 13(8), pp. 701-715.

31. Wright, T. and Hayes, W. (1976) Tensile Testing of Bone Over a Wide Range of Strain Rates; Effects of Strain Rate, Microstructure and Density. *Medical and Biological Engineering*, pp. 671-680.

32. Wright, V. (1990) Post-Traumatic Osteoarthritis – A Medico-Legal Minefield. British *Journal of Rheumatology*, 29, pp.474-478.

33. Zeng, Y., Cowin, S.C., and Weinbaum, S. (1994) A Fiber Matrix Model for Fluid Flow and Streaming Potentials in the Canaliculi of an Osteon. *Annals of Biomedical Engineering*, 22(3), pp. 280-292.

34. Zhang, D., Weinbaum, S., and Cowin, S.C. (1998) Estimates of the Peak Pressures in Bone Pore Water. *Journal of Biomechanical Engineering*, 120(6), pp. 697-703.

TABLES

Table 1: Impact Data for High and Low Rate of Loading on Paired Subjects

	Time To Peak Force (ms)		Contact Duration (ms)		Peak Force (kN)		Input Energy (Nm)	
Rate of Loading	High*	Low	High*	Low	High	Low	High	Low
Specimen I.D.								
99-370	4.63	50.0	10.76	226	3.49	3.42	21.71	4.87
99-535	5.53	52.0	10.96	224	5.35	5.80	#	13.91
99-571	5.33	55.0	10.46	228	5.11	5.05	44.95	20.90
99-729	5.83	57.0	15.54	228	3.23	2.58	28.04	9.76
99-750	4.48	56.0	9.46	228	4.65	3.92	28.44	17.23
99-775	3.34	55.0	8.12	229	5.25	5.36	22.03	21.73
00-524	4.43	49.0	10.4	165	3.66	3.90	24.48	7.00
00-540	2.64	66.0	6.52	222	6.11	5.97	13.82	30.67
Average	4.9	54.2	10.3	218.8	4.6	4.5	26.2	15.8
Std. Dev.	0.9	2.6	2.6	23.4	1.0	1.2	9.6	8.6

* – significantly different from impacted limb in low rate of loading group (t-test, $p < 0.05$)
# - Outlier

Table 2: Contact Area and Pressure Data for High and Low Rate of Loading on Paired Subjects

	Retro-Patellar Contact Area (mm^2)		Retro-Patellar Contact Pressure (MPa)		Anterior Contact Area (mm^2)	
Rate of Loading	High	Low	High	Low	High	Low
Specimen I.D.						
99-370	734.3	N/A	9.8	N/A	869.5	N/A
99-535	478.8	443.9	19.3	17.4	1051.2	523.1
99-571	745.1	895.8	12.1	13.1	515.2	816.9
99-729	#	377.3	15.2	12.0	749.1	531.8
99-750	478.8	623.9	12.6	10.5	563.3	462.9
99-775	967.8	605.3	17.6	17.6	713.4	569.5
00-524	637.1	317.9	11.2	14.0	834.1	420.4
00-540	#	846.7	11.8	15.9	625.5	783.4
Average	749.6	587.3	13.7	14.4	740.1	586.9
Std. Dev.	185.8	224.1	3.3	2.7	176.5	153.9

- Outlier
N/A – Pressure film data lost

Table 3: Frequency of Injury Following High and Low Rate of Loading Experiments on Paired Subjects

	Gross Fractures		Histological Fractures		Occult Microcracks	
Rate of Loading	High	Low	High	Low	High	Low
Specimen I.D.						
99-370	1	0	2	0	2	0
99-535	0	0	1	1	0	0
99-571	0	0	0	0	2	1
99-729	1	0	4	2	4	4
99-750	0	0	0	0	2	1
99-775	1	1	2	1	3	3
Total	3	1	9	4	13	9
Range			(0-4)	(0-2)	(0-4)	(0-4)

Table 4: Mechanical Properties of Retropatellar Articular Cartilage Post Trauma (Avg ± SD).

Time Point	Limb	E_{11} (MPa)	E_{33} (MPa)	G_{13} (MPa)	υ_{13}	k_1 ($m^4/Ns10^{-15}$)	k_3 ($m^4/Ns10^{-15}$)
4.5 Months Low [a]	Imp	3.64 ± 1.49^{+}	0.81 ± 0.17^{+}	0.19 ± 0.05	0.12 ± 0.02	7.66 ± 2.89^{+}	2.42 ± 1.24
	Unimp	5.34 ± 2.19	1.03 ± 0.18	0.17 ± 0.02	0.12 ± 0.05	5.19 ± 2.84	2.54 ± 1.44
High [a]	Imp	3.82 ± 1.30^{+}	0.82 ± 0.23^{+}	0.22 ± 0.05	0.10 ± 0.03	7.59 ± 3.71^{+}	5.92 ± 3.75$^{+\#}$
	Unimp	6.30 ± 1.83	1.15 ± 0.30	0.16 ± 0.08	0.10 ± 0.02	4.83 ± 3.14	2.70 ± 1.86
12 Months Low [b]	Imp	4.15 ± 2.21^{+}	0.98 ± 0.44^{+}	0.21 ± 0.04	0.11 ± 0.03	6.15 ± 2.86	4.32 ± 3.48
	Unimp	5.56 ± 2.18	1.26 ± 0.36	0.21 ± 0.07	0.13 ± 0.04	4.39 ± 1.82	2.58 ± 1.59
High [a]	Imp	2.93 ± 0.94^{+}	0.78 ± 0.23^{+}	0.25 ± 0.14	0.10 ± 0.03	6.70 ± 2.62^{+}	4.20 ± 1.92^{+}
	Unimp	5.96 ± 2.42	1.14 ± 0.25	0.21 ± 0.14	0.11 ± 0.03	4.43 ± 2.49	2.55 ± 1.93

Imp – impacted limb, Unimp – unimpacted limb

+ – significantly different from contralateral unimpacted limb (paired t-test, $p < 0.05$)

– significantly different from impacted limb in low rate of loading group (t-test, $p <$ 0.0)

Table 5: Subchondral Bone Thickness (mm) at the Center of the Patella and the Midline of the Lateral and Medial Facets (Avg ± SD).

Time Point	Limb	Lateral	Center	Medial
4.5 Months				
Low [a]	Imp	0.44 ± 0.08^{+}	0.67 ± 0.07^{+}	0.45 ± 0.11
	Unimp	0.40 ± 0.08	0.56 ± 0.14	0.41 ± 0.08
High [a]	Imp	0.38 ± 0.09^{+}	0.74 ± 0.16^{+}	0.39 ± 0.10^{+}
	Unimp	0.30 ± 0.05	0.53 ± 0.17	0.32 ± 0.07
12 Months				
Low [b]	Imp	0.63 ± 0.15^{+}	0.97 ± 0.24^{+}	0.64 ± 0.14
	Unimp	0.58 ± 0.11	0.78 ± 0.18	0.58 ± 0.21
High [a]	Imp	0.85 ± 0.20$^{+\#}$	1.33 ± 0.48^{+}	0.85 ± 0.23$^{+\#}$
	Unimp	0.66 ± 0.21	0.83 ± 0.36	0.59 ± 0.13

Imp – impacted limb
Unimp – unimpacted limb
+ – significantly different from contralateral unimpacted limb (paired t-test, $p < 0.05$)
# – significantly different from impacted limb in low rate of loading group (t-test, $p < 0.0$)

Table 6: Total Fissure Length (Avg ± SD) from Gross Photographs of the Rabbit Patellae, and the Average Fissure Depth (Avg ± SD) and the Number of Fissures (median (range)) from Histological Sections.

Time Point	Limb	Total Fissure Length (mm)	Average Fissure Depth (%)	Number of Fissures (#)
4.5 Months				
Low [a]	Imp	9.2 ± 5.2 [+]	37 ± 14 [+]	2.5 (0-6) *
	Unimp	2.4 ± 2.8	5 ± 12	0 (0-2)
High [a]	Imp	11.2 ± 5.8 [+]	36 ± 24 [+]	4 (2-5) *
	Unimp	3.1 ± 3.6	7 ± 18	0 (0-1)
12 Months				
Low [b]	Imp	11.2 ± 8.3	34 ± 18 [+]	1 (0-10)
	Unimp	6.3 ± 5.5	9 ± 12	1 (0-5)
High [a]	Imp	25.7 ± 8.8 [+#]	42 ± 15 [+]	7 (4-12) * [$]
	Unimp	4.4 ± 4.3	23 ± 20	2 (0-8)

Imp – impacted limb
Unimp – unimpacted limb
+ – significantly different from contralateral unimpacted limb (paired t-test, $p < 0.05$)
* – significantly different from contralateral unimpacted limb (Signed Rank test, $p < 0.05$)
# – significantly different from impacted limb in slow group (t-test, $p < 0.05$)
$ – significantly different from impacted limb in slow group (Rank Sum test, $p < 0.05$)

FIGURES

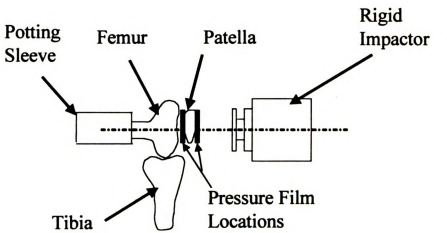

Figure 1: A 5.7 x 5.7 cm, 6061-T6 aluminum rigid interface with a mass of 4.5 kg was accelerated in a horizontal impact sled by a pneumatic cannon. The rigid interface impacted the joint. The pressure sensitive film was inserted into the joint to capture patellofemoral joint contact pressure and area, as well as the contact pressure and area on the anterior surface of the patella. High, medium, and low pressure film were stacked in the patellofemoral joint. The anterior surface of the patella had stacked low and medium pressure film.

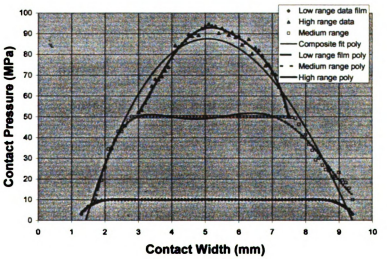

Figure 2: This chart indicates the useable pressure ranges for the low, medium, and high pressure film. The low pressure film had a useable range of 3MPa to 10MPa. The useable range for the medium pressure film was between 10MPa and 49MPa. The high pressure film was not used since pressures from past experiments never exceeded 49MPa (reproduced from reference 22).

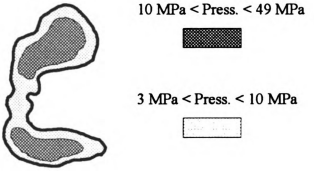

Figure 3: The digitized images of the medium and low pressure films were combined to obtain the contact pressure distribution and contact area.

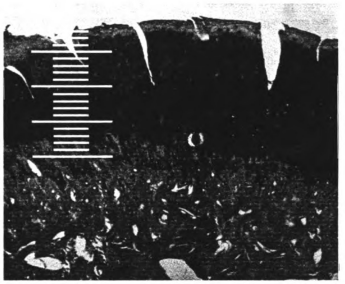

Figure 4: The number and average depth of the surface fissures was measured at 40x with a calibrated eye-piece by one investigator using the histological sections of the patellae.

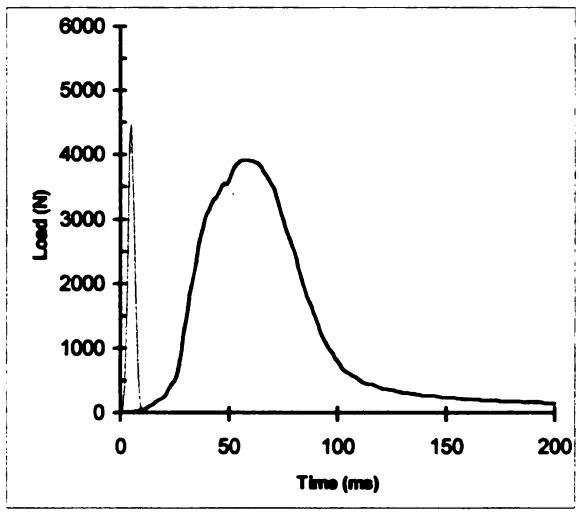

Figure 5: This chart shows typical load versus time responses for the high and low rate of loading experiments. Both tests showed a nearly symmetrical haversine. The peak loads were not significantly different between the tests. The contact durations for each of these tests were significantly different.

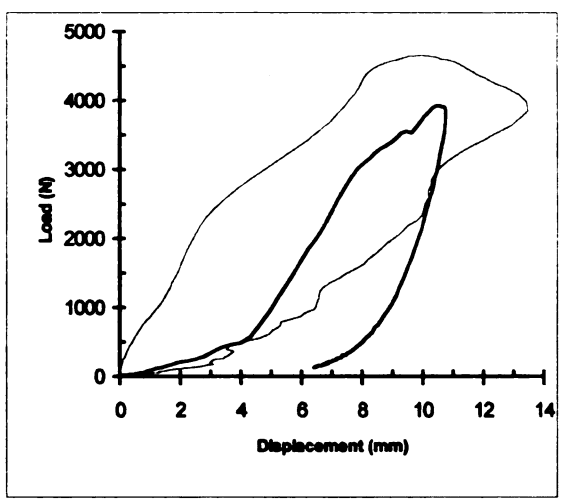

Figure 6: Typical load-displacement curves for the high and low rate of loading experiments.

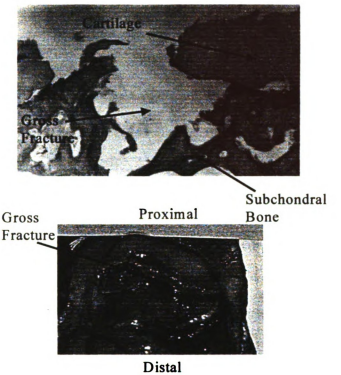

Figure 7: This shows a gross fracture of the patella that was readily observable on the retropatellar surface.

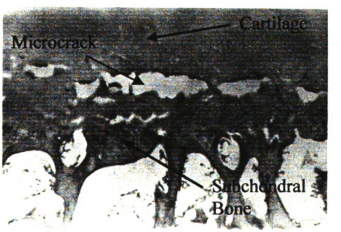

Figure 8: This histological slide of the patella shows a horizontal microcrack near the zone of calcified cartilage between hyaline cartilage from the underlying subchondral bone.

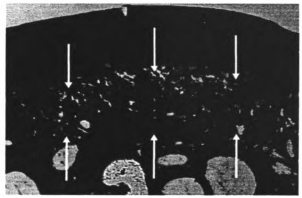

(A)

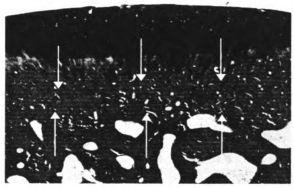

(B)

Figure 9: The traumatized rabbit patellae in the high rate of loading experiments (A) resulted in a significant increase in subchondral bone thickness compared to the impacted patellae in the low rate of loading experiments (B) under the midline of the medial and lateral facets, with the same trend apparent in the center of the patellae.

(A)

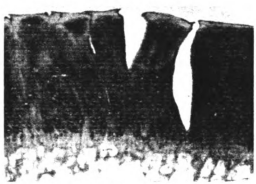

(B)

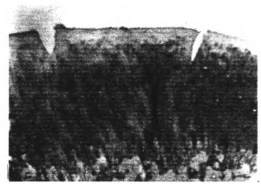

(C)

Figure 10: Representative histological sections of the rabbit retropatellar cartilage for unimpacted (A), impacted at a high rate of loading (B), and impacted at a low rate of loading (C). Notice the average fissure depth to be between 30 and 40% of the cartilage thickness, and deeper fissures tended to exist following high versus low rate of loading experiments at 12 months post trauma.

CHAPTER 6

POLYSULPHATED GLYCOSAMINOGLYCAN TREATMENTS CAN MITIGATE DECREASES IN STIFFNESS OF ARTICULAR CARTILAGE IN A TRAUMATIZED ANIMAL JOINT

Ewers BJ and Haut RC

ABSTRACT

A single, blunt impact to the rabbit patello-femoral joint has been shown to cause a decrease in the stiffness of retropatellar cartilage and an increase in the thickness of underlying bone. Polysulphated glycosaminoglycan (PSGAG) treatments, on the other hand, have been shown to inhibit the degradation of articular cartilage, and possibly increase synthesis of collagen and glycosaminoglycans in experimental studies on diseased joints. The aim of the current study was to examine the effect of early PSGAG treatments on cartilage using an *in vivo* post-trauma animal model. The study used 24 Flemish Giant rabbits in three groups: control, impacted, and impacted with treatment. Treatment consisted of intramuscular injections the day of insult and every four days thereafter for six weeks. At 30 weeks post-trauma mechanical tests were performed on the retropatellar cartilage to determine its mechanical stiffness. The patellae were also grossly evaluated for surface lesions on the retropatellar cartilage, and histologically processed to measure the thickness of subchondral bone. The group receiving no treatment had a statistically significant decrease in stiffness (modulus) for the impacted versus contralateral, unimpacted cartilage and versus the control group. The degradation

in mechanical stiffness, however, was not observed in the group receiving treatment. There was also a significant increase in the underlying thickness of the subchondral plate on the impacted patellae compared to the contralateral, unimpacted sides for both the treated and untreated groups. In conclusion, the PSGAG treatments mitigated a decrease in mechanical stiffness (modulus) of retropatellar articular cartilage at 30 weeks post-trauma. The mechanism by which the mechanical stiffness of the cartilage was preserved is currently unknown.

INTRODUCTION

A single, severe blunt insult to the rabbit patello-femoral joint has been shown to cause changes in retropatellar cartilage and underlying subchondral bone (Newberry et al., 1998). This includes a decrease in stiffness of the retropatellar articular cartilage, starting at three months post-trauma versus unimpacted controls. Studies with human cartilage have also shown that degenerated tissue has a decreased stiffness via indentation testing (Kempson et al., 1971) and a decrease in equilibrium modulus has been correlated with this degeneration (Armstrong and Mow, 1982). The thickness of the subchondral plate underlying retropatellar cartilage is greater than that of the contralateral, unimpacted patella. Such early changes have been hypothesized leading to further softening of the articular cartilage, erosion, and eventually osteoarthrosis (OA) in the joint (Radin et al., 1984). Since there can often be a single known incident, or trauma, which could initiate this disease process a contraceptive treatment, such as a "chondroprotective" drug, may prove to be effective in slowing or mitigating changes in joint tissues post-trauma.

The etiology of OA is known to involve an increase in extracellular matrix turnover, which eventually leads to a net loss of proteoglycans and collagen from the

articular cartilage. These changes result in degradation of cartilage and ultimately degeneration of the joint (Bayliss, 1992). Polysulfated glycosaminoglycans (PSGAG) have been used clinically in Europe and in the veterinary community for the treatment of diseased joints. PSGAG have been shown to decrease the rate of synthesis of certain degradative enzymes in these degenerating joints (Howell et al., 1986; May et al., 1988). In addition to inhibiting degradation, *in vitro* experiments have shown that PSGAG can stimulate a net increase in collagen and glycosaminoglycan synthesis in tissue explants (Glade, 1990). While animal models of OA have been used to study PSGAG treatments (Fubini et al., 1993; Gaustad and Larsen, 1995; Golding et al., 1983; Howell et al., 1986), the effectiveness of PSGAG treatment has not been examined in a post-trauma model. Mazieres et al. (1993) has shown a positive effect of the anti-inflammatory drug diacerhein on the histological appearance of traumatized patellae with a post-contusion model of OA using New Zealand rabbits. Our model uses Giant Flemish rabbits along with a post-trauma exercise protocol and documents the mechanical stiffness of traumatized cartilage over time. The mechanical properties of articular cartilage have been suggested to be a better indicator of its ability to function as a weight bearing material than its histological appearance (Armstrong and Mow, 1982).

The aim of the current study was to evaluate whether early, intramuscular injections of PSGAG would be effective in mitigating the previously recorded softening of retropatellar articular cartilage following a severe, blunt trauma to the patello-femoral joint in a rabbit model. We hypothesized that these early treatments would help preserve the mechanical stiffness (modulus) of the retropatellar articular cartilage, even in the presence of impact generated surface lesions.

METHODS AND MATERIALS

A total of twenty-four mature Flemish Giant rabbits (5.0 ± 0.5 kg, 6-8 months of age) were used in the study. Sixteen animals received a blunt insult to the right patello-femoral joint. Eight animals served as a control population, and did not receive an insult. The impact protocol has been described in earlier studies (Newberry et al., 1998). Briefly, a 1.33 kg mass with a flat 1 in. diameter impact surface was dropped from 0.46 m onto the right hind limb, which was flexed approximately 120^0. During the impact the animals were maintained at a surgical plane of anesthesia using Isoflurane and oxygen (2% Isoflurane). The impactor was stopped electronically to prevent multiple impacts. A load transducer (Sensotec, Columbus OH : model 31/1432, 500 lb capacity) recorded the impact load at 10 kHz.

After trauma, all animals received one injection of Butorphenol for post-surgical pain. Eight animals were treated with the veterinary drug Adequan® 100 mg/ml (Luitpold Pharmaceuticals), which is a semi-synthetic glycosaminoglycan containing primarily chondoitin sulphate with three to four esters per disaccharide unit and a molecular weight of 3000 to 15000 daltons. The treatment consisted of 2 mg/kg injections every four days for six weeks beginning on the day of the insult. The remaining eight impacted animals received no treatment.

After a five day period of rest following the impact, a daily exercise program was initiated for all animals, including the non-impacted control group. Previous studies have shown that with exercise the decrease in stiffness of cartilage and increase in thickness of subchondral bone is accelerated in time (Newberry et al., 1997; Newberry et al., 1998). This program consisted of ten minutes of exercise, five days a week, on a treadmill

running at 0.3 mph (Oyen-Tiesma et al., 1998). The exercise schedule lasted the entire length of the study. The animals were housed in individual cages (48" x 24" x 19") when not being exercised. This study was approved by the MSU All-University Committee on Animal Use and Care.

All twenty-four animals were sacrificed after thirty weeks. Immediately after sacrifice, the patellae were excised for mechanical indentation tests on the retropatellar cartilage. The patellae were immersed in a room-temperature phosphate buffered saline bath during the indentation tests. These tests were performed with a custom built instrument that used a computer operated stepper motor (Physik Instruments, Waldbronn, Germany : model M-168.30) to indent the cartilage. A fixture, which held the patella with its retropatellar surface facing the indenter, allowed X-Y-Z movement to position the site of indentation. A camera mount (Bogen, Italy) attached to the base of the fixture allowed for rotation of the patellae, to insure that the indentation was normal to the cartilage surface. A 1 mm diameter flat, non-porous probe was pressed into the cartilage 0.1 mm in 30 ms and maintained for 150 seconds. The resistive loads were measured (Data Instruments, Acton MA : model JP - 25, 25 lb capacity), amplified, and collected at 1000 Hz for the first second and 20 Hz thereafter. After the tissue was allowed to recover for 5 minutes, the probe was replaced with a needle that was slowly pressed into the cartilage to determine the thickness of cartilage at that location. The above procedure was performed at two sites approximately one indentor diameter away from the surface lesions on the lateral retropatellar facet (Figure 1).

The mechanical data from the indentation tests on the cartilage were analyzed using an elastic analysis due to Hayes et al. (1972). This analysis assumed an infinite

elastic layer (cartilage) bonded to a rigid half space (bone). It allowed the determination of two shear moduli for the cartilage. These were based on the load at 30 milliseconds (an instantaneous shear modulus – G_U) and at 150 seconds (a relaxed shear modulus – G_R).

After the mechanical tests, each patella was stained with India ink to highlight surface lesions and photographed. The patellae were then placed in 10% buffered formalin for a week, and decalcified in 20% formic acid for another week. Tissue blocks were cut medial to lateral across the patellae in the area known to produce high contact pressure during impact to the joint (Newberry et al., 1998). The tissue blocks were processed in paraffin, and a minimum of six sections, 8 μ thick, were cut medial to lateral. The sections were stained with Safranin O-Fast Green and examined under light microscopy at 12-400 power. The thickness of the subchondral bone plate underlying retropatellar cartilage was measured at 25x with a calibrated eye-piece at the center of each facet and mid-line of the patella by a single investigator (BE), using existing methods (20) (Figure 2).

A mixed design two-factor ANOVA with S-N-K post-hoc testing was used to evaluate the differences in shear modulus (stiffness) and subchondral bone thickness between limbs and groups. Limb was the repeated factor with group being the independent factor. Significant statistical differences were reported for $p < 0.05$.

RESULTS

Examination after impact and ensuing daily observations by a veterinary technician (J.A.) indicated no noticeable joint effusions, and the rabbits did not appear to favor their impacted limbs. Gross visual examinations of the patellae after wiping with India ink indicated surface fissures on the retropatellar articular cartilage in 15 of 16

impact cases. These lesions typically ran proximal to distal on the lateral facet, near the central ridge of the patella (Figure 1). PSGAG treatments did not have an effect on the gross appearance of these surface lesions. The impacted patellae in the treated group still had typical impact-induced surface lesions (Figure 3). No surface lesions were seen on the retropatellar surfaces of the unimpacted, contralateral or control patellae.

The mechanical data was lost for one animal in the impacted group. There was a statistically significant decrease in G_U of the retropatellar cartilage on the impacted patella versus the controls at this 30 week timepoint (Table 1). There were no significant differences in subchondral bone thickness between the impacted limb from the non-treated or PSGAG-treated groups compared to controls at any location on the patella. In contrast, G_U of the impacted cartilage from the PSGAG-treated group was not different from that of controls or the unimpacted, contralateral limb of the impacted treated or non-treated groups. The relaxed modulus G_R from the impacted (non-treated) group was not different from controls. On the other hand, this measure of tissue stiffness was significantly less than that of its contralateral, unimpacted limb. This significant difference in G_R between limbs was not present in the PSGAG-treated group.

From the histological sections of the patellae no significant differences were measured in the subchondral plate thicknesses between left and right limbs at any location on the patella in the control group (Table 2). In contrast, there was a significant increase in thickness of the subchondral plate underlying retropatellar cartilage at the medial and central locations in the impacted versus the contralateral, unimpacted patellae. Animals receiving PSGAG treatments after impact also indicated significant increases in the thickness of the subchondral plate on impacted versus contralateral, unimpacted

patellae at these same two locations. There was also a trend for subchondral plate thickening in impacted versus unimpacted patellae at the lateral location.

DISCUSSION

The results supported our hypothesis that the stiffness (modulus) of retropatellar cartilage would not degrade significantly, post-trauma for animals injected early with PSGAG. After six weeks of treatment immediately following insult the 39 % decrease in stiffness for impacted versus unimpacted, control retropatellar cartilage was mitigated in the model. On the other hand, early PSGAG treatment did not appear to have an effect on the gross appearance of impact-induced surface lesions on the retropatellar cartilage. The PSGAG treatments also did not mitigate the thickening of the subchondral plate underlying retropatellar cartilage that had previously been measured versus the contralateral unimpacted patella in this post-trauma animal model.

Our results compare well with earlier studies using this model. Newberry et al. (1998), observed a statistically significant (40 %) reduction in the instantaneous modulus (G_U) of impacted retropatellar cartilage versus unimpacted, controls at six months post-trauma. Similar to the previous study (Newberry et al., 1998), we also documented a significant decrease in the relaxed modulus (G_R) of the impacted cartilage compared to the contralateral unimpacted limb, but not compared to controls. The appearance of the impact-induced surface lesions on the retropatellar cartilage was also similar to earlier studies (Newberry et al., 1998). Finally, we observed a 23 % increase in the thickness of the subchondral plate at the central location for the impacted limbs compared to contralateral, unimpacted limbs. Newberry et al. (1998) documents a 29 % increase at six months post-trauma.

The PSGAG treatment did not grossly appear to heal the mechanically induced surface lesions in our trauma model. This result was consistent with others who have shown no effect of PSGAG treatment on healing cartilage defects (Barr et al., 1994; Trotter et al., 1989). In our trauma model statistical changes in thickness of underlying bone versus controls is not documented until 12 months after trauma. A longer duration study would be needed to document the effect of PSGAG treatments on the underlying bone in a more chronic setting. Armstrong et al.(1994) observed that subchondral bone thickening was mitigated or slowed after regular treatment of the joint with hyaluronan (HA) in a sheep meniscectomy model. This effect was believed to be an indirect result of the treatments by an improvement in the quality of the overlying cartilage. In our model, Ewers et al.(1998), recently showed that slight changes in the overlying cartilage properties theoretically would have no significant affect on the underlying bone stresses which might cause subchondral bone remodeling. In contrast, the effect might be different for the sheep tibial-femoral joint because of a different geometry. On the other hand, the remodeling of bone underlying impacted joint cartilage in our model may be due to the acute overstressing generated during blunt impact. PSGAG treatments may not significantly affect this remodeling post-trauma. These issues need further study.

Impaction of the patello-femoral joint in the current study may have overstressed retropatellar cartilage and damaged the extracellular matrix leading to an increased hydration of the tissue (Donahue et al., 1983). The damaged matrix and the increased hydration of the cartilage may be the cause for the decrease in the modulus of the tissue post-trauma. Previous research, by others, suggests that the equilibrium response of cartilage in an indentation test (approximated by G_R in the current study) is controlled by

the content and integrity of tissue proteoglycans (Jurvelin et al., 1988). Furthermore, they suggested that G_U may be more reflective of the content and integrity of collagen in the tissue (Mizrahi et al., 1986). Yet, these investigators also suggest that tissue proteoglycans can play a role in determining the structural integrity of the collagen network by affecting its pretension. The unrelaxed and relaxed shear moduli are "apparent" material properties that are derived from modeling the cartilage as a single-phase, elastic layer. The unrelaxed modulus is related to tissue permeability, fluid pressure, and matrix properties. The impact may have caused the tissue to become more permeable causing the decrease in G_U. A possible mechanism for the action of the PSGAG treatments on traumatized cartilage might involve its ability to alter the content of proteoglycans post-insult by either increased synthesis or inhibited degradation. For example, Glade et al.(1990) showed increased synthesis of proteoglycan by chondrocytes in culture when exposed to PSGAGs. Hannan et al.(1987), also showed less depletion of tissue proteoglycans with PSGAG treatments versus no treatments in a canine meniscectomy model. This increase in proteoglycans could cause the permeability to be lowered, resulting in a restoration of G_U.

Another potential effect of the PSGAG treatments may have been to help return normal loading to the impacted limb, mitigating a small increase in the stiffness of cartilage on the unimpacted contralateral limb that has been documented to become statistically significant at one year post-trauma in our model (Newberry et al., 1998). On the other hand, our studies have not been able to actually quantify a favoring of the impacted limb in our model. The possibility of complementary effects of PSGAG treatment and altered joint loading, or with or without post-trauma exercise will also need

to be investigated in future studies. Another limitation of the current study was the absence of histochemical and histological analyses of the treated and non-treated retropatellar cartilage.

In conclusion, this investigation suggested positive effects of early PSGAG treatments on mechanical stiffness (modulus) of retropatellar cartilage following severe blunt trauma to the rabbit patello-femoral joint. The applicability of these results to the human scenario will need to be explored in clinical studies.

ACKNOWLEDGMENTS

This study was supported by a grant for the Centers for disease Control and Prevention (R49/CCR503607). Its contents are solely the responsibility of the authors and do not necessarily represent the official views of the Centers for Disease Control and Prevention. The authors wish to gratefully acknowledge Jane Walsh for her preparation of the histological sections, Jean Atkinson for her care of the animals and Cliff Beckett for technical assistance.

REFERENCES

1. Armstrong CG, Mow VC: Variations in the intrinsic mechanical properties of human articular cartilage with age, degeneration, and water content. *J Bone Joint Surg [Am]* 64:88-94, 1982.

2. Armstrong S, Read R, Ghosh P: The effects of intraarticular hyaluronan on cartilage and subchondral bone changes in an ovine model of early osteoarthritis. *J Rheumatol* 21:680-688, 1994.

2. Barr AR, Duance VC, Wotton SF, Waterman AE: Influence of intra-articular sodium hyaluronate and polysulphated glycosaminoglycans on the biochemical composition of equine articular surface repair tissue. *Equine Vet J* 26:40-42, 1994.

4. Bayliss MT: Metabolism of animal and human osteoarthritic cartilage. In: *Articular Cartilage and Osteoarthritis*, 1st ed, pp 487-500. Ed by KE Kuettner, R Schleyerbach, JG Peyron, VC Hascall. New York, Raven Press, 1992.

5. Donahue JM, Buss D, Oegema TR Jr, Thompson RC Jr: The effects of indirect blunt trauma on adult canine articular cartilage. *J Bone Joint Surg [Am]* 65:948-957, 1983.

6. Ewers BJ, Newberry WN, Garcia JJ, Haut RC: Alterations in the mechanical properties of bone underlying articular cartilage in a traumatized joint. *44th ann. meeting ORS* 459, 1998.

7. Fubini SL, Boatwright CE, Todhunter RJ, Lust G: Effect of intramuscularly administered polysulphated glycosaminoglycan on articular cartilage from equine joints injected with methylprednisolone acetate. *Am J Vet Res* 54:1359-1365, 1993.

8. Gaustad G, Larsen S: Comparision of polysulpated glycosaminoglycan and sodium hyaluronate with placebo in treatment of traumatic arthritis in horses. *Equine Vet J* 27:356-362, 1995.

9. Glade MJ: Polysulphated glycosaminoglycan accelerates net synthesis of collagen and glycosaminoglycans by arthritic equine cartilage tissues and chondrocytes. *Am J Vet Res* 51:779-785, 1990.

10. Golding J, Ghosh P: Drugs for osteoarthrosis II. The effect of glycosaminoglycan polysulfate ester (Arteparon) on proteoglycan aggregation and loss from articular cartilage of immobilized rabbit knee joints. *Curr Ther Res* 34:67-80, 1983.

11. Hannan N, Ghosh P, Bellenger C, Taylor T: Articular cartilage damage produced by meniscectomy in the canine. *J Orthop Res* 5:47-59, 1987.

12. Hayes WC, Keer LM, Herrmann G, Mockros LF: A mathematical analysis for indentation tests of articular cartilage. *J Biomech* 5:541-551, 1972.

13. Howell DS, Carreno MR, Pelletier JP, Muniz OE: Articular cartilage breakdown in a lapine model of osteoarthritis: action of glycoaminoglycan polysulfate ester (GAGPS) on proteoglycan enzyme activity, hexuronate, and cell counts. *Clin Orthop* 213:69-76, 1986.

14. Jurvelin J, Säämänen A-M, Arokoski J, Helminen HJ, Kiviranta I, Tammi M: Biomechanical properties of the canine knee articular cartilage as related to matrix proteoglycans and collagen. *Eng Med* 17:157-162, 1988.

15. Kempson GE, Spivey CJ, Swanson SAV, Freeman MAR: Patterns of cartilage stiffness on normal and degenerate human femoral heads. *J Biomech* 4:597-609, 1971.

16. May SA, Hooke RE, Lees P: The effect of various drugs used in the treatment of equine degenerative joint disease on equine stromelysin (proteoglycanase). *Br J Pharmacol* 93:281, 1988.

17. Mazières L, Berdah M, Thiéchart, Viguier G: Étude de la diacetylrheine sur un modèle post-contusif d'arthrose expérimentale chez le lapin. *Rev Rhum [Ed Fr]* 60:77S-81S, 1993.

18. Mizrahi J, Maroudas A, Lanir Y, Ziv I Webber TJ: The "instantaneous" deformation of cartilage: effects of collagen fiber orientation and osmotic stress. *Biorheology* 23:311-330, 1986.

19. Newberry WN, Zukosky DK, Haut RC: Subfracture insult to a knee joint causes alterations in the bone and in the functional stiffness of overlying cartilage. *J Orthop Res* 15:450-455, 1997.

20. Newberry WN, MacKenzie CD, Haut RC: Blunt impact causes changes in bone and in cartilage in a regularly exercised animal model. *J Orthop Res* 16:348-354, 1998.

21. Oyen-Tiesma M, Atkinson J, Haut RC: A method for promoting regular rabbit exercise in orthopaedics research. *Contemporary Topics in Laboratory Animal Science* 37:77- 80, 1998.

22. Radin EL, Martin RB , Burr DB, Caterson B, Boyd RD, Goodwin C: Effects of mechanical loading on the tissues of the rabbit knee. *J Orthop Res* 2:221-234, 1984.

23. Trotter GW, Yovich JV, McIlwraith CW, Norridin RW: Effects of intramuscular polysulphated glycosaminglycan on chemical and physical defects in equine articular cartilage. *Can J Vet Res* 43:224-230, 1989.

TABLES

Table 1: Instantaneous (unrelaxed) shear modulus (G_U) and relaxed shear modulus (G_R) of the articular cartilage for each group (Ave ± SD).

Group		G_U (MPa)	G_R (MPa)
CONT	Right	0.936 ± 0.137	0.285 ± 0.071
	Left	0.949 ± 0.138	0.278 ± 0.062
NO PSGAG	Impacted	0.570 ± 0.156 $^{+\$*}$	0.226 ± 0.062 $^{+}$
	Unimpacted	1.081 ± 0.276	0.323 ± 0.092
PSGAG	Impacted	0.940 ± 0.180	0.297 ± 0.066
	Unimpacted	0.910 ± 0.253	0.311 ± 0.077

CONT - control group (n=8)
NO PSGAG - no treatment (n=7)
PSGAG - 6 weeks of treatment (n=8)

\+ - Significantly different from unimpacted side
$ - Significantly different from controls
* - Significantly different from impacted side on PSGAG group

Table 2: Subchondral plate thickness at three locations for each group (Ave ± SD, n=8).

Group		Medial (mm)	Central (mm)	Lateral (mm)
CONT	Right	0.45 ± 0.09	0.62 ± 0.21	0.46 ± 0.11
	Left	0.41 ± 0.08	0.62 ± 0.20	0.46 ± 0.12
NO PSGAG	Impacted	0.48 ± 0.09 $^{+}$	0.64 ± 0.09 $^{+}$	0.43 ± 0.08
	Unimpacted	0.38 ± 0.06	0.52 ± 0.12	0.38 ± 0.06
18 PSGAG	Impacted	0.54 ± 0.14 $^{+}$	0.84 ± 0.19 $^{+}$	0.50 ± 0.10
	Unimpacted	0.41 ± 0.12	0.52 ± 0.15	0.33 ± 0.06

CONT - control group
NO PSGAG - no treatment
PSGAG - 6 weeks of treatment

\+ - Significantly different from unimpacted side

FIGURES

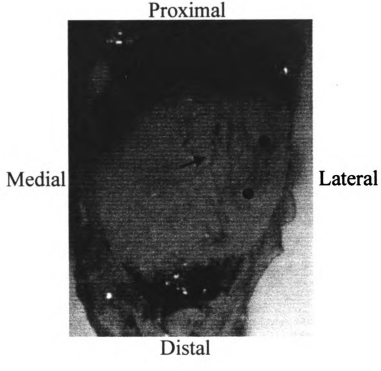

Figure 1: Impact fissures were found on the lateral side of the central ridge between the patellar facets (➡). Indentation tests were conducted at two locations along the lateral facet (●) (x7.5).

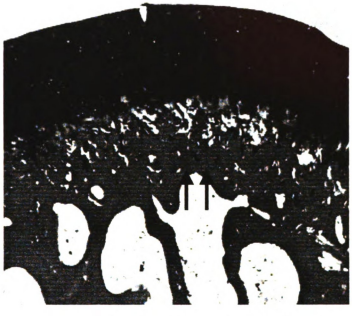

Figure 2: The subchondral bone thickness was measured at three locations: midline of the patella, and at the midline of the medial and lateral facets. The thickness was measured with a calibrated eyepiece between the tidemark and trabecular bone (→).

(A)

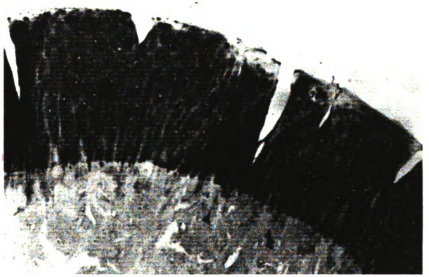

(B)

Figure 3: No differences were grossly observed in the histological appearance of lesions in the retropatellar cartilage of the impacted (A) and impacted with PSGAG treatment (B) groups.

CHAPTER 7

THE EXTENT OF MATRIX DAMAGE AND CHONDROCYTE DEATH IN MECHANICALLY TRAUMATIZED ARTICULAR CARTILAGE EXPLANTS DEPENDS ON RATE OF LOADING

Ewers BJ, [+]Dvoracek-Driksna D, [+]Orth MW, and Haut RC

SUMMARY

Mechanical loads can lead to matrix damage and chondrocyte death in articular cartilage. This damage has been implicated in the pathogenesis of secondary osteoarthritis. Studies on cartilage explants with the attachment of underlying bone at high rates of loading have documented cell death adjacent to surface lesions. On the other hand, studies involving explants removed from bone at low rates of loading suggest no clear spatial association between cell death and matrix damage. The current study hypothesized that the observed differences in the distribution of cell death in these studies are attributed to the rate of loading. Ninety bovine cartilage explants were cultured for two days. Sixty explants were loaded in unconfined compression to 40 MPa in either a fast rate of loading experiment (~900 MPa/s) or a low rate of loading experiment (40 MPa/s). The remaining thirty explants served as a control population. All explants were cultured for four days after loading. Matrix damage was assessed by measuring the total length and average depth of surface lesions and the release of glycosaminoglycans to the culture media. Explants were sectioned and stained with calcein and ethidium bromide homodimer to document the number of live and dead cells. Greater matrix damage was

documented in explants subjected to a high rate of loading, compared to explants exposed to a low rate of loading. The high rate of loading experiments resulted in cell death adjacent to fissures, whereas more dead cells were observed in the low rate of loading experiments and a more diffuse distribution of dead cells was observed away from the fissures. In conclusion, this study indicated that the rate of loading can significantly affect the degree of matrix damage, the distribution of dead cells, and the amount of cell death in unconfined compression experiments on explants of articular cartilage.

INTRODUCTION

Excessive levels of mechanical load can generate matrix damage and chondrocyte death in articular cartilage (Jeffrey et al., 1995). Matrix damage has been documented following severe blunt impacts to a joint using an animal model of osteoarthrosis (OA) (Newberry et al., 1998), and clinically it is seen in the early stages of OA (3). Chondrocyte death, leading to a reduction in tissue cellularity or chondrocyte malfunction, has been suggested to facilitate development of OA (Blanco et al., 1998; Buckwalter, 1995). Death of chondrocytes has also been shown to result in long-term degradation of cartilage *in vivo* (Simon et al., 1976).

Studies using cartilage explants with the attachment of underlying bone have documented matrix damage and cell death following blunt insult at high rates of loading. Oyen-Tiesma et al. (1999), using a single insult of 53 MPa in 250 ms (212 MPa/s) onto an explant of cartilage, documented that cell death correlated with the degree of mechanical disruption to the matrix. The study observed that cell death occurred adjacent to surface fissures, and the investigators did not observe cell death in specimens without visible damage to the matrix. Another study, using a single insult of load ranging from 30

to 50 MPa with a time to peak ranging from 40 to 100 ms (350 – 1250 MPa/s), showed cell death adjacent to fissures in 12 of 15 specimens (Repo and Finlay, 1977).

Other studies, using cartilage explants without underlying bone and for low rates of loading have also documented matrix damage and cell death. Torzilli et al. (1999), using a single impact of 20 MPa in 571 ms (35 MPa/s), documented surface fibrillation into the middle zone of cartilage directly under the indentor. Cell death was also localized under the indentor, but extended throughout the thickness of the explant. Quinn et al. (1998) saw no clear spatial association between cracks in the matrix and cell viability. That study used a very low rate of loading that compressed explants to 50 % strain in 15 seconds, and the load was held for one hour.

The distribution of cell death with respect to visible matrix damage is inconsistent between these two types of studies. Interestingly, these studies exhibit two important differences that may help explain the contrasting results: high rate of loading with the attachment of bone, and a lower rate of loading on explants without bone. The constraint of the underlying bone has been suggested to have a protective effect on the matrix of cartilage during mechanical loading (Jeffrey et al., 1995). Articular cartilage exhibits a flow-dependent viscoelastic behavior due to its biphasic composition (Mow et al., 1980). Studies have suggested that at high rates, loads on this biphasic tissue are mainly supported by the fluid phase, while for lower rate experiments or at equilibrium, the loads are supported by the solid phase (Ateshian and Wang, 1995; Mow et al., 1980).

Our previous study using unconfined compression of cartilage explants documented an increase in matrix damage and cell death with increasing load for two different loading rates (Ewers et al., 2000). The study also suggested that at a severe load

level, the higher rate of loading (~900 MPa/s) produced more matrix damage compared to a lower rate of loading (40 MPa/s). Furthermore, it grossly appeared that the low rate of loading experiments resulted in more cell death than the high rate of loading experiments especially at an applied pressure of 40 MPa.

The aim of the current study was to investigate the effect of loading rate on the extent of matrix damage and cell death in severely traumatized explants of articular cartilage. Based upon the rate dependent nature of cartilage and earlier studies (Chen et al., 1999; Ewers et al., 2000), we hypothesized that the extent of matrix damage would be higher in high versus low rate of loading experiments, while cell death would be greater in low versus high rate experiments.

METHODS AND MATERIALS

Bovine forelegs were obtained within three hours of slaughter (18-24 months of age). The legs were cut just above the knee joint leaving the metacarpal joints intact. The legs were rinsed with distilled water, skinned and then rinsed again prior to opening the knee joint under a laminar flow hood. A 6.35 mm punch with a smooth edge was used to make 90 plugs, approximately 15 from the metacarpal surfaces of each limb. The plugs were separated from the underlying bone using a scalpel. The specimens were placed in a petri dish containing Dulbecco's Modified Eagle's Medium (DMEM): F12 (Gibco, USA #12500-039). All explants were washed three times (10 minutes each wash) in DMEM: F12. Approximately 60 mg of cartilage (2 explants) was placed randomly in wells. Each well contained one ml of DMEM: F12 supplemented with 50 μg/ml ascorbic acid, 20% fetal bovine serum, additional amino acids, and antibiotics (penicillian 100 units/ml, streptomycin 1.0 μg/ml, amphotericin B 0.25 μg/ml) (Rosselot et al., 1992). The explants

were allowed to equilibrate in this media for two days in a humidity-controlled incubator (37^0 C, 7.2% CO_2, NuAire, Plymouth, MN).

After equilibration, thirty explants (15 wells) were randomly assigned to a non-impact control group. The remaining specimens were assigned to either a high rate (45 milliseconds to peak, ~900 MPa/s, n=30) or low rate (1 second to peak, 40 MPa/s, n=30) impact test group. The thickness of each explant was measured using a digital micrometer (Digimatic, Mitutoyo Corp., Japan). Each specimen was loaded to a peak load of 1247 N (~ 40 MPa) using a single haversine load-time pulse. The specimens were placed between two highly polished stainless steel plates in an unconfined compression experiment using a servo-hydraulic machine (Instron, model 1331, Canton, MA). During this entire process sterility was maintained. Peak load, time to peak load, and maximum displacement were recorded in each experiment. After loading, the explants were washed in media three times (ten minutes each wash) before placing them in pre-assigned wells. One ml of media was added to each well. Media were collected from each well and replaced daily for four days post-test.

One day post-test five explants from each group were randomly chosen for the cell viability study. Two 1 mm slices were cut from the center of each explant using a specialized cutting tool. The sections were stained with a kit containing calcein and ethidium bromide homodimer (Live/Dead & Viability/Cytotoxicity, Molecular Probes, Oregon). All specimens were viewed in a florescence microscope (Leica DM LB (frequency: 50-60 Hz), Lecia Mikroskopie und Systeme GmgH, Wetlzar, Germany). Full thickness digital images (100x) of the explant were taken at the center of impact over a 2.5 mm length for each slice (Spot Digital Camera, Diagnostic Instruments Inc.). Cell

viability was quantified by manually counting the dead (red) and viable (green) cells for each explant using image software (Sigma Scan, SPSS Inc., Chicago, IL). The data from the two slices were averaged for each explant. The above procedure was repeated on another five explants from each group four days post-test. The remaining explants, not used for the cell viability study, were stained with India ink to highlight surface fissures. Surface photographs were made of each explant. Two full width sections of each explant were used to estimate the depth of these surface lesions. The total length of the surface fissuring was measured in the photographs, and their average depth through the thickness was documented using image software (Sigma Scan, SPSS Inc., Chicago, IL).

Following the last collection from each well, the media were quantitatively analyzed for nitric oxide and glycosaminoglycans. Nitric oxide was determined as previously described and documented as the concentration of nitrite in the media per well per day (Orth et al., 1999). The content of glycosaminoglycan in each well was determined using the DMB assay (Chandrasekhar et al., 1987). Chondroitin sulphate was used as a standard.

The data for lesion length and depth and chondrocyte viability was subjected to an ANOVA with SNK post-hoc tests. Nitric oxide and glycosaminoglycan concentrations were analyzed every day post-test with an ANOVA and SNK post-hoc tests. T-tests were used at each strain level to compare axial stress generated for high and low loading rate experiments. Statistical significance was indicated at $p < 0.05$.

RESULTS

The peak load generated in the high rate of loading group was not significantly different compared to that in the low rate of loading group (1245 ± 13 N). The time to

peak was 43.0 ± 2.3 ms (~930 MPa/s) and 1.00 ± 0.01 seconds (40 MPa/s) for the high and low rate of loading groups, respectively. The maximum strain produced in specimens from the high rate group was significantly decreased relative to the low rate group (0.409 ± 0.074 versus 0.476 ± 0.088). The stress generated at strains ranging from 0.1 to 0.5 in the high rate of loading experiments was significantly greater than that generated in the low rate of loading experiments (Figure 1).

Gross observations after loading indicated surface fissures existed across the top surface for all loaded explants (Figure 2). No fissures were observed on the sides or bottoms of any loaded or control explants. Two unimpacted, control explants had one superficial lesion each. There was a statistically significant greater total length of fissuring, and average depth of the fissuring for both test groups compared to controls, as expected (Table 1). Importantly, the specimens loaded at the high rate had a significantly greater total length and average depth of surface lesions than measured on explants loaded at the low rate.

Cell viability was not significantly different in any group between one and four days post-test, so the data were pooled. No differences were seen in the total number of cells between groups (Table 1). Since at the edge (approximately 5 % of the diameter) of each specimen there was a small region of cell death due to the punch (22), this region was not included in the digital analysis. While there was a significant increase in the number of dead cells and percentage of dead versus live cells for both test groups compared to controls, in explants subjected to a low rate of loading the number of dead cells and the percentage of dead to live cells was significantly higher than in explants subjected to a high rate of loading. Qualitatively it was observed that the distribution of

dead cells from the high loading rate experiments was typically near the surface fissures (Figure 3). In contrast, following the low rate of loading experiments a more diffuse distribution of dead cells was present throughout the explant. However, in this study, only total number of dead cells within the defined area of full thickness to 2.5 mm slices was quantified using the image analysis software. Differences in distribution of dead cells among different locations within the defined area were not quantified. Our cell viability assay does not distinguish between apoptosis and necrosis. However, in a preliminary study (unpublished observation) we observed all cell death occurring by three hours, which suggests that the majority of cells are dying by necrosis, not apoptosis.

One day after loading the explants there was a significant increase of NO in specimens from the high rate of loading group compared to controls (Figure 4). This was followed by an increase of NO in specimens from both test groups compared to controls at two days. The amount of NO returned to control levels in both test groups at day three. No NO was measured in the media of any group after four days. Glycosaminoglycan released to the media increased for both traumatized groups compared to controls each day post-test (Figure 5). A significantly greater amount of glycosaminoglycan was released to the media from those explants subjected to a high rate of loading (96 $\pm$ 6 μg/ml) than from those exposed to a low rate of loading (74 $\pm$ 6 μg/ml) after one day in culture. After two days, however, the amount of glycosaminoglycan released to the media from explants subjected to the low rate of loading (85 $\pm$ 7 μg/ml) was greater than that released from specimens exposed to the high rate of loading (75 $\pm$ 4 μg/ml). At days three and four there were no significant differences in the amount of glycosaminoglycan released to the media between the test groups of explants.

DISCUSSION

Our hypothesis was supported in the current study. We documented greater matrix damage in the explants subjected to a high rate of loading compared to explants exposed to a low rate of loading. The high rate of loading experiments resulted in cell death adjacent to fissures, whereas the low rate of loading experiments produced a more diffuse distribution of cell death away from the fissures. Interestingly, we found that the low rate of loading experiments produced more cell death compared to the high rate of loading experiments at a given applied pressure.

The applied pressure in the current study was chosen based upon a previous study that documented significant matrix damage and cell death with both the high and low rates of loading (Ewers et al., 2000). Furthermore, the high rate of loading (~900 MPa/s) and the low rate of loading (40 MPa/s) are representative of the previous two sets of studies examining matrix damage and cell death. The current study was consistent with this previous study in that a low rate of loading grossly resulted in more cell death compared to a high rate of loading. The earlier study also suggested that a higher rate of loading would result in more matrix damage versus a lower rate of loading.

The results of the current study compare well to previous studies of others. Chen et al. (1999) using a repetitive loading protocol on cartilage explants, documented increased water content, indicative of matrix damage, compared to controls for an impact event with a peak stress of 2.5 MPa for a 30 MPa/s or greater maximum stress rate. On the other hand, a smoothly rising load did not result in increased water content until the peak stress was 10 MPa for a 30 MPa/s or greater maximum stress rate. In the current study the high rate of loading resulted in cell death largely adjacent to fissures, which has

also been documented in previous studies using higher rates of loading (Oyen-Tiesma et al., 1999; Repo and Finlay, 1977). The low rate of loading experiment produced a more diffuse distribution of cell death, which is similar to previous studies that documented no clear spatial association between cell death and matrix fissures with lower rates of loading (Quinn et al., 1998; Torzilli et al., 1999). Loening et al. (1999), however, using a low rate of loading (32 MPa/s) on cartilage explants documented chondrocyte apoptosis before detectable mechanical damage as measured by glycosaminoglycan (GAG) release, water content, and altered material properties.

The increase in NO released into the media after loading at one and two days post-test was similar to previous studies that documented a marginally significant increase in NO one day after severe compression (Loening et al., 1999). However, the concentrations of NO were very low relative to cytokine-stimulated NO production (unpublished observation). Thus the relevance of the released NO during loading needs to be clarified. The current study documented an increase in GAGs released into the media for both rate of loading experiments compared to controls out to four days post-trauma. This result was similar to a previous study that documented an increase in proteoglycan release into the media out to six days post-loading (Quinn et al., 1998). Based upon a previous study, the content of proteoglycan in bovine articular cartilage is approximately 32 μg/mg (Homandberg et al., 1992). During two days of equilibration the DMB assay indicated an approximate 10% loss of GAG. On average the loaded explants lost approximately 12% more GAG after four days, while the control explants lost approximately 6%. The greater release of GAGs for the high rate of loading experiments compared to the low rate of loading group at one day post-test may be the result of more

matrix damage, allowing for the release of GAGs to the media. On the other hand, at two days post-test the low rate of loading experiments produced a higher level of GAG released to the media than for the high rate of loading group. This result might have been caused by the higher cell death for the low rate of loading experiments resulting in a cell-mediated degradation of proteoglycans after two days in culture. It is unclear if this loss of GAG represents cell-mediated degradation or a direct loss due to matrix damage (Kurz et al., 2000). At this time the mechanism of GAG release into the media is unknown and would require further investigation.

The observed differences between the high and low rate of loading experiments may be due to the flow-dependent viscoelastic behavior of articular cartilage. Since cartilage is biphasic, faster rates of loading result in more of the load being supported by the fluid phase, causing an increase in tissue fluid pressure. These large fluid pressures result in correspondingly larger tensile stresses in the solid matrix, which may be responsible for producing gross fissuring of the articular cartilage (Garcia et al., 2000). However, a contact analysis of transversely isotropic, biphasic cartilage showed no changes in contact area out to one second after application of joint load, suggesting a minimal rate of loading effect over this time frame (Donzelli et al., 1999). Conversely, a non-linear, biphasic model of cartilage may result in an increased percentage of the load being carried by the fluid at large deformations (Garcia et al., 2000). Cartilage, when modeled as a non-linear, biphasic material, may result in significant differences in the stress field for high and low rate of loading experiments, which would help explain the findings of the current study. A further complexity in the analysis of the stress field results from the fissures that are generated during the loading of these explants. Fissures

would cause large stress concentrations, dramatically altering the stress field. Thus, it is clear that the stress field is not uniform through these explants, and further computational modeling is needed to describe the stress causing surface lesions and cell death.

One limitation of the current study was that the cartilage was removed from the underlying bone before loading. Bone is known to constrain the cartilage, and this has been suggested to have a protective effect on the cartilage matrix during loading (Jeffrey et al., 1995). Thus, a layer of underlying bone would likely alter the state of stress in the cartilage, and therefore change the stress state around fissures to alter the propagation of these lesions and the distribution of dead cells. It was interesting to note that in the current study, even without the constraint of the underlying bone, visible matrix damage was limited to the surface of the explant. Furthermore, the intent of this study was to explain a contradiction in the literature dealing with the influence of loading rate on matrix damage and cell death for explanted cartilage tissue. This study does not address the response of an in vivo joint to blunt loading. However, clinical studies do indicate that surface lesions and dead cells are characteristics of degenerative joint diseases such as OA (Brandt et al., 1986; Simon et al., 1976). Another limitation of this study was that it examined only a severe load level. The rate of loading effects may not be as apparent at lower levels of loading, but future studies are warranted at less severe levels of load. A final limitation is that the equilibration and possible subsequent swelling may have resulted in the tissue becoming more sensitive to mechanical loading. The increase in water content would lead to relatively more tensile stresses developed in the solid phase during impact that could enhance the extent of matrix damage (Garcia et al., 2000).

However, this effect needs further study, as does the effect of a loss of lateral constraint in the tissue explants.

In conclusion, this study indicated that the rate of loading can significantly affect the degree of matrix damage, the distribution of dead cells, and the amount of cell death in unconfined compression experiments on explants of articular cartilage. The role played by rate of loading on a joint and the pathogenesis of a chronic disease such as OA will need further investigation.

ACKNOWLEDGMENT

This study was supported by a grant for the Centers for disease Control and Prevention (R49/CCR503607). Its contents are solely the responsibility of the authors and do not necessarily represent the official views of the Centers for Disease Control and Prevention. The authors wish to gratefully acknowledge Cliff Beckett for technical assistance.

REFERENCES

1. Ateshian GA, Wang H (1995) A theoretical solution for the frictionless rolling contact of cylindrical biphasic articular cartilage layers. *J Biomech* 28:1341-1355.

2. Blanco FJ, Guitian R, Vazquez-Martul E, de Toro FJ, Galdo F (1998) Osteoarthritis chondrocytes die by apoptosis. A possible pathway for osteoarthritis pathology. *Arthritis Rhuem* 41:284-289.

3. Brandt KD, Mankin HJ, Shulman LE (1986) Workshop on etiopathogenesis of osteoarthrits. *J Rhuematol* 13:1126-1160.

4. Buckwalter JA (1995) Osteoarthritis and articular cartilage use, disuse, and abuse: experimental studies. *J Rhuematol Suppl* 43:13-15.

5. Chandrasekhar S, esterman MA, Hoffman HA (1987) Microdetermination of proteoglycans and glycosaminoglycans in the presence of guanidine hydrochloride. *Anal Biochem* 161:103-108.

6. Chen C-T, Burton-Wurster N, Lust G, Bank RA, Tekoppele JM (1999) Compositional and metabolic changes in damaged cartilage are peak-stress, stress-rate, and loading duration dependent. *J Orthop Res* 17:870-879.

7. Donzelli PS, Spilker RL, Ateshian GA, Mow VC (1999) Contact analysis of biphasic transversely isotropic cartilage layers and correlations with tissue failure. *J Biomech* 32:1037-1047.

8. Ewers BJ, Dvoracek-Driksna D, Orth MW, Haut RC (2000) Matrix damage and chondrocyte death in articular cartilage depends upon loading rate. *Transactions 46th ORS* (abstract).

9. Garcia JJ, Altiero NJ, Haut RC (2000) An approach for the stress analysis of transversely isotropic biphasic cartilage under impact load. *J Biomech Eng*, 122:1-8.

10. Homandberg GA, Meyers R, Xie D (1992) Fibronectin fragments cause chondrolysis of bovine articular cartilage slices in culture. *J Bio Chem* 267(6):3597-3604.

11. Jeffrey JE, Gregory DW, Aspden RM (1995) Matrix damage and chondrocyte viability following a single impact load on articular cartilage. *Arch Biochem Biophys* 322:87-96.

12. Kurz B, Jin M, Patwari P, Lark MW, Grodzinsky AJ (2000) Biosynthetic response and mechanical properties of articular cartilage after injurious compression: The importance of strain rate. *Transactions 46th ORS* (abstract).

13. Loening AM, Levenston ME, James IE, Nuttal ME, Hung HK, Gowen M, Grodzinsky AJ, Lark MW (1999) Injurious compression of bovine articular cartilage induces chondrocyte apoptosis before detectable mechanical damage. *Transactions 45th ORS* (abstract).

14. Mow VC, Kuei SC, Lai WM, Armstrong CG (1980) Biphasic creep and stress relaxation of articular cartilage in compression: Theory and experiments. *J Biomech Eng* 102:73-84.

15. Newberry WN, Mackenzie CD, Haut RC (1998) Blunt impact causes changes in bone and cartilage in a regularly exercised animal model. *J Orthop Res* 16:348-354.

16. Orth MW, Fenton JI, Chlebek-Brown KA (1999) Biochemical characterization of cartilage degradation in embryonic chick tibial explant cultures. *Poultry Science* 78:1596-1600.

17. Oyen-Tiesma M, Deloria LB, Meglitsch T, Oegema TR, Lewis JL (1999) Cell death after cartilage impact depends on matrix damage. *Transactions 45th ORS* (abstract).

18. Quinn TM, Grodzinsky AJ, Hunziker EB, Sandy JD (1998) Effects of injurious compression on matrix turnover around individual cells in calf articular cartilage explants. *J Orthop Res* 16:490-499.

19. Repo RU, Finlay JB (1977) Survival of articular cartilage after controlled impact. *J Bone Joint Surg [Am]* 59: 1068-1076.

20. Rosselot G, Reginato AM, Leach RM (1992) Development of growth hormone an insulin-like growth factor I on cultured post-embryonic growth plate chondrocytes. *In Vitro Cell Dev Biol* 28A:235-244.

21. Simon WH, Richardson S, Herman W, Parsons JR, Lane J (1976) Long-term effects of chondrocyte death on rabbit articular cartilage in vivo. *J Bone Joint Surg [Am]* 58:517-526.

22. Tew SR, Kwan APL, Hann A, Thompson BM, Archer CW (2000) The reactions of articular cartilage to experimental wounding: Role of apoptosis. *Arth Rheum* 43:215-225.

23. Torzilli PA, Grigiene R, Borrelli Jr. J, Helfet DL (1999) Effect of impact load on articular cartilage: Cell metabolism and viability, and matrix water content. *J Biomech Eng* 121:433-441.

TABLES

Table 1: Quantification of matrix damage and chondrocyte viability for control (Control), high rate of loading experiments (High), and low rate of loading experiments (Low) (Avg ± SD).

	Control	High	Low
Matrix Damage [a]			
Total fissure length (mm)	0.2 ± 0.5	62.4 ± 15.7 *	52.1 ± 11.4 *+
Average fissure depth (%)	1.5 ± 4.4	34.5 ± 10.5 *	23.0 ± 8.2 *+
Chondrocyte Viability [b]			
Total cells (#)	163 ± 59	177 ± 45	172 ± 55
Dead cells (#)	17 ± 10	83 ± 29 *	122 ± 35 *+
Dead cells (%)	9 ± 6	47 ± 12 *	66 ± 13 *+

a - n = 18
b - n = 10
* - significantly greater versus control group by ANOVA.
+ - significantly different versus high rate of loading experiments by ANOVA.

FIGURES

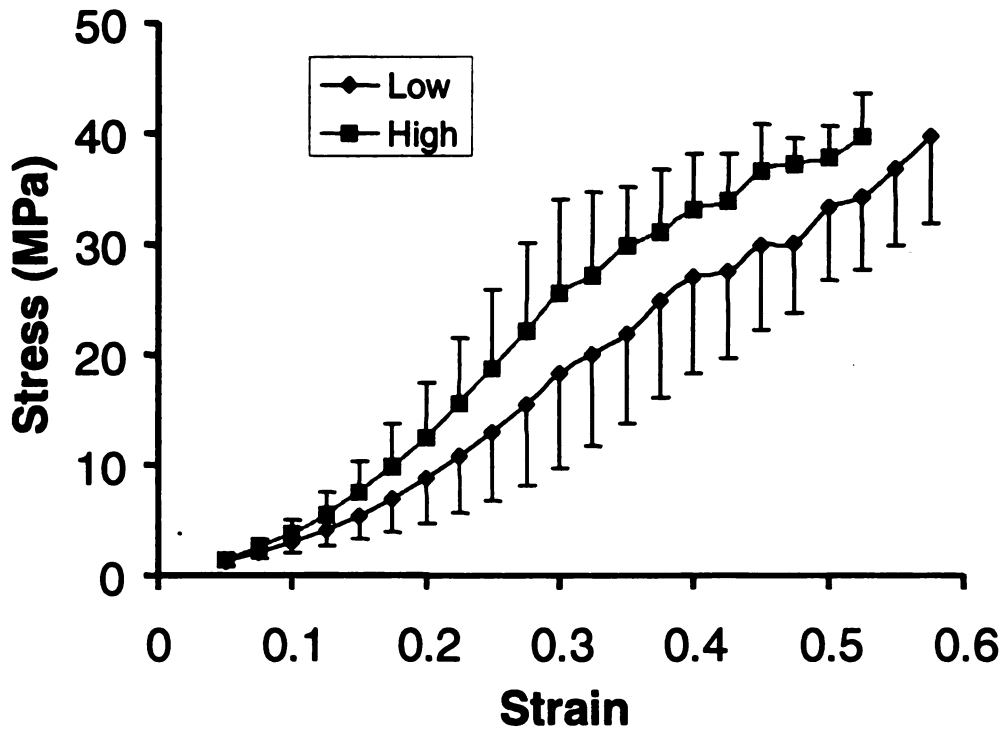

Figure 1: The average stress-strain responses of cartilage in unconfined compression for high (■) and low (◆) rate of loading experiments (Ave ± SD). There was a significant increase in the stress generated in the high rate of loading experiments compared to the low rate of loading experiments for compressive strains levels ranging from 0.1 to 0.5 ($p < 0.05$).

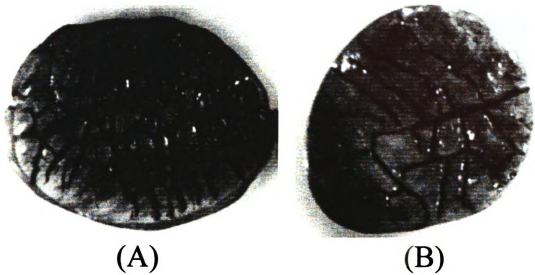

Figure 2: The surfaces of the cartilage explants were wiped with India ink to highlight surface fissures. Typical specimens are shown from the high rate of loading group (**A**) and from the low rate of loading group (**B**).

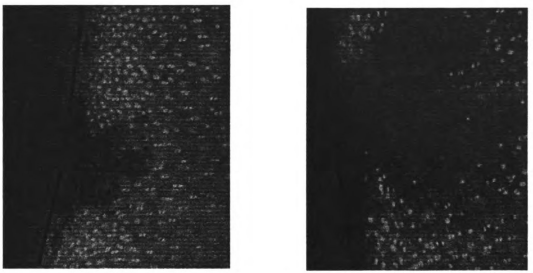

(A) (B)

Figure 3: In the stained sections of the explants it was impossible to distinguish the dead cells in the grayscale image. The image was digitally altered to make the background gray, the live cells appear as light gray points and the dead cells appear as black points. The sections are oriented with the surface to the left. The cartilage surface and fissure have been outlined in these sections, since they are difficult to distinguish. The high rate of loading experiments typically showed cell death adjacent to the surface fissure (**A**). The low rate of loading experiments typically indicated a greater range of cell death with dead cells beyond the fissure (**B**).

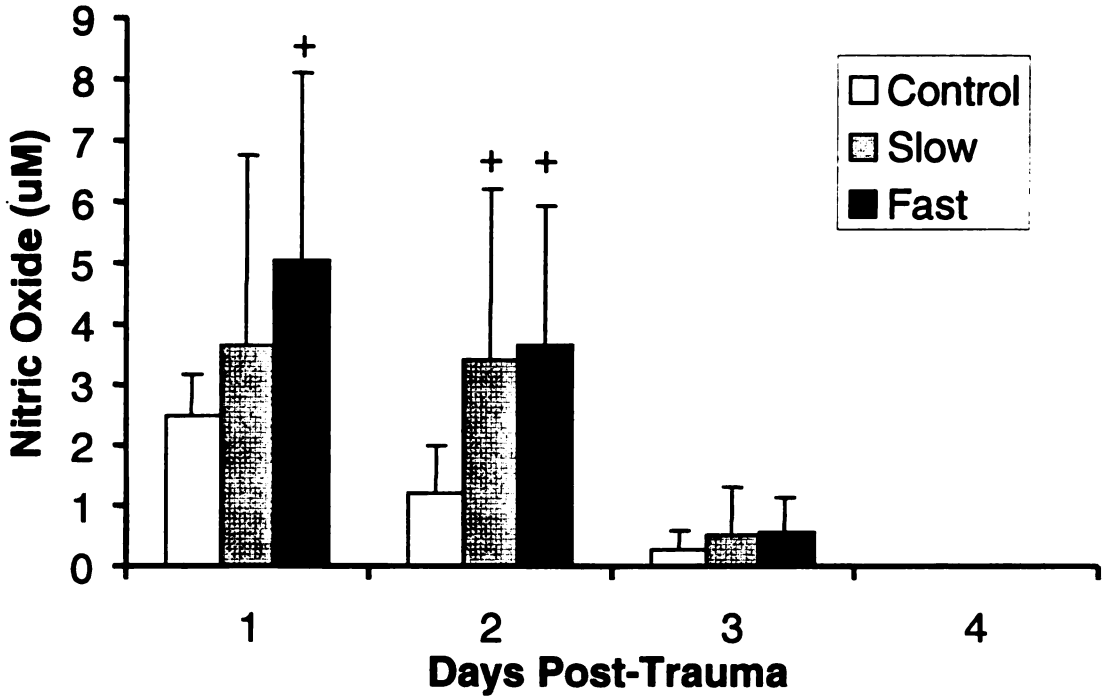

Figure 4: The average amount of nitric oxide (NO) released into the media per well each day post-test for control (Control), high rate of loading experiments (High), and low rate of loading experiments (Low) (Ave ± SD, n=12). The (+) symbol indicates a statistically significant increase in NO release compared to controls at that day post-test ($p < 0.05$).

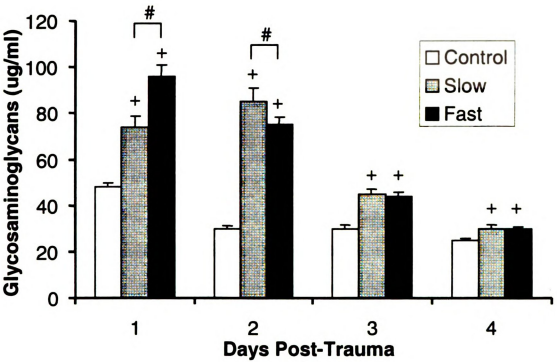

Figure 5: The average glycosaminoglycan released into the media each day post-test control (Control), high rate of loading experiments (High), and low rate of loading experiments (Low) (Ave ± SD, n=12). The (+) symbol indicates a statistically significant increase in glycosaminoglycan release compared to controls at that day post-test ($p < 0.05$). The (#) symbol indicates a statistically significant difference between high rate of loading experiments and low rate of loading experiments ($p < 0.05$).

CHAPTER 8

THEORETICAL MODELS OF CARTILAGE EXPLANTS AND CORRELATIONS WITH EXPERIMENTAL MATRIX DAMAGE AND CELL DEATH AFTER IMPACTING LOADS

Ewers BJ, Krueger JA, +Dvoracek-Driksna D, +Orth MW, Haut RC

ABSTRACT

Excessive mechanical loading of articular cartilage can lead to matrix damage and chondrocyte death. The relationship between this damage and secondary osteoarthritis is still unknown. In vitro studies of explants have suggested that matrix damage and cell death correlate with the state of stress and strain produced by applied boundary tractions. Recently, however, confocal microscopy has shown that local matrix strains differ from the strains produced in adjacent cells under physiological loading. The current study documents mechanically induced matrix damage and cell death in explants, and then attempts to correlate the mechanical damage with the state of stress and strain in the matrix and embedded cells. Thirty bovine cartilage explants were equilibrated for two days. Ten served as controls and the remaining randomly underwent unconfined compression to 30 MPa at either a high (~667 MPa/s) or low rate of loading (30 MPa/s). Matrix damage and cell viability were documented for each group. The experimentally determined displacements for both the high and low rate experiments were then applied to isotropic and transversely isotropic computational models of the explant, with or without depth-dependent, matrix material properties. The amount of displacement on a

cell was then linearly interpolated and applied to a computational model of the cell. The isotropic model with depth-dependent material properties best associated areas of high stress with matrix damage and predicted the lateral expansion profiles documented in the recent literature. The current study also suggested that the extent of cell strain in each layer was most influenced by the shape of the cell, not the depth-dependent material properties of the matrix.

INTRODUCTION

Osteoarthritis (OA) is a disease affecting diarthrodial joints and is characterized by full thickness loss of articular cartilage resulting in bone-on-bone contact and joint pain. OA may cost society $54 billion annually in treatment and lost workdays (Hamermann, 1989). Excessive and abnormal mechanical loading of cartilage has been implicated in the pathogenesis of OA. Clinically, matrix damage of cartilage, such as surface fissuring, and chondrocyte death have been documented in osteoarthritic cartilage (Kim et al., 2000). However the role of acute injuries, such as those given above, in the mechanism of a post-traumatic, secondary OA are not well understood.

In vitro studies, using isolated cartilage explants, have attempted to correlate excessive mechanical loading with cell death and matrix damage. In hallmark studies Repo and Finlay (1977), using tissue explants on bone and subjected to a single impact of 25 MPa pressure, document cell death localized around fissures in the superficial layer of the cartilage. Torzilli et al. (1999) also documents cell death in the superficial zone of cartilage explants without bone at lower applied pressure (10 MPa). Chen et al. (1999) showed that matrix damage occurs in the same area under repetitive loading with peak boundary pressures of 2.5 MPa. Ewers et al. (2000) document in cartilage explants

without underlying bone that the rate of loading can affect the distribution of cell death. They found that a low rate of loading (40 MPa/s) causes cell death deeper in the explant compared to that occurring in a high rate of loading (800 MPa/s) experiment to the same peak load. Matrix damage, on the other hand, is primarily located in the superficial layer of the explant for both rates of loading.

The above in vitro studies have been used in attempts to correlate the state of stress and strain in a loaded cartilage explant with the locations and degree of matrix damage and cell death, by considering only the levels of applied boundary traction. Clearly, comparing studies when some explant studies have underlying bone and others do not is difficult. It is evident that with bone attached to the explant there is a distribution of tissue stress through its depth as one approaches the attached bone. Boundary tractions are also not necessarily representative of the state of tissue stress and strain through the explant thickness in the case of no underlying bone, primarily because the material properties of cartilage are known to be depth-dependent (Roth and Mow, 1980; Schingal et al., 1997). This factor may play a significant role in the non-uniform distribution of matrix damage and cell death documented in previous experimental, in vitro studies.

The state of stress and strain in the explant matrix may also be quite different than that in adjacent cells. Guilak et al. (1995) have experimentally shown with confocal microscopy that local matrix strains, in fact, are different than strains produced in adjacent cells under physiological levels of loading. Guliak and Mow (2000) have subsequently generated a computational model of cartilage cells embedded in a cartilage matrix. Their study suggests that large differences in the elastic properties of the cell and

adjacent matrix result in nearly double the strains in the cell versus the adjacent matrix. The previous study, however, did not specifically examine the effect of depth-dependent changes in the material properties of the matrix.

The object of the current study was to extend the modeling efforts of Guilak and Mow (2000) in the analysis of an impact event where cell death occurs, and attempt to correlate the distribution of matrix damage and cell death with the state of stress and strain in the explant matrix and the embedded cells. The current study will also begin to address some of the effects of depth-dependent material properties of cartilage. Tissue shear stress and tensile strains have previously been correlated with acute fissuring of cartilage (Atkinson et al., 1998). Large cell strains have also been hypothesized to cause significant leakage of fluorescent indicators across cell membranes in preliminary studies (Guliak et al., 1995). This suggests that membrane damage and the possibility of cell death may occur from excessive cell strain (Guliak et al., 1995). We hypothesize that matrix damage will correlate with high tissue stress, based on previous studies from our laboratory, and that cell death will be associated with high cell strain. For both hypotheses, we also believe that the depth-dependent material properties of the explant matrix should be considered in theoretical models.

METHODS

Mechanical Loading of the Explants

One pair of bovine forelegs were obtained from a local abattoir within six hours of slaughter, and skinned prior to opening the knee joint under a laminar flow hood. A 6-mm diameter biopsy punch was used to make 30 plugs from the metacarpal surfaces. The plugs of cartilage were removed from the underlying bone with a scalpel. The specimens

were placed in Dulbecco's Modified Eagle's Medium (DMEM):F12 (Gibco, #12500-039, and allowed to equilibrate for two days in a humidity controlled incubator (37° C, 7.2% CO_2, NuAire, Plymouth, MN). Ten explants were randomly assigned to a non-impact control group. The remaining explants were loaded to 850 N (~30 MPa) using a high rate, computer controlled haversine pulse (50 ms to peak, n=10) or a low rate pulse (1 s to peak, n=10). The specimens were loaded between two highly polished stainless steel plates in unconfined compression using a servo-hydraulic testing machine (Instron, model 1331, Canton, MA). After the impact loads were applied, 2 explants (approximately 50 mg of cartilage) were placed in each well with 1 ml of media. Cell viability was determined 24 hours post-impact using established techniques. Briefly, three 0.5 mm thick slices per explant were stained with Calcein AM and Ethidium Homodimer (Live/Dead & Viability/Cytotoxicity, Molecular Probes, Oregon). Specimens were viewed in a florescence microscope (Lecia DM LB, Lecia Mikroskopie und Systeme GmgH, Germany), and full thickness digital images were made of the center 3-mm of each slice (Spot Digital Camera, Diagnostic Instruments Inc.). Each full thickness slice was divided into three layers: superficial (top 20%), middle (50%), and deep (bottom 30%). A blinded observer (MK) quantified cell viability by manually counting live and dead cells in each zone using image software (Sigma Scan, SPSS Inc., IL). The percentage of dead cells in each zone was calculated (# dead cells / # total cells). ANOVA with SNK post-hoc tests were used to determine statistical differences in cell death in each zone for the two rates of loading, and versus controls. Data were documented as the mean ± one standard deviation. Statistical significance was indicated at $p<0.05$.

Computational Model

The geometry of the computational model (Abaqus 5.8, Hibbit, Karlsson & Sorenson Inc., RI) consisted of an axisymmetric 6-mm diameter disk of cartilage one mm thick, which corresponds to the average thickness of cartilage disks taken from bovine metacarpal joints (Ewers et al., 2000). Since it was assumed that the stainless steel surfaces in the impact experiments resulted in near frictionless interfaces with the cartilage explant, the boundary conditions for the model corresponded to a simple, unconfined compression test. The bottom nodes were fixed in the axial (thickness) direction. The top nodes on the model were vertically displaced with the average deformation recorded in either the high or the low rate of loading experiment. The mesh consisted of 300 eight-noded poroelastic elements (CAX8P). The model was divided into the same three layers as used for the cell viability experiments. For the non-layered model, each layer was given the same material properties. A biphasic analysis was used for the layered and non-layered models with either an isotropic (I) or transversely isotropic (TI) solid skeleton (Table 1). Under unconfined compression the axial direction was in compression, while the radial direction was in tension. The TI model allowed for an approximation of the differences in the compressive and tensile moduli of the cartilage explant, as given in the literature (Table 1). The axial modulus (E_{33}) was determined from Schingal et al. (1997) by averaging the confined compression modulus in each layer. Poisson's ratios were assumed zero, per Cohen et al. (1993) in each layer. The radial modulus (E_{11}) was taken from Roth and Mow (1980) by averaging the tensile moduli parallel and perpendicular to superficial split-lines for each zone. The remaining material property (out-of-plane shear modulus - G_{13}) was assumed to behave in an isotropic

manner, ie: $G_{13} = E_{33} / 2(1+\nu_{13})$. The permeability of the cartilage (k) was assumed isotropic, as given by Cohen et al. (1993). The fraction of solid volume (ϕ^s) was also taken from Cohen et al. (1993). For the isotropic model the radial and axial elastic moduli were averaged for each layer. The maximum shear stresses and the tensile strains were averaged in each layer of the matrix.

To approximate the state of strain in cells, an axisymmetric elastic microscopic cell model (Abaqus 5.8) was derived from the macroscopic cartilage model (Figure 1). The cell model combined the geometry and assumed material properties of both the cell and the pericellular matrix, per Guliak (2000). In the superficial layer, the geometry of the chondrocyte was assumed to be elliptical with a height of 5 μm and a width of 15 μm, as experimentally measured by Guilak et al.(1995). In the middle and deep zones, a spherical shape was assumed with a diameter of 15 μm (Guliak et al., 1995). The pericellular matrix was assumed to be 2.5 μm thick (Guliak and Mow, 2000; Lee et al., 1997). Both the cell and the pericellular matrix were assumed isotropic with an elastic modulus of $9.5x10^{-4}$ MPa and $1.5x10^{-3}$ MPa, respectively, and nearly incompressible (ν = 0.499) (Jones et al., 1999; Jones et al., 1997). The material properties of the matrix in the cell model were the same as those used in the macroscopic explant model. The mesh for the cell model consisted of 1550 and 1034 eight-noded axisymmetric elements (CAX8) for the elliptical and spherical cell shapes, respectively. The displacements between the nodes from one element along the axis of symmetry in the center of each layer of the macroscopic model were linearly interpolated for use as a distributed displacement boundary condition in the cell model. The average tensile (ε_1) and average maximum shear (γ_{MAX}) strains were determined in cells for each layer.

RESULTS

Unconfined compression of the cartilage explants resulted in experimental impact loads of 848 ± 11 N and 838 ± 21 N for the low and high rate of loading tests, respectively. These data were not statistically different ($p > 0.05$). The time to peak load was 1.00 ± 0.05 s and 45.0 ± 2.5 ms for the low and high rate of loading experiments, respectively ($p < 0.05$). Analysis of the load-displacement data from the experiments indicated that the low rate of loading experiments resulted in slightly more axial deformation of the explant than in the high rate of loading experiments, 0.32 ± 0.04 mm and 0.29 ± 0.04 mm, respectively. The axial deformations, however, were not significantly different ($p > 0.05$). Matrix damage was observed in all specimens (both rate of loading experiments) as minor lesions in the superficial zone with no observable radial variation (Figure 2).

Cell death was produced in all loaded specimens. Cell death did not have any observable radial variation in the loaded explants. The total percentage of dead cells following the low rate of loading experiments was significantly greater than that produced in the high rate of loading experiments, 51 ± 16% versus 33 ± 16%, respectively. Both cases resulted in significantly more dead cells than in controls (0.63 ± 0.85%). For the high and low rate of loading experiments there were significantly more dead cells in the superficial layer of the explant than in the deeper zones (Figure 3). In the superficial and middle zones a significantly higher percentage of dead cells existed in the low versus the high rate of loading experiments (Figure 4).

Using the average experimental deformations generated in the low and high rate of loading experiments, the computational explant models indicated slightly larger shear stresses and tensile strains in the matrix for the low rate of loading than for the high rate of loading models (Table 2). As expected, the non-layered computational models showed no radial or depth-dependent differences in maximum shear stresses within the matrix (Figure 5A). While the layered computational models showed only a minor radial-dependent distribution of shear stress, they did indicate depth-dependencies in maximum shear stress (Figure 5B). The layered models indicated a 5 and a 2.3 fold increase in the maximum shear stress in the superficial layer compared to the deep zone, for the isotropic and transversely isotropic models, respectively (Table 2). This region of high shear stress in the layered models corresponded with the region of experimentally produced matrix damage in the superficial layer of the explants.

The non-layered computational models showed no radial or depth-dependent differences in tensile strain in the matrix (Figure 6A). The layered models, however, indicated both radial and depth-dependent differences in matrix tensile strains. The isotropic layered model did not show significant radial-dependent changes in matrix tensile strains in the superficial and middle layers, but there was a significant increase in tensile strain in the deep layer near the edge of the model (Figure 6B). Yet, the experiments did not produce any matrix damage in this region of the explant. On average, the isotropic layered model indicated a 33% increase in matrix tensile strain through the depth of the explant. The transversely isotropic model showed large radial-dependent variations in tensile strains in all layers, with the largest strain near the edge of the explant (Figure 6C). On average, the transversely isotropic model indicated little

variation in matrix tensile strain through the depth of the explant (Table 2). Overall, the variations in maximum tensile strain in the explant models did not correspond well with the locations of matrix damage in the experiments.

The cell models resulted in larger strains in the cells than in the local matrix. As in the macroscopic explant models, due to more deformation in the low compared to high rate of loading models, the cell models indicated slightly larger tensile and shear cell strains in the low rate of loading than in the high rate of loading experiments (Table 3). The cell models indicated that the strains were minimum in the center of the cells and maximum near the periphery, with a concentric distribution that varied radially by less than 10%. The computational cell models from the non-layered explant models indicated similar average tensile strains between layers (3% variance). The cell models for the layered, isotropic explant model indicated approximately a 24% lower tensile strain in the superficial layer than in the deep layer. This was in contrast to more cell death in the superficial than in the deep zone. The layered transversely isotropic cell model also showed minor variations in tensile strains between layers (10%), and the results were also in contrast to the observed distribution of dead cells in the corresponding experiments.

The computational cell models from the non-layered explant models indicated approximately 34 and 27% increases in average shear strain for the isotropic and transversely isotropic models, respectively, in the superficial layer compared to the middle and deep zones. These results corresponded better with the experiments where significantly more dead cells were observed in the superficial layer than in the deeper layers. The layered models also indicated approximately 20 and 15% increases in average

cellular shear strain in the superficial layer compared to the deeper layers for the isotropic and transversely isotropic models, respectively.

The non-layered models also exhibited large cellular shear strains in the superficial layer compared to the deeper zones. This result indicated that the large cellular strains generated in the superficial layer may be due to the cell shape, not necessarily the depth-dependent material properties of the matrix. A small parametric study was performed by inserting a spheroidal shape cell into the superficial layer of the cartilage for the transversely isotropic, layered cell model. When the superficial cells were modeled as spheroids, rather than ellipsoids the average tensile strains were only slightly decreased from 0.36 to 0.35. On the other hand, the average cellular shear strains were more dramatically reduced from 0.62 to 0.52 for the ellipsoid versus the spheroidal cell models, respectively.

DISCUSSION

The object of the current study was to correlate the distribution of matrix damage and cell death with the state of stress and strain in the explant matrix and the embedded cells. We hypothesized that matrix damage would correlate with high tissue stress and that cell death would be associated with high cell strain. For both hypotheses, we also theorized that the depth-dependent material properties of the explant matrix would have to be considered in the theoretical models. Both matrix damage and extensive cell death were documented in the superficial layer following impact in this study. As hypothesized, a theoretical model with depth-dependent material properties was found to have high shear stresses in the superficial zone, which corresponds to the documented location of matrix damage. On the other hand, depth-dependent material properties were not found to

produce high cell strains corresponding to regions of cell death. High cell strain related more to cell shape than to depth dependent changes in material properties.

Jurvelin et al. (1997), using an optical measuring system, noted that under unconfined compression the superficial cartilage layer underwent a smaller lateral expansion than the deep region immediately after ramp loading. After ramping down to 10% compression in 3 seconds, they documented 72% less lateral expansion in the superficial layer compared to the deep zone. In order to correctly approximate this depth-dependent lateral expansion with a theoretical model, there was a need to include the depth-dependent material properties of the cartilage. The current study indicated that the isotropic, layered model did a better job than the TI layered model of predicting the distribution of lateral expansion in the deep versus the superficial layers. However, the isotropic layered model exhibited only a 34% decrease of lateral expansion in the superficial layer compared to the deep zone. The discrepancy between the earlier experimental data by Jurvelin et al. (1997) and the current theoretical model may be due to the timeframe used for loading the explant. Li et al. (2000) recently developed a fibril reinforced, poroelastic model of cartilage that took into account depth-dependent material properties of the tissue. They modeled unconfined compression and applied ramp compression in 5 seconds. The study noted that the percentage decrease in lateral expansion in the superficial region versus the deep zone changed from 58, 61, and 78%, in 5, 20, and 40 seconds, respectively. Therefore, following Li's (2000) observations, it is likely that a loading time of less than 5 seconds, like the 1 second and 50 milliseconds used in the current study, would result in less than 58% variation in lateral expansion with depth.

The current study also suggested that an important parameter influencing the extent of cell strain was the shape of the cell. Ellipsoidal versus spherical cells in the superficial zone resulted in increased shear strain, which corresponded with the notion of cell death. Previously, Baer and Setton (2000) examined the influence of cell geometry on the micromechanical environment of intervertebral disc cells. In one part of the study, they modeled the matrix as transversely isotropic and applied a lateral load resulting in constant nominal strains for both ellipsoidal and spheroidal cells. They also noticed that the cell strains were decreased when the cell was modeled as ellipsoidal versus spherical. However, the contrasts between our findings and those of Baer and Setton (2000) may be attributed to modeling differences. First, the major to minor cell axis ratio was 3:1 for ellipsodial cartilage cells in the current study; whereas, Baer and Setton (2000)used a ratio of 10:1 for the ellipsoidal intervertebral disc cells. The current study also loaded the cells in the axial direction under large nominal strains (30%), while Baer and Setton (2000) loaded the cells in the lateral direction under small nominal strains (5%).

In the current study, cellular strains were approximately twice as large as the local nominal matrix strain, which supports the findings of previous embedded cell models. Guilak and Mow (2000) determined that when the elastic modulus of a cell is two or more orders of magnitude less than that of the surrounding matrix, the peak strains in the cell are also two times greater than the local matrix strain. Experimentally Guliak et al.(1995) recorded a 27–37% increase in cell strain versus local matrix strain, in contrast to the 74-121% in the current model. The Guilak et al study, however, was performed with a physiological loading, which results in a 15% surface-surface strain. In the current study, the model was subjected to approximately 30% strain for high and low rates of

loading. This suggested that the material properties of cells used in the current model may be inadequate for large deformations. A possible solution to this problem may be to incorporate a stiffening effect into the material properties of the cells for large strains and high strain rates.

The biphasic model in the current study was not able to account for differences in compression for high and low rate of loading experiments. While the deformations recorded between the two rate of loading experiments were not statistically significant in this study, previous studies with larger sample sizes have shown significantly more deformation in the low versus high rate of loading experiments (Ewewrs et al., 2000). The permeabilities used in the models were taken from the literature and are based on fitting long duration relaxation experiments, unlike the very short times exhibited in impact tests. This is supported by a previous study that examined contact analysis for biphasic materials (Donzelli et al., 1999). The study showed no change in contact area for times to one second after applying a load. To fully model the apparent fast relaxation characteristics of cartilage under an impact, a model that incorporates a viscoelastic solid phase may be needed (Suh and Bai, 1998).

A limitation of the current computational models was that actual experimental loads could not be applied. This was due to the low modulus values used for the tissue layers, based on the literature. Atkinson et al. (1998), using an isotropic elastic model for the cartilage to model an impact event, suggested that the elastic modulus of cartilage needs to be approximately 20 times that determined in small deformation experiments. Previous studies have already attempted to model a nonlinear stiffening effect for the impact response of cartilage (Garcia et al., 2000; Li et al., 2000). More studies will be

needed to incorporate the nonlinear, viscoelastic effects into cartilage models for the impact event. The material properties used in the current study also led to strains in cells that exceeded the limits of infinitesimal theory. In order to remedy this problem, there will also be a need to determine some of the nonlinear material properties of cells under impact load scenarios. Although the current study was not able to estimate the absolute values of cellular strain in different layers of cartilage under impact, it has provided information on some of the factors that will be needed in models to more accurately represent cellular strains in various layers of the tissue.

Since matrix and cell stresses and strains were not uniform throughout the modeled tissue, boundary tractions may not be the best indicator of matrix damage or cell death. The current study showed that areas of high matrix stress correspond with areas of matrix damage by incorporating depth-dependent material properties for the cartilage. The study also indicated that depth-dependent, isotropic models could better predict experimentally observed variations of lateral expansion from unconfined compression experiments than a transversely isotropic model. Cell shape was also determined to be an important parameter when examining cellular strains under impact loading.

In summary, the current study has helped confirm the need to take into account depth dependent variations in cellular shapes and material properties to understand better the mechanisms of cell death and matrix damage of cartilage from blunt impact loading. Future studies must also consider models of structures such as the cell membrane and its cytoskeleton to more completely understand the mechanism of cell death from blunt impacting loads.

ACKNOWLEDGEMENTS

This study was supported by a grant for the Centers of Disease Control and Prevention (R49/CCR503607). Its contents are solely the responsibility of the authors and do not necessarily represent the official views of the Centers of Disease Control and Prevention. The authors with to gratefully acknowledge Cliff Beckett and Masaya Kitagawa for technical assistance.

REFERENCES

1. Atkinson, TS, RC Haut, and NJ Altiero. (1998) Impact-induced fissuring of articular cartilage: an investigation of failure criteria. *J Biomech Eng.* 120:181-187.

2. Baer, AE and LA Setton. (2000) The micromechanical environment of intervertebral disc cells: effects of matrix anisotropy and cell geometry predicted by a linear model. *J Biomech Eng.* 122:245-251.

3. Chen C-T, N Burton-Wurster, G Lust, RA Bank, and JM Tekoppele. (1999) Compositional and metabolic changes in damaged cartilage are peak-stress, stress-rate, and loading-duration dependent. *J Orthop Res.* 17:870-879.

4. Cohen, B, TR Gardner, and GA Ateshian. (1993) The influence of transverse isotropy on cartilage indentation behavior: a study of the human humeral head. *Transactions 39Th ORS (abstract).*

5. Donzelli, PS, RL Spilker, GA Ateshian, and VC Mow. (1999) Contact analysis of biphasic transversely isotropic cartilage layers and correlations with tissue failure. *J Biomech.* 32:1037-1047.

6. Ewers, BJ, D Dvoracek-Driskna, MW Orth, and RC Haut. (2000) The extent of matrix damage and chondrocyte death in mechanically traumatized articular cartilage explants depends on rate of loading. *J Orthop Res.* in press.

7. Flores, RH and MC Hochberg. (1998) "Definition and classification of osteoarthritis." In: *Osteoarthritis*, edited by KD Brandt, M Doherty, and LS Lohmander. New York: Oxford University Press, pp1-12.

8. Garcia, JJ, NJ Altiero, and RC Haut. (2000) Estimation of in situ elastic properties of biphasic cartilage based on a transversely isotropic hypo-elastic model. *J Biomech Eng.* 122:1-8.

9. Guilak F and VC Mow. (2000) The mechanical environment of the chondrocyte: a biphasic finite element model of cell-matrix interactions in articular cartilage. *J Biomech.* 33:1663-1673.

10. Guilak F, A Ratcliffe, and VC Mow. (1995) Chondrocyte deformation and local tissue strain in articular cartilage: a confocal microscopy study. *J Orthop Res*, 13:410-421.

11.Hamerman, D. (1989) The Biology of osteoarthritis, *New Eng Journal of Med* 320:1323-1330.

12. Jones, WR, GM Lee, SS Kelley, and F Guilak. (1999) Viscoelastic properties of chondrocytes form normal and osteoarthritic human cartilage. *Transactions 45th ORS.*

13. Jones, WR, HP Ting-Beall, GM Lee, SS Kelley, RM Hochmuth et al, (1997) Mechanical properties of human chondrocytes and chondrons from normal and osteoarthritic cartilage. *Transactions 43rd ORS* (Abstract).

14. Jurvelin, JS, MD Buschmann, and EB Hunziker. (1997) Optical and mechanical determination of Poisson's ratio of adult bovine humeral articular cartilage. *J Biomech.* 30:235-241.

15. Kim, HA, YJ Lee, SC Seong, KW Choe, and YW Song. (2000) Apoptotic chondrocyte death in human osteoarthritis. *J Rheumatol.* 27(2):455-462.

16. Lee, Gm, TA Paul, M Slabaugh, and SS Kelley. (1997) The pericellular matrix is enlarged in osteoarthritic cartilage. *Transactions 43rd ORS (abstract).*

17. Li, LP, MD Buschmann, and A Shirazi-Adl. (2000) A fibril reinforced nonhomogeneous poroelastic model for articular cartilage: inhomogeneous response in unconfined compression. *J Biomech.* 33:1533-1541.

18. Repo RU and JB Finlay. (1977) Survival of articular cartilage after controlled impact. *J Bone Joint Surg [AM].* 59:1068-1078.

19. Roth, V and VC Mow, (1980) The intrinsic tensile behavior of the matrix of bovine articular cartilage and it variation with age. *J Bone Joint Surg.* 62-A:1102-1117, 1980.

20. Schinagl, RM, D Gurskis, AC Chen, and RL Sah. (1997) Depth-dependent confined compression modulus of full-thickness bovine articular cartilage. *J Orthop Res.* 15:499-506.

21. Suh, JK and S Bai. (1998) Finite element formulation of biphasic poroviscoelastic model for articular cartilage. *J Biomech Eng.* 120:195-201.

22. Torzilli, PA, R Grigiene, J Borrelli, Jr., and DL Helfet. (1999) Effect of impact load on articular cartilage: cell metabolism and viabiltiy, and matrix water content. *J Biomech Eng.* 121:433-441.

TABLES

Table 1: Matrix biphasic material properties for the non-layered isotropic (I) and transversely isotropic (TI) and layered transversely isotropic (TI) models.

Material property	Layered TI			Non-Layered	
	Superficial	Middle	Deep	I*	TI*
E_{33} (MPa)	0.16§	0.60§	1.78§	0.69	0.46
E_{11}(MPa)	28.0#	8.8#	1.8#	0.69	5.80
ν_{12}	0.0	0.0	0.0	0.0	0.0
ν_{13}	0.0	0.0	0.0	0.0	0.0
G_{13}(MPa)	0.08	0.30	0.89	0.345	0.37
κ (x10-^{15}m^4/Ns)	5.1*	5.1*	5.1*	3.0	5.1
ϕ^s	0.25*	0.25*	0.25*	0.25	0.25

* – Cohen et al. (1993)
§ – Schingal et al. (1997)
# – Roth and Mow (1980)

Table 2: Average maximum shear stress (τ_{MAX}) (MPa) and tensile strain (ε_1) for each region and rate of loading for the non-layered and layered isotropic (I) and transversely isotropic (TI) models.

Rate of Loading	Region	Non-Layered				Layered			
		I		TI		I		TI	
		τ_{MAX}	ε_1	τ_{MAX}	ε_1	τ_{MAX}	ε_1	τ_{MAX}	ε_1
Low	Superficial	0.33	0.16	1.08	0.16	2.61	0.14	1.26	0.21
	Middle	0.33	0.16	1.08	0.16	1.12	0.16	0.82	0.20
	Deep	0.33	0.16	1.08	0.16	0.55	0.21	0.55	0.22
High	Superficial	0.30	0.145	0.98	0.145	2.37	0.13	1.12	0.18
	Middle	0.30	0.145	0.98	0.145	0.99	0.14	0.72	0.17
	Deep	0.30	0.145	0.98	0.145	0.49	0.19	0.47	0.19

Table 3: Average maximum tensile strains (ε_1) and maximum shear strain (γ_{MAX}) in the cell for each region and rate of loading for the non-layered and layered isotropic (I) and transversely isotropic (TI) models.

Rate of Loading	Region	Non-Layered				Layered			
		I		TI		I		TI	
		ε_1	γ_{MAX}	ε_1	γ_{MAX}	ε_1	γ_{MAX}	ε_1	γ_{MAX}
Low	Superficial	0.35	0.68	0.30	0.59	0.28	0.61	0.43	0.71
	Middle	0.34	0.51	0.31	0.47	0.33	0.50	0.40	0.58
	Deep	0.34	0.51	0.31	0.47	0.38	0.54	0.45	0.62
High	Superficial	0.32	0.62	0.27	0.54	0.26	0.54	0.36	0.62
	Middle	0.31	0.46	0.28	0.42	0.30	0.44	0.33	0.50
	Deep	0.31	0.46	0.28	0.42	0.33	0.45	0.37	0.53

FIGURES

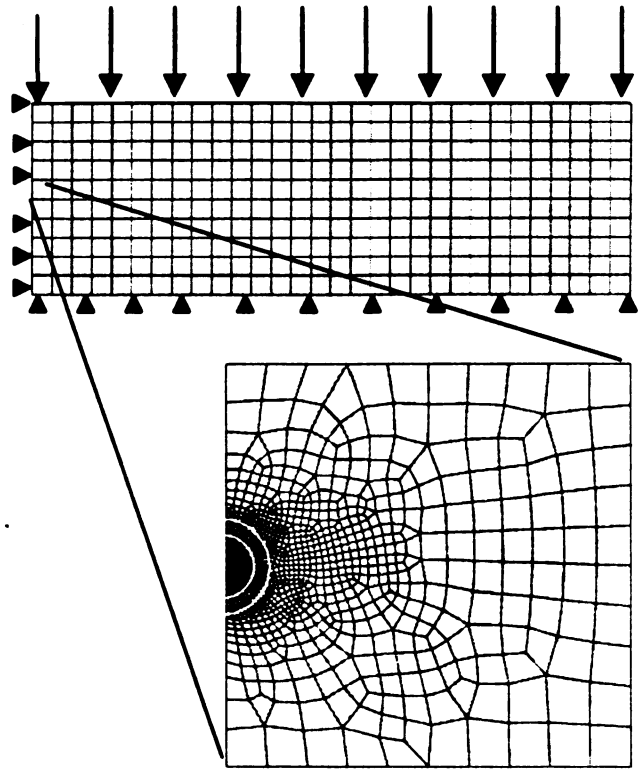

Figure 1: A biphasic axisymmetric finite element model was developed for a cartilage explant under unconfined compression. From this solution a linear interpolation of the displacements was used as the boundary condition for a 100 x 100 μm model of an axisymmetric cell embedded in the matrix. Cell models were constructed in the superficial, middle, and deep layers of the explant.

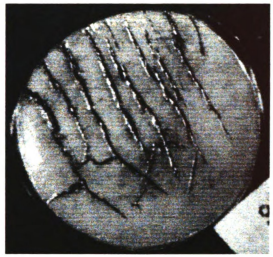

(a)

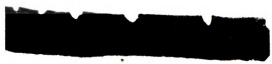

(b)

Figure 2: Matrix damage was always observed as small surface fissures (a), extending only into the superficial layer (b).

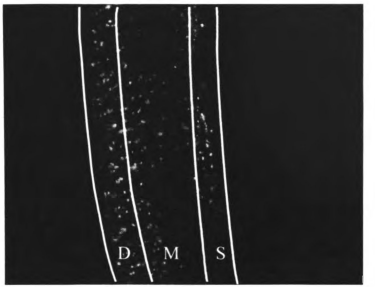

Figure 3: From stained sections dead cells appeared red and live cells appeared green. In these grayscale pictures, the dead cells are dark while the live cells appear bright. Cell death was observed throughout the thickness of the cartilage, however, the superficial layer (S) showed the largest percentage of cell death, followed by the middle zone (M). Minor degrees of cell death also appeared in the deep zone (D).

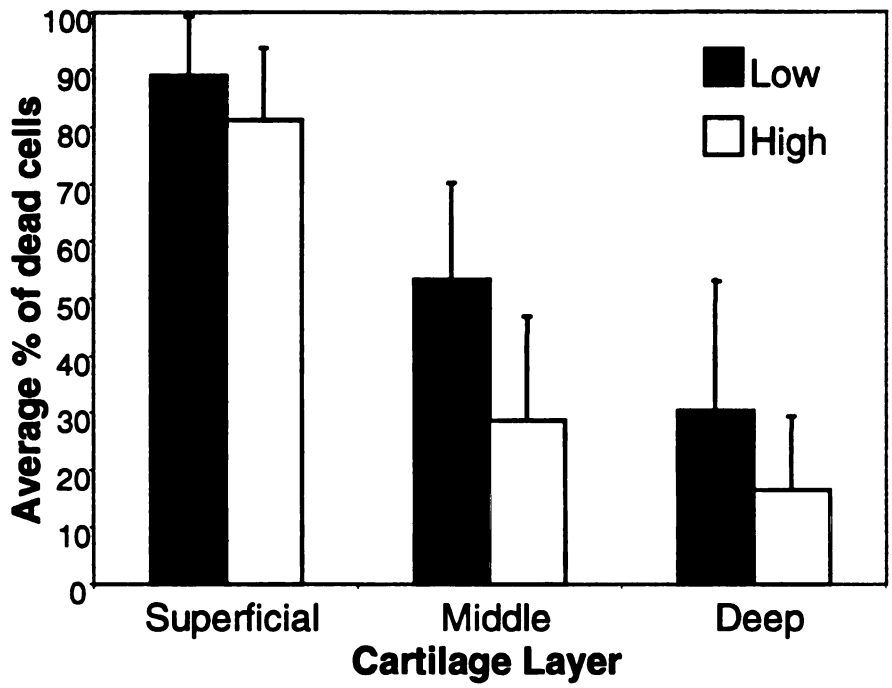

Figure 4: There was significantly more cell death in the low versus high rate of loading experiments (♦). There was also significantly more cell death in the middle zones for the low compared to high rate of loading experiments (♦). Minimal cell death occurred in the deep zone for both rate of loading experiments.

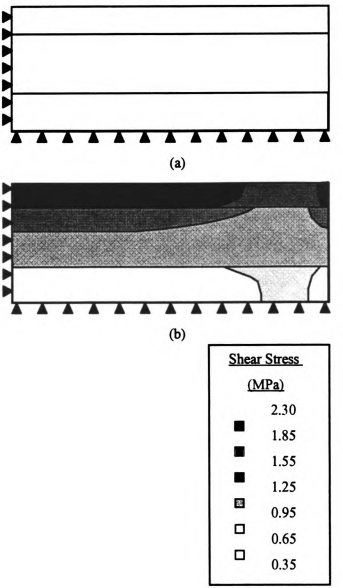

Figure 5: There were no radial or depth-dependent distributions of maximum shear stress in the isotropic non-layered explant model (A). On the other hand, the isotropic layered model indicated depth-dependent variations in maximum shear stresses, with the largest stresses appearing in the superficial layer (B).

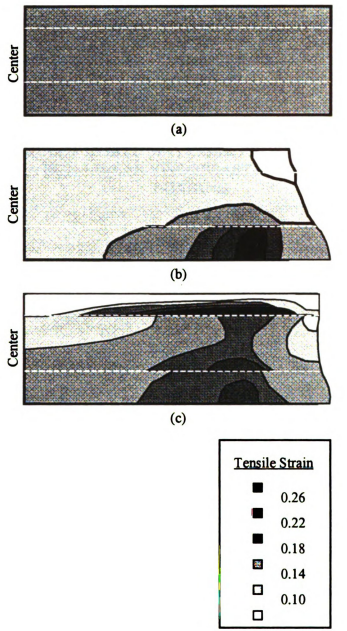

Figure 6: This figure shows the deformed explant. There were no radial or depth-dependent variations in tensile strain for the isotopic non-layered model (A). In contrast, the isotropic, layered model exhibited large tensile strains in the deep region and smaller lateral expansion in the superficial layer (B). The transversely isotropic, layered model also indicated similar levels of average tensile strain in the superficial and deep layers (C).

CHAPTER 9

DETERMINATION OF IN SITU MATERIAL PROPERTIES OF CARTILAGE BASED ON A NON-LINEAR VISCOELASTIC MODEL FOR IMPACT LOADING

Benjamin James Ewers

ABSTRACT

A method was developed to determine the nonlinear isotropic viscoelastic properties of articular cartilage from in situ indentation testing for modeling of articular cartilage under impact loading scenarios. The infinitesimal viscoelastic properties were determined by fitting force-time curves from a non-porous flat-ended indentor experiment for loads times less than one second. A commercial finite element code was employed to solve the problem of a viscoelastic layer indented by a flat-ended indentor. The components of a first order Prony series were then determined. The non-linear isotropic material properties were estimated by fitting force-displacement curves obtained from large deformation indentation relaxation tests on cartilage using a non-porous spherical indentor. The curve consisted of peak forces obtained at the initial stage of rapid indentation versus the associated displacements. A commercial finite element code was employed to solve the problem of a hyperelastic layer indented by a rigid sphere. The components of the strain energy function could then be determined. Near incompressibility was assumed to model the rapid loading. The method was applied to

indentation data from bovine cartilage to document the non-linear viscoelastic material properties for impact loading. The method was validated using experimental data from unconfined compression of bovine cartilage.

INTRODUCTION

Osteoarthritis (OA) is a disease affecting diarthrodial joints and is characterized by full thickness loss of articular cartilage resulting in bone-on-bone contact and joint pain. Clinically, matrix damage of cartilage, such as surface fissuring, and chondrocyte death have been documented in osteoarthritic cartilage (Kim et al., 2000). Excessive and abnormal mechanical loading of cartilage has been implicated in the pathogenesis of OA. However the role excessive or abnormal mechanical loading plays in the mechanism of a post-traumatic, secondary OA are not well understood.

Repo and Finlay (1977), using tissue explants on bone and subjected to a single impact, document cell death localized around fissures in the superficial layer of the cartilage. Torzilli et al. (1999) also document cell death and fissuring of cartilage following a single impact in explants without the attachment of underlying bone. In vitro studies have also been used in attempts to correlate the state of stress and strain in loaded cartilage with the locations and degree of matrix damage and cell death. Atkinson et al. (1998) using impacts on isolated rabbit tibial plateaus suggested that maximum shear stress is the best predictor of cartilage fissuring. Large matrix strains corresponding to large cell strains have been hypothesized to cause significant leakage of florescent indicators across cell membranes in preliminary studies (Guliak et al., 1995). This suggests that membrane damage and the possibility of cell death may occur from excessive cell strain (Guliak et al., 1995). Recently, Ewers et al. (2001) modeling an

explant under impact loading suggest that shear stress correlates with matrix damage and large cell strains correlates with areas of extensive cell death.

However, it is difficult to use the infinitesimal material properties of cartilage for modeling impact scenarios because of the large deformations. Atkinson et al. (1998), using an isotropic elastic model for the cartilage to model an impact event, suggested that the elastic modulus of cartilage needs to be approximately 20 times that determined in small deformation experiments. This is in support of a previous study that documented stiffening effects of cartilage due to high strain rates during impact experiments (Oloyede et al., 1992). Therefore, there is a need to take into account the non-linear stiffening effect of cartilage for modeling impact experiments.

Cartilage is composed of a fluid and solid phase and as such, has been modeled as a biphasic material with fluid flow being responsible for the time-dependent creep and stress-relaxation behavior (Mow et al., 1980). However, the instantaneous response of biphasic cartilage is equivalent to that of an incompressible elastic material (Armstrong et al., 1984; Ateshian et al., 1994). In addition, the shear stresses in a cartilage layer under impact loading are the same for an incompressible elastic and biphasic material at time zero (Garcia et al., 1998). A previous study that examined contact analysis for biphasic materials, shows no change in contact area for times out to one second after applying a load, suggesting little or no fluid flow (Donzelli et al., 1999). Under one second of loading, however, there is extensive relaxation of cartilage from in situ indentation tests (Newberry et al., 1988). Ewers et al. (2000) also supports this result and show that the rate of loading under one second can affect the deformation and possibly the state of stress in unconfined compression experiments on bovine cartilage. They found that a low

rate of loading (40 MPa / 1 second) caused more deformation and cell death deeper in the explant compared to a high rate of loading (40 MPa / 50 milliseconds) experiment to the same peak load. On the other hand, matrix damage was more extensive with the higher rate of loading suggesting larger shear stresses were developed assuming high tissue shear stresses are responsible for matrix damage. To fully model the apparent fast relaxation characteristics of cartilage under impact loading, a model that incorporates a viscoelastic solid phase may be needed (Suh and Bai, 1998).

The object of the current study was to model cartilage for impact loading as a non-linear viscoelastic material and determine the material properties from in-situ indentation testing. This will allow for improved modeling of cartilage under impact loading and assist with understanding the mechanisms of matrix damage and cell death due to excessive mechanical loading.

METHODS AND MATERIALS

Theoretical background

The infinitesimal shear modulus (G) was assumed to be viscoelastic and the reduced relaxation function ($g_R(t)$) was modeled using a Prony series:

$$g_R(t) = \frac{G_R(t)}{G_O} = 1 - \sum_{i=1}^{N} G_i^P (1 - e^{t/\tau})$$

As a first approximation we assumed only one term:

$$g_R(t) = \frac{G_R(t)}{G_O} = 1 - G^P (1 - e^{t/\tau})$$

G_O is the instantaneous shear modulus, so there are only two parameters to determine the viscoelastic Prony series: G^P and τ, where G^P corresponds to the amount of relaxation, while τ determines the shape of the relaxation curve.

In a hyperelastic formulation the Cauchy stress is:

$$\sigma_{ij} = \frac{2}{J} F_{ik} \left(\frac{\partial W}{\partial C_{km}} \right) F_{jm}$$

Where F_{ik} is the deformation gradient, C_{km} is the right Cauchy-Green deformation tensor, J is the determinant of the deformation gradient, and W is a strain-energy function. The appropriate stress-strain relationship in terms of derivatives of the strain-energy function with respect to the strain invariants for an arbitrary isotropic compressible material is:

$$\sigma_{ij} = 2J \frac{\partial W}{\partial I_3} \delta_{ij} + \frac{2}{J} \left(\frac{\partial W}{\partial I_1} + I_1 \frac{\partial W}{\partial I_2} \right) B_{ij} - \frac{2}{J} \frac{\partial W}{\partial I_2} B_{ik} B_{kj}$$

Where B_{ij} is the left Cauchy-Green deformation tensor, I_1, I_2, and I_3 are the strain invariants of the left Cauchy-Green deformation tensor. We chose a strain energy function that has been used to model the non-linear stiffening of large arteries (Simon et al., 1998). This is a "generalized" Fung strain-energy function of the form:

$$W = \frac{1}{2} C_O (e^{\phi} - 1)$$

$$\phi = C_1 (\bar{I}_1 - 3) + C_2 (\bar{I}_2 - 3) + K(J-1)^2$$

The bar above the strain invariants indicates they are the deviatoric strain invariants:

$$\bar{I}_1 = J^{-2/3} I_1 \qquad\qquad \bar{I}_2 = J^{-4/3} I_2$$

This strain-energy function can be incorporated into a commercial finite element code using a user-defined isotropic hyperelastic function, UHYPER (ABAQUS, version 5.8; Hibbit, Karlsson, & Sorensen, Inc.). This involves taking derivatives of the strain-energy function with respect to I_1, I_2, and J (A.1-A.2). This strain-energy function is stress free in the undeformed configuration. Therefore there are four independent coefficients. The two infinitesimal elastic constants (G_O, ν) were expressed in terms of the four coefficients of the strain energy function, by a theoretical pure shear test and a uniform triaxial test (B.1-B.2). Since we were interested in impact loading the cartilage was assumed to be nearly incompressible (ν=0.49).

In a pilot study using bovine cartilage it was determined that the strain-energy function stated above did not give a good fit to the experimental data. The exponential form had stiffened too rapidly for the experimental deformations. Therefore, the exponential term in the strain-energy function was expanded and the higher order terms dropped:

$$e^{\phi} = 1 + \phi + \frac{1}{2}\phi^2 = \psi$$

The strain energy function was put in the form:

$$W = \frac{1}{2} C_O \psi$$

Using the expanded version of the strain energy function in UHYPER (A.3) flattened the load-displacement curve at the higher strains giving a better fit of the pilot experimental data (Figure 1).

To fully model the cartilage as a non-linear viscoelastic material we need to determine six material parameters: four coefficients of the strain-energy function, and two coefficients in the Prony series.

Experiment

Indentation relaxation experiments were performed on cartilage from a fresh bovine metacarpal joint. The joint was opened and placed in phosphate buffered saline (pH 7.2) and mounted in a fixture with the cartilage surface facing an indentor probe that was attached to a stepper micrometer (M-168.30, PI Physik Instrumente, Auburn, MA).

The following procedure was performed at each of four sites. First a plane-ended non-porous cylindrical indentor of 1.0 mm diameter was pressed 0.1 mm into the cartilage at an average velocity of 2.5 mm/s and maintained for 150 seconds. For two of the sites, after a period of five minutes, a spherical non-porous indentor was pressed 0.05 mm into the cartilage at 2.5 mm/s and maintained for 150 seconds. This procedure for the spherical indentor was subsequently repeated while increasing the indentation depth to 0.1, 0.15, 0.2, 0.225, and 0.25 mm with a wait period of five minutes between tests. For the other two sites the above procedure with the spherical indentor was done in reverse order: first 0.25 mm, then 0.225, 0.2, 0.15, 0.1, and finally the 0.05 mm indentation depth. In all of the above tests the resistive loads were measured (Data Instruments, Acton MA: model JP - 25, 25 lb capacity), amplified, and collected at 1000 Hz for the

first second, and 20 Hz thereafter. Finally tissue thickness was measured at three locations around each testing site by pressing a needle into the cartilage to determine tissue thickness at that location. The thickness at the testing site was assumed to be an average of the three measured thicknesses.

A spherical shape indentor was used to help avoid damage to the tissue at the large deformations. However, to help determine if tissue damage was occurring at the large deformations, a second indentation test was performed to examine the difference in peak loads between repeated tests. Finally to examine the effect of repeated testing on a single site the fifth set of indentation experiments were performed with the spherical indentor at various locations. First the spherical indentor was pressed into the cartilage followed by a five-minute wait period, then the tissue thickness was determined at that site. The indentor was moved to the next site and the second indentation depth experiment was performed. This procedure was repeated for all indentation depths.

From the peak resistive load of the flat-ended indentor experiments the "instantaneous" shear modulus (G_O) was determined based on an elastic analysis at the four sites and averaged (Hayes et al., 1972):

$$G_O = \frac{P}{8awk}$$

Where P is the peak load, a is the indentor radius (0.5 mm), w is the indentation depth (0.1 mm) and κ is a geometric factor depending on the indentor radius and thickness of the elastic layer. The force-time plots of the four flat-ended indentor experiments were averaged and plotted over one second. The relaxation that occurred by one second was due to the viscoelastic nature of the cartilage because we are assuming no fluid flow

during this time frame. A computational model was constructed for a linear viscoelastic layer bonded to a rigid half space and indented by a rigid cylindrical flat-ended probe. The geometry consisted of a large, axisymmetric cylindrical disk of cartilage with a thickness determined from the average experimental cartilage thickness. The bottom nodes were fixed in space while the nodes under the indentor were displaced 0.1 mm in 50 ms and maintained for 1 second. The mesh consisted of 394 eight-noded quadrilateral elements (CAX8). The infinitesimal elastic modulus was based on the average experimental G_O and the assumption of $\nu = 0.49$. The two viscoelastic parameters (G^P, τ) were varied until the computational load data fit the experimental relaxation data.

From the five experiments performed with the spherical indentor an average curve of peak load versus normalized displacement (strain) was determined directly under the center of the indentor. A computational model was constructed of a hyperelastic layer bonded to a rigid half space indented by a rigid spherical probe. The geometry consisted of a large, axisymmetric cylindrical disk of cartilage with a thickness determined from the average experimental cartilage thickness. The bottom nodes were fixed in space while the spherical rigid indentor was displaced to 0.3 mm (50 % strain) while predicting the resistive loads. The mesh consisted of 440 eight-noded quadrilateral elements (CAX8). In order to fit the experimental force-displacement curves, two coefficients (C_0 and C_1) were adjusted in this model. The other two coefficients could then be found in terms of the infinitesimal elastic constants (G_O, ν) using equations (B.1-B.2).

In order to validate this method of determining non-linear viscoelastic material properties of bovine cartilage unconfined compression was modeled at two rates of loading. A 6.0 mm diameter punch with a smooth edge was used to make 32 plugs from

the metacarpal surfaces of bovine forelegs. The plugs were separated from the underlying bone using a scalpel. The specimens were assigned to either a high rate (50 milliseconds to peak, 600 MPa/s, n=16) or low rate (1 second to peak, 30 MPa/s, n=16) test group. The thickness of each explant was measured using a digital micrometer (Digimatic, Mitutoyo Corp., Japan). Each specimen was loaded to a peak load of 840 N (~ 30 MPa) using a single haversine load-time pulse. The specimens were placed between two highly polished stainless steel plates in an unconfined compression experiment using a servo-hydraulic machine (Instron, model 1331, Canton, MA). Peak load, time to peak load, and maximum displacement were recorded in each experiment. A computational model was constructed assuming a hyper-viscoelastic layer. The geometry consisted of a large, axisymmetric cylindrical disk of cartilage with a thickness determined from the average experimental cartilage thickness. The material properties were those determined using the above procedures. The bottom nodes were fixed in the axial direction, but allowed to move radially. The top nodes were displaced downward. For the high rate of loading model the top nodes were displaced to the average displacement from the experiments in 50 ms, while the low rate of loading model had the average experimental displacements applied in 1 second. The mesh consisted of 300 eight-noded quadrilateral elements (CAX8). The theoretical load was then compared to the average experimental load for each rate of loading experiment.

RESULTS

The average cartilage thickness was 0.60 ± 0.05 mm for these experiments. The elastic infinitesimal analysis of the four indentation relaxation experiments with the flat-ended indentor resulted in $G_O = 3.2 \pm 0.4$ MPa. The load relaxed from 50 milliseconds to

1 second in these relaxation tests approximately 56 %. As a first approximation $G^P = 0.5$ and τ was varied from 0.4 to 0.08 (Figure 2). As expected, as τ decreased the relaxation of load was faster. However, for $G^P = 0.5$ there was not enough relaxation at one second. In the second attempt $G^P \cong 0.6$, and the computational model fit the peak load and load at one second (Figure 3). However, using a one term Prony series the relaxation curve was not fit well. Since we were interested in using these material properties for impact loading, we were mostly interested in fitting early relaxation part of the curve. Therefore the best fit for the early relaxation (< 100 milliseconds) was $G^P = 0.625$ and $\tau = 0.08$. Future studies will need to use a two term Prony series to better model the relaxation behavior of cartilage for the entire one second of relaxation.

The experimental data from the spherical indentation tests indicate that there was no difference in peak load between the first and second tests at displacements between 0.15 – 0.25 mm (Figure 4). This indicated that the tissue was not damaged at 50 % strain with the spherical indentor. The experimental data for the four sites of testing showed no differences in the peak load versus strain curve whether the test sequence was varied starting at the small or large displacement tests (Figure 5). Furthermore, when testing each location once on the opposite plateau there was no difference in the peak load versus strain curve compared to the repeated indentation sites.

When attempting to fit the experimental peak load versus strain data with the hyperelastic function, it was not fitting the curve correctly at the smaller strains. It can be shown by linearly extrapolating the flat-ended indentation relaxation data backward that there is an approximate 30 % reduction in load between time zero and 50 milliseconds (Figure 6). This translated into a true instantaneous shear modulus of 4.2 MPa. When

using G_O = 4.2 MPa the hyperelastic energy-function could now fit the experimental peak load versus strain data reasonably well (Figure 7). I determined that the one set of strain-energy coefficients that best fit the experimental data over the entire strain range was: C_O = 6.0, C_1 = 0.68, C_2 = 0.02, K = 35.25.

Analysis of the experimental unconfined compression tests on the bovine cartilage explants indicated that the high rate of loading resulted in an average peak load of 803 ± 42 N and an average peak strain of 0.46 ± 0.06. On the other hand, the low rate of loading experiments resulted in an average peak load of 857 ± 36 N and an average peak strain of 0.56 ± 0.12. Using the average strains as input boundary conditions in the model along with the four coefficients of the strain-energy function determined above, a hyperelastic model of unconfined compression did a reasonable job predicting the peak load for the high rate of loading experiments, but drastically over estimated the peak load for the low rate experiments (Figure 8). In contrast, when the cartilage was modeled as a hyper-viscoelastic material, with the estimated material properties determined above the predicted peak load was 670 and 706 N for the high and low rate of loading experiments, respectively. While the hyper-viscoelastic model slightly under predicts the experimental peak load for both rate of loading experiments (~17 %), the same trend is followed. Experimentally, there was a 6.3 % decrease in average peak load for the high versus low rate of loading experiments. The computational model predicted a decrease of 5.1 %. The high rate of loading model, with less deformation compared to the low rate of loading model, predicted a tissue shear stress of 5.65 MPa versus 5.0 MPa for the low rate of loading explant model.

DISCUSSION

The object of the current study was to develop a non-linear viscoelastic model of cartilage for impact loading, and determine material properties from in-situ indentation tests. The current study indicated that all six material properties for a hyper-viscoelastic model could be determined from in situ indentation testing. The estimated material properties could then be used to predict responses of cartilage in unconfined compression test performed at two rates of loading.

Other investigators have modeled bovine cartilage as a biphasic material with a viscoelastic solid phase. Suh and DiSilvestro (1999) used a simplified relaxation function with a discrete spectrum to model the viscoelastic solid phase and determined τ_S and τ_L, where τ_S is the short-term relaxation time and τ_L is the long time constant. For short times it can be assumed that the relaxation of the Suh and DiSilvestro (1999) model is only due to relaxation of the solid phase (no fluid flow), so that τ_S with τ from the current study can be compared. The previous study documented τ_S = 0.02 s versus τ = 0.08 s of the current study.

In the current study, the unconfined compression of bovine cartilage explants indicated, as expected, that there was more tissue deformation for the low versus high rate of loading experiments. Excessive deformation has been suggested to cause cell death by possibly damaging the cell membrane (Guliak et al., 1995). Interestingly, the hyper-viscoelastic model in the current study found that while there is more deformation in the low rate of loading experiments, the high rate of loading impacts would result in increased shear stresses. These high shear stresses have been implicated in acute fissuring of articular cartilage due to impact loading (Newberry et al., 1998; Atkinson et al., 1998). The hyper-viscoelastic modeling of the current study is in support of a previous study that

documented increased fissuring of cartilage explants under unconfined compression at a high versus low rate of loading (Ewers et al., 2001).

There were a number of limitations in the current study. First, the hyper-viscoelastic material properties for cartilage determined using this method are only appropriate for loading under one second, where there is no fluid flow, such as impact scenarios. For loading times greater than this, there is the need to model the cartilage as a biphasic material. A biphasic model has the advantage of being able to separate the solid and fluid stresses in the cartilage. This may provide important since solid tensile stresses have been implicated in cartilage fissuring (Garcia et al., 1998). The relaxation of the cartilage could not be fitted precisely over the entire one second with a single term in the Prony series thus future studies will need to incorporate at least one additional term like previous investigators (Suh and Bai, 1998). This study did not take into account the known depth-dependent material properties of cartilage (Schingal et al., 1997). These depth-dependent material properties may need to be taken into account to predicate experimental deformations and matrix damage (Ewers et al., 2001). For instance, in the current study the homogenous computational model predicts a constant shear stress, but experimentally matrix damage is initiated in the superficial layer. Likewise, the current homogenous model predicts a constant lateral expansion, but experimentally the lateral expansion of cartilage under unconfined compression is not constant. Future studies can use the current method to determine the hyper-viscoelastic material properties in different layers of cartilage. Finally, there are many sets of material properties that could estimate the experimental response of cartilage under indentation testing. Therefore the material properties determined with this method are not unique. There is a need to incorporate an

optimization scheme to get the material properties that "best" fit the experimental data, so other laboratories can predict the same material properties using these techniques.

In conclusion, the hyper-viscoelastic material properties of cartilage were determined from in situ indentation testing and used to predict other impact loading scenarios. Previous studies have used an elevated elastic modulus to model impact scenarios to get appropriate displacements. Modeling the cartilage as hyperelastic allows for experimental loads to be used as boundary conditions and the appropriate displacements can be obtained. The use of a hyperelastic model is critical because the state of tissue stress will vary between a model using an elevated elastic modulus and a model incorporating a hyperelastic material for contact impact modeling. Since cartilage has fast relaxation behavior that can not be accounted for by fluid flow, a viscoelastic model is imperative for modeling impact scenarios. The current study allows for the determination of these viscoelastic properties, so that the effect of different rates of loading on cartilage stress and strain can be investigated with computational models. Therefore, this study will help with modeling impact experiments to be able to better understand mechanisms behind mechanically induced matrix damage and cell death that could possibly lead to a chronic degradative disease such as OA. Future studies will need to examine the depth-dependent material properties of cartilage.

REFERENCES

1. Armstrong, C. G., Lai, W. M. and Mow, V. C., (1984) An Analysis of the Unconfined Compression of Articular Cartilage. *Journal of Biomechanical Engineering* 106, pp. 165-173.

2. Ateshian, G. A., Lai, W. M., Zhu, W. B. and Mow, V. C., (1994) An Asymptotic Solution for the Contact of Two Biphasic Cartilage Layers. *Journal of Biomechanics* 27, pp. 1347-1360.

3. Atkinson, TS, RC Haut, and NJ Altiero. (1998) Impact-induced fissuring of articular cartilage: an investigation of failure criteria. *J Biomech Eng*. 120:181-187.

4. Donzelli, PS, RL Spilker, GA Ateshian, and VC Mow. (1999) Contact analysis of biphasic transversely isotropic cartilage layers and correlations with tissue failure. *J Biomech*. 32:1037-1047.

5. Ewers, BJ, D Dvoracek-Driskna, MW Orth, and RC Haut. (2000) The extent of matrix damage and chondrocyte death in mechanically traumatized articular cartilage explants depends on rate of loading. *J Orthop Res*. in press.

6. Ewers BJ, Dvoracek-Driskna D, MW Orth MW, Haut RC (2001) Theoretical models of cartilage explants and correlations with experimental matrix damage and cell death after impacting loads. *Annal of Biomedical Eng* in review.

7. Garcia JJ, Altiero NJ, Haut RC (1998) An approach for the stress analysis of transversely isotropic biphasic cartilage under impact load. *J Biomech Eng* 120:608-613.

8. Guilak F, A Ratcliffe, and VC Mow. (1995) Chondrocyte deformation and local tissue strain in articular cartilage: a confocal microscopy study. *J Orthop Res*, 13:410-421.

9. Hayes, W. C., Keer, I. M., Herrmann, and Mockros, I. E., (1972) A Mathematical Analysis for Indentation Tests of Articular Cartilage. *Journal of Biomechanics* 5, pp. 541-551.

10. Kim, HA, YJ Lee, SC Seong, KW Choe, and YW Song. (2000) Apoptotic chondrocyte death in human osteoarthritis. *J Rheumatol*. 27(2):455-462.

11. Mow VC, Kuei SC, Lai WM, Armstrong CG (1980) Biphasic creep and stress relaxation of articular cartilage in compression: Theory and experiments. *J Biomech Eng* 102:73-84.

12. Newberry, W. N., Mackenzie, C. D., and Haut, R. C., (1998) Blunt Impact Causes Changes in Bone and Cartilage in a Regularly Exercised Animal Model. *Journal of Orthopaedic Research* 16, pp. 348-354.

13. Oloyede A, Flaachsmann R, Broom ND (1992) The dramatic influence of loading velocity on the compressive response of cartilage. *Connective Tissue Research* 27:211-224.

14. Repo RU and JB Finlay. (1977) Survival of articular cartilage after controlled impact. *J Bone Joint Surg [AM]*. 59:1068-1078.

15. Schinagl, RM, D Gurskis, AC Chen, and RL Sah. (1997) Depth-dependent confined compression modulus of full-thickness bovine articular cartilage. *J Orthop Res* 15:499-506.

16. Suh, JK and S Bai. (1998) Finite element formulation of biphasic poroviscoelastic model for articular cartilage. *J Biomech Eng.* 120:195-201.

17. Suh JK, DiSilvestro MR (1999) Biphasic poroviscoelastic behavior of hydrated biological soft tisue. J Applied Mech 66:528-535.

18. Torzilli, PA, R Grigiene, J Borrelli, Jr., and DL Helfet. (1999) Effect of impact load on articular cartilage: cell metabolism and viabiltiy, and matrix water content. *J Biomech Eng.* 121:433-441.

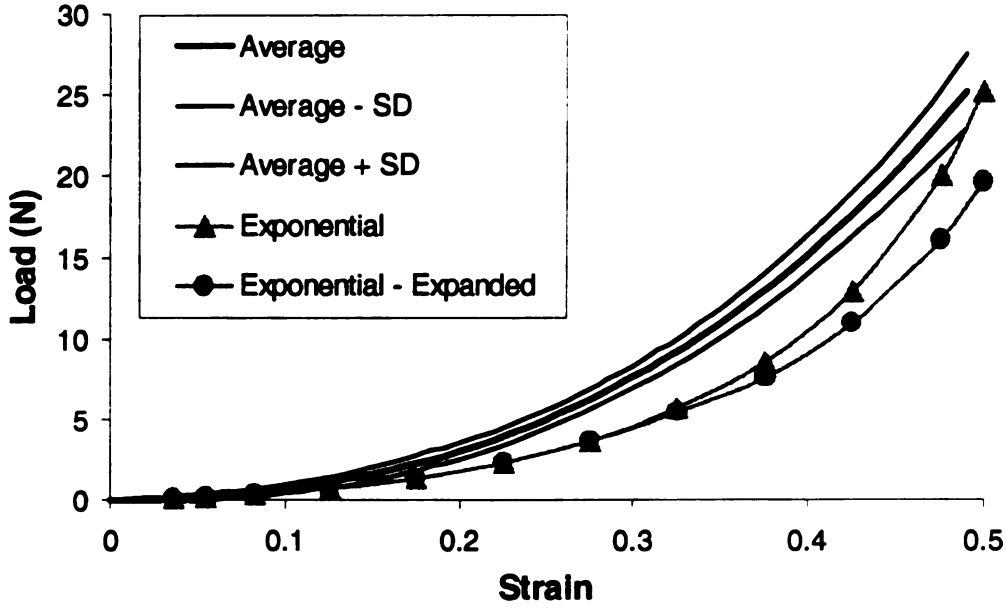

Figure 1: Experimental load-strain curves for indentation of a rigid sphere into bovine articular cartilage (Average ± one standard deviation). Gray lines show the computational models using the same coefficients of the strain-energy function. Notice that for strains less than 30 % the models predict the same load, thereafter the expanded form of the strain-energy function flattens out. The expanded form had a similar shape as the experimental data.

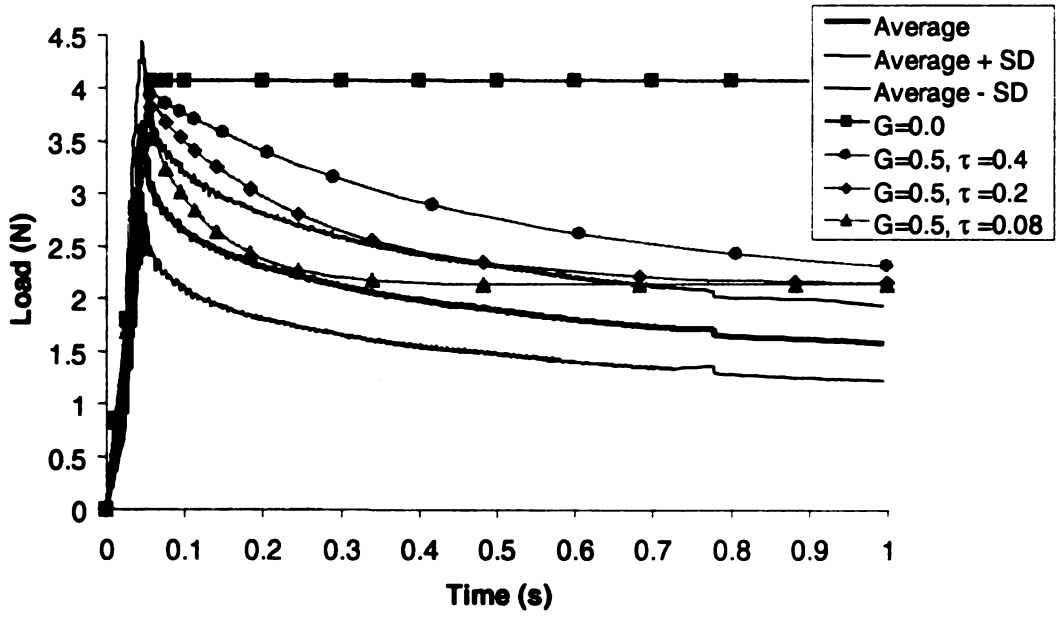

Figure 2: First attempt to model the relaxation of bovine cartilage. Notice there was not enough relaxation. Decreasing τ caused the load to relax faster.

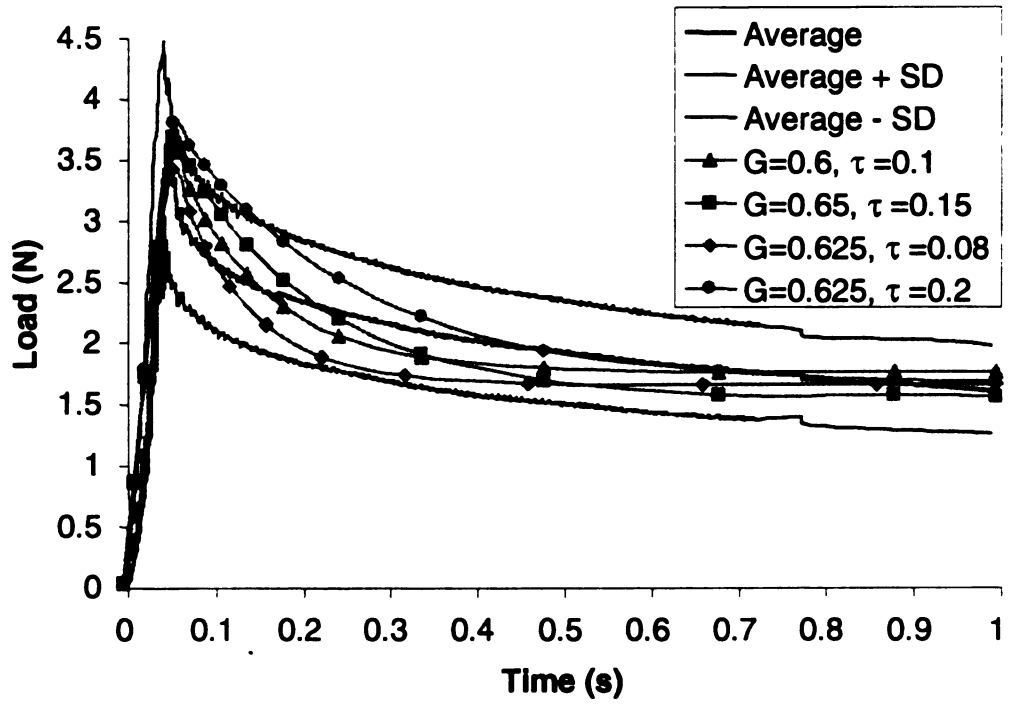

Figure 3: Final curve fitting of the relaxation experiments. With only a one term Prony series it is hard to get a good fit of the relaxation. Because impacts are generally under 100 ms, we took the best fitting curve from that region ($G^P = 0.625$, $\tau = 0.08$).

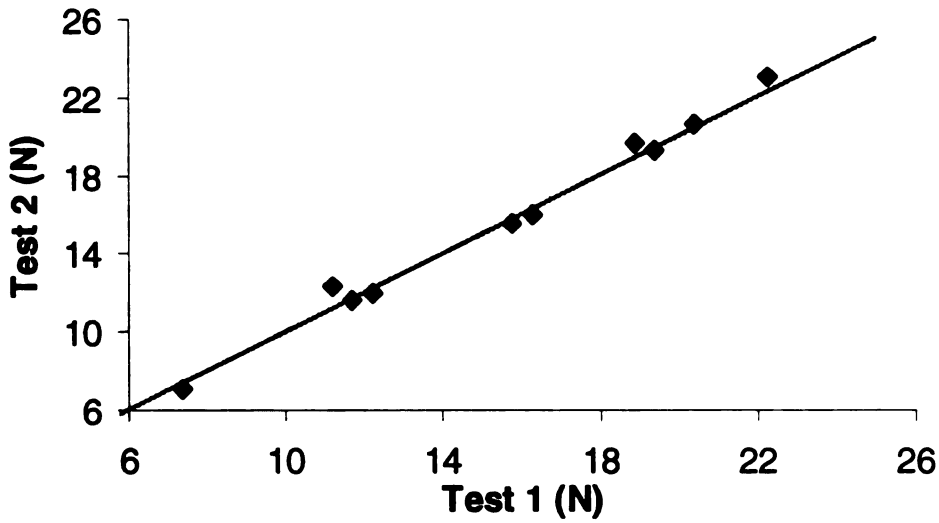

Figure 4: Peak load for repeated indentation tests with the spherical indentor for displacements greater than 0.15 mm. The line represents zero error. Notice no trend for the second test to be above or below the line suggesting that there is no tissue damage due to the first indentation test.

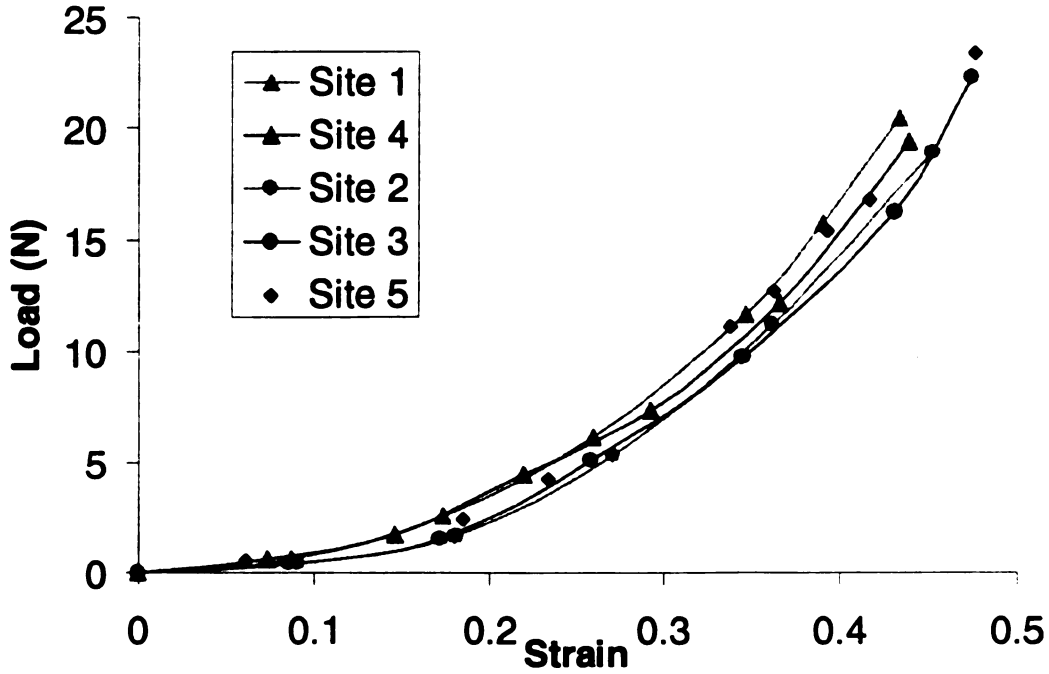

Figure 5: The experimental peak load versus strain curves for all the testing sites. Sites 1 through 4 were all repeated measures. Sites 1 and 4 went from small to large displacements, while sites 2 and 3 went from large to small displacements. Site 5 had only one indentation test per location to examine the influence of repeated tests on the load-displacement response of cartilage. Notice how site 5 falls within the experimental data from the repeated sites indicating that it was reasonable to conduct repeated tests on the cartilage using a spherical indentor.

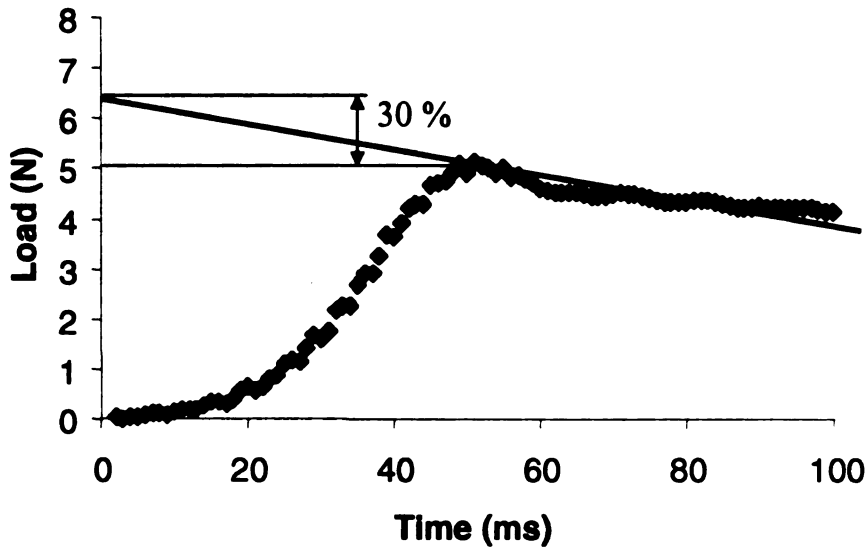

Figure 6: By linearly extrapolating to determine an instantaneous load, there is an approximate 30 % reduction in load from 0 to 50 ms.

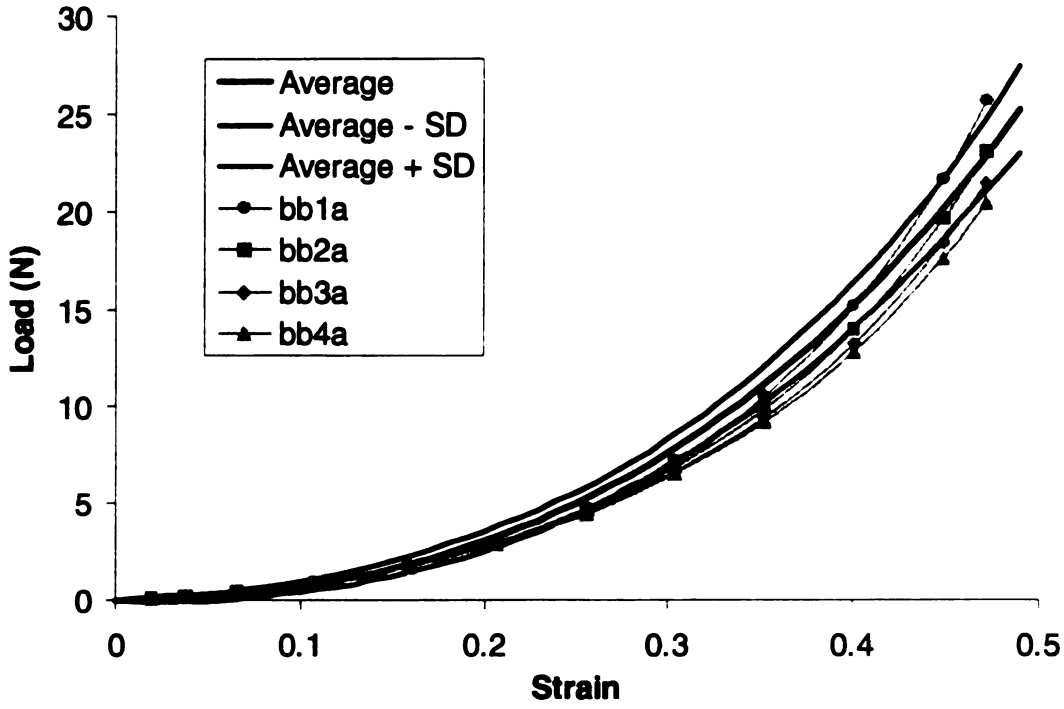

Figure 7: The average experimental peak load versus strain curve along with the computational model with four possible sets of strain-energy coefficients. This assumed that the instantaneous shear modulus was $1.3*G_O$ based on the amount of relaxation in 50 milliseconds. The one set that best fit the experimental data over the entire strain range was bb2a ($C_O = 6.0$, $C_1 = 0.68$, $C_2 = 0.02$, $K = 35.25$).

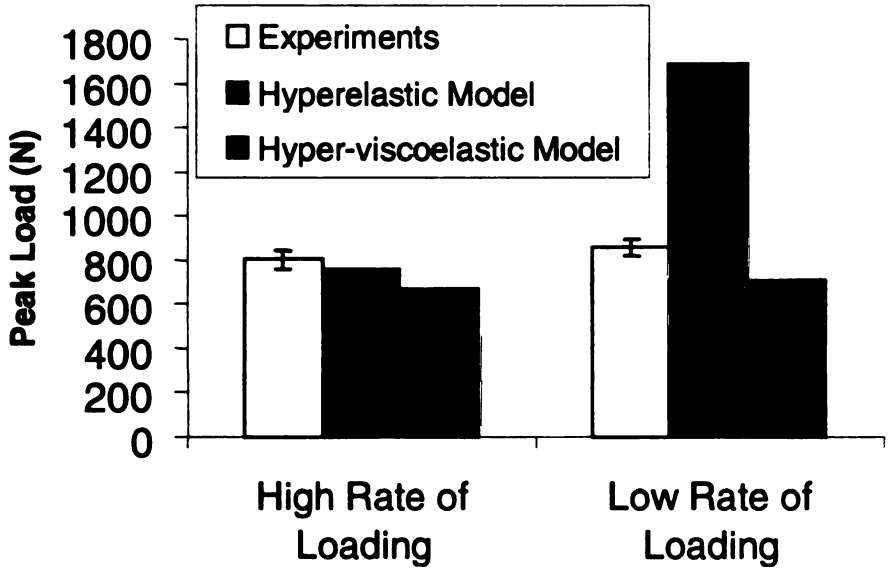

Figure 8: Experimental peak load from the unconfined compression experiments and the peak load prediction from the hyperelastic and hyper-viscoelastic models. Deformation was the input boundary condition. Notice that the hyper-viscoelastic slightly under predicted the peak experimental load.

APPENDIX A

A.1 Variables to define for user-defined isotropic hyperelastic subroutine

Variables given

BI1 – first deviatoric strain invariant
BI2 – second deviatoric train invariant
AJ – determinant

Variables that need to be defined

U – strain energy function

$UI1(1) = \partial U / \partial \bar{I}_1$

$UI1(2) = \partial U / \partial \bar{I}_2$

$UI1(3) = \partial U / \partial J$

$UI2(1) = \partial^2 U / \partial \bar{I}_1^{\,2}$

$UI2(2) = \partial^2 U / \partial \bar{I}_2^{\,2}$

$UI2(3) = \partial^2 U / \partial J^2$

$UI2(4) = \partial^2 U / \partial \bar{I}_1 \partial \bar{I}_2$

$UI2(5) = \partial^2 U / \partial \bar{I}_1 \partial J$

$UI2(6) = \partial^2 U / \partial \bar{I}_{21} \partial J$

$UI3(1) = \partial^3 U / \partial \bar{I}_1^{\,2} \partial J$

$UI3(2) = \partial^3 U / \partial \bar{I}_2^{\,2} \partial J$

$UI3(3) = \partial^3 U / \partial \bar{I}_2 \partial \bar{I}_1 \partial J$

$UI3(4) = \partial^3 U / \partial \bar{I}_1 \partial J^2$

$UI3(5) = \partial^3 U / \partial \bar{I}_2 \partial J^2$

$UI3(6) = \partial^3 U / \partial J^3$

A.2 UHYPER for the "generalized" exponential Fung strain-energy equation

```
*USER SUBROUTINE
      SUBROUTINE UHYPER(BI1,BI2,AJ,U,UI1,UI2,UI3,TEMP,NOEL,CM)
      IMPLICIT DOUBLE PRECISION (A-H,O-Z)
      CHARACTER*8 CM
      PARAMETER (ZERO=0.0D0)
      DIMENSION UI1(3),UI2(6),UI3(6)
      C0=21.0
      C1=0.185
      C2=0.005476
      CK=9.65
      PHI=C1*(BI1-3.0)+C2*(BI2-3.0)+CK*(AJ-1)**2
      U=0.5*C0*(EXP(PHI)-1.)
      DUDPHI=0.5*C0*EXP(PHI)
      DU2DPHI2=DUDPHI
      DU3DPHI3=DUDPHI
      UI1(1)=DUDPHI*C1
      UI1(2)=DUDPHI*C2
      UI1(3)=DUDPHI*2.*CK*(AJ-1)
      UI2(1)=DU2DPHI2*C1*C1
      UI2(2)=DU2DPHI2*C2*C2
      UI2(3)=DU2DPHI2*2.*CK*(1.+2.*CK*(AJ-1.)**2)
      UI2(4)=DU2DPHI2*C1*C2
      UI2(5)=DU2DPHI2*C1*2.*CK*(AJ-1.)
      UI2(6)=DU2DPHI2*C2*2.*CK*(AJ-1.)
      UI3(1)=DU3DPHI3*C1*C1*2.*CK*(AJ-1.)
      UI3(2)=DU3DPHI3*C2*C2*2.*CK*(AJ-1.)
      UI3(3)=DU3DPHI3*C1*C2*2.*CK*(AJ-1.)
      UI3(4)=DU3DPHI3*C1*2.*CK*(1.+2.*CK*(AJ-1.)**2)
      UI3(5)=DU3DPHI3*C2*2.*CK*(1.+2.*CK*(AJ-1.)**2)
      UI3(6)=DU3DPHI3*CK**2*(AJ-1)*(12.+8.*CK*(AJ-1)**2)
      RETURN
      END
```

A.3 UHYPER for the expanded exponential strain-energy equation

```
*USER SUBROUTINE
      SUBROUTINE UHYPER(BI1,BI2,AJ,U,UI1,UI2,UI3,TEMP,NOEL,CM)
      IMPLICIT DOUBLE PRECISION (A-H,O-Z)
      CHARACTER*8 CM
      PARAMETER (ZERO=0.0D0)
      DIMENSION UI1(3),UI2(6),UI3(6)
      C0=6.0
      C1=0.68
      C2=0.02
      CK=35.25
      D1=(BI1-3.0)
      D2=(BI2-3.0)
      D3=(AJ-1.0)
      TEMP=1+C1*D1+C2*D2+CK*D3**2+0.5*C1**2*D1**2+0.5*C2**2*D2**2
     1    +0.5*CK**2*D3**4+C1*C2*D1*D2+C1*CK*D1*D3**2+C2*CK*D2*D3**2
      U=0.5*C0*(TEMP)
      UI1(1)=0.5*C0*C1*(1+C1*D1+C2*D2+CK*D3**2)
      UI1(2)=0.5*C0*C2*(1+C2*D2+C1*D1+CK*D3**2)
      UI1(3)=C0*CK*(D3+CK*D3**3+C1*D1*D3+C2*D2*D3)
      UI2(1)=0.5*C0*C1**2
      UI2(2)=0.5*C0*C2**2
      UI2(3)=C0*CK*(1+3*CK*D3**2+C1*D1+C2*D2)
      UI2(4)=0.5*C0*C1*C2
      UI2(5)=C0*C1*CK*D3
      UI2(6)=C0*C2*CK*D3
      UI3(1)=0.0
      UI3(2)=0.0
      UI3(3)=0.0
      UI3(4)=C0*C1*CK
      UI3(5)=C0*C2*CK
      UI3(6)=6*C0*CK**2*D3
      RETURN
      END
```

APPENDIX B

Relationships between the infinitesimal elastic constants (G_O, ν) and the coefficients of the strain-energy function.

The following two independent theoretical problems were used to relate the infinitesimal elastic constants to the coefficients of the strain-energy function. For rapid loading it was assumed that the cartilage was nearly incompressible ($\nu = 0.49$).

B.1 Pure shear. The infinitesimal shear modulus is related to the derivatives of the strain energy function by the following well known function

$$G_O = 2\left(\frac{\partial W}{\partial I_1} + \frac{\partial W}{\partial I_2}\right)$$

evaluated in the undeformed configuration ($I_1=3$, $I_2=3$, $I_3=1$). Using the strain energy function in the current study yields the equation:

$$G_O = C_O(C_1 + C_2)$$

B.2. Uniform triaxial loading assuming equal stretches.

$$\sigma = \sigma_1 = \sigma_2 = \sigma_3 \qquad \lambda = \lambda_1 = \lambda_2 = \lambda_3$$

Then the strain invariants are $I_1 = 3\lambda^2$, $I_2 = 3\lambda^4$, $I_3=\lambda^6$, and the equation for the stresses:

$$\sigma = 2\lambda^3 \frac{\partial W}{\partial I_3} + \frac{2}{\lambda}\frac{\partial W}{\partial I_1} + 4\lambda\frac{\partial W}{\partial I_2}$$

The derivative of the stress with respect to stretch evaluated in the undeformed configuration is equal to three times the bulk modulus (B):

$$\left.\frac{d\sigma}{d\lambda}\right|_{\lambda=1} = 3B$$

Evaluated with the "generalized" Fung strain energy function gives:

$$B = C_O(K - C_1 - 2C_2)$$

Where B is the bulk modulus and is related to the shear modulus G_O and ν by:

$$B = \frac{2G_O(1+\nu)}{3(1-2\nu)} = C_O(K - C_1 - 2C_2)$$